Impact of VUV Photons on SiO_2 and Organosilicate Low-k Dielectrics: General Behavior, Practical Applications and Atomic Models.

M. R. Baklanov[1,2], V. Jousseaume[3,4], T. Rakhimova[5], D. Lopaev[5], Yu. Mankelevich[5],

V. V. Afanas'ev[6], L. Shohet[7], S. W. King[8], and E. T. Ryan[9]

[1] *North China University of Technology, 100144 Beijing, China*

[2] *Moscow Technological University (MIREA), 119454 Moscow, Russia*

[3] *Université Grenoble Alpes, F-38000 Grenoble, France*

[4] *CEA, LETI, MINATEC Campus, F-38054 Grenoble, France*

[5] *Skobeltsyn Institute of Nuclear Physics, Lomonosov Moscow State University, 119991, Moscow, Russia.*

[6] *Department of Physics and Astronomy, University of Leuven, B-3001 Leuven, Belgium.*

[7] *Plasma Processing and Technology Laboratory and Department of Electrical and Computer Engineering, University of Wisconsin-Madison, Madison, WI 53706, USA*

[8] *Logic Technology Development, Intel Corporation, Hillsboro, Oregon 97124, USA*

[9] GLOBALFOUNDRIES*, Albany, NY 12203, USA*

CONTENTS.

I. INTRODUCTION.

UV light assisted processes are widely used in semiconductor technology. The most important and traditional applications include lithography, thin film curing, and wafer cleaning (removal of organic residues, water purification, etc.) Incidental UV phenomena related to plasma processing (dry etch, plasma assisted chemical vapor deposition (PECVD), resist strip, barriers deposition) are also very important for technology development and high-volume manufacturing (HVM) because these could be responsible for degradation of IC devices and adverse influence on their reliability and yield.

In the case of back-end-of-line (BEOL) interconnect technology, which is the major interest of this review, UV light application historically was mainly motivated by the need to remove organic porogen from organosilicate (OSG) films, also called carbon-doped glass or SiCOH, to create porous SiCOH, or pSiCOH films. Porosity lowered the film's dielectric constant, k, which enables one to reduce the

interconnect wiring capacitance contribution to the RC signal delay in integrated circuits.[1,2] These films are generically called low-k dielectrics. The UV-based low-k film curing (λ > 200 nm) proved superior to thermal annealing and electron beam curing.[3,4] Thermal annealing was slow and did not adequately increase Si-O-Si crosslinking because copper in-diffusion limited the thermal budget to <400^{o}C, while E-beam curing could generate electrical current in the front-end fabricated circuits and produce X-rays potentially damaging Si-based devices.[5] Thus the UV curing became the established technology of choice used in HVM.

The advent of UV curing and the realization that photons play a significant role in plasma-induced damage to pSiCOH motivated research into the mechanisms of UV/VUV photon interactions in pSiCOH films and in other materials used in BEOL nanofabrication. Integrated circuits require multiple levels of interconnect wires insulated by SiCOH low-k materials with vias connecting one level of wiring to another.[6] Each interconnect wiring level is fabricated sequentially, i.e., after completing the previous one. Thus, during UV curing of a pSiCOH film used in the fabrication of a particular interconnect wiring level, all the materials in the previously fabricated interconnect levels underneath can be exposed to UV photons. One consequence was a UV-induced change in stress from compressive to tensile in SiCNH films used to passivate the top Cu surface.[7,8,9] Films with modestly compressive or neutral stress are desired because tensile films can induce cracking during the chip packaging process. Thus, there was a need to understand how UV light affects all the films used to fabricate BEOL interconnects.

Today the mechanisms of UV/VUV photon interactions with pSiCOH and other films used in interconnect fabrication are fairly well understood after nearly two decades of research. And this understanding has allowed engineers to both control the damaging effects of photons and utilize the UV light for material engineering and nanofabrication processes.

In general, progressively smaller nanostructures are increasingly fragile and require gentler nanofabrication methods. For example, ion bombardment during plasma processing can damage or deform the silicon fin in fin field-effect transistors (FinFETs), which motivated the development of softer plasma processes. The need for gentle processing such as plasmaless or ion-free etching and deposition is increasing, and for some fabrication processes UV-based methods are a promising alternative to plasma-based methods.

In this paper, the current status of the UV based low-k dielectric technology will be overviewed. The first section will provide a short introduction into low-k materials, which were developed over the

last 20 years, and report on the present level of understanding of the photochemical reactions responsible for UV curing (selective porogen phase removal, creation of porous structure and strengthening of the OSG matrix). The second section will be devoted to mechanisms of low-k damage by VUV photons happening during the plasma processing. The third section will analyze the nature and atomic models of defects in SiO2 and OSG materials due exposure into UV/VUV photons. The last section will review current, potential near term, and longer-term applications of UV- and VUV-assisted processing for advanced manufacturing. Current applications are those now used in high volume manufacturing, or for which HVM capable tools are available. Potential near-term applications are those in development on HVM-capable tools. Potential long-term applications are those in various stages of development or research. Applications have been mostly limited to UV light since commercial UV systems are more readily available, and use the advantage of UV photons having a significantly larger penetration depth than VUV light in most of dielectric materials.

II. UV curing of OSG low-k films.

II.1. Introduction to low dielectric constant (low-k) films.

Downscaling of integrated circuits (IC) brings new challenges to semiconductor technology. Besides smaller dimensions, new materials and new integration schemes are required. In advanced interconnects, resistive-capacitive (RC) delay (product of the resistance R of the metal lines and their inter-capacitance C), dynamic power consumption, and cross-talk noise are becoming the main obstacles for the downscaling. The need to decrease RC requests introduction of new materials into interconnects. The conventional SiO_2 inter-metal dielectric has been replaced by materials with lower dielectric constant k (SiO_2 has k-value of 4.2), so-called "low-k" materials, while Al was replaced by Cu as a conductor with lower resistivity.[1,2]

Dielectric constant of materials is described by the Clausius–Mossotti equation,

$$\frac{k-1}{k+2} = \sum_i \frac{N_i \alpha_i}{3\varepsilon_0} \qquad \text{(II.1)}$$

where $k=\varepsilon/\varepsilon_0$, ε and ε_0 are the dielectric constants of the material and vacuum, *N* is the number of molecules per unit volume (density) and α_i is the total polarizability, including electronic (α_{el}), ionic (α_{ion})

and dipolar (α_{dip}) polarizabilities ($\alpha_i = \alpha_{el}+\alpha_{ion}+\alpha_{dip}$). According to this equation, the dielectric constant of materials can be reduced by decreasing the total polarizability and density. Early generations of low-k dielectrics were obtained by doping the traditional SiO_2 with fluorine and carbon during the chemical vapor deposition (CVD) of the materials. Fluorine substitution lowers the k value by decreasing the polarizability and increasing the free volume. These kinds of dielectrics typically have a k -value in the range of 3.0–3.5.[10]

Different low dielectric constant materials from organic polymers to zeolites and metal-organic frameworks have been evaluated as possible low dielectric constant candidates for ULSI interconnects during the last 2 decades. Organic polymers have chemical bonds with low polarizability and, therefore, they are able to provide the lowest k values (2.6–3.0) without requiring the introduction of porosity. They were very popular in the beginning but the efforts to integrate organic materials into ICs have not been successful. In addition to poor mechanical and thermal properties, the key problems were related to the relatively high coefficient of thermal expansion (CTE) with respect to other components of integrated circuits.[11,12,13,14,15,16,17] Materials like zeolites,[18,19,20,21,22,23] boron carbonitrides [24,25,26] and metal-organic frameworks (MOF) [27,28,29] have excellent mechanical properties that is extremely important so that they can sustain a complete integration (including packaging) but they are hardly compatible with existing damascene technology because of crystalline structure and intergranular voids [30] (zeolites and MOF) and change of their chemical composition during the plasma and chemical etching. At the end, organosilicate glasses (OSG) remain the major materials for interconnect technology because they have properties similar to traditional SiO_2, use the similar (often same) technological equipment and have better compatibility with damascene integration technology.[31] The introduction of carbon groups into silica matrix can both reduce the density of the material (and thus k-value) and the total polarizability. However, the only carbon incorporation into a silica matrix shows its limits in terms of k-value reduction. Depending on the precursors used, deposition conditions and the carbon content in the layer, the dielectric constant can be lowered to 2.7-3.0 without artificial porosity. [32,33] Then a second breakthrough was reached by introducing porosity in the insulating matrix. The objective here was to decrease the film density further, leading to a decrease of the dielectric constant.[2-34]

Thin low-k films can be obtained by liquid, gas phase and plasma deposition methods, such as dip-coating, spin-coating and plasma enhanced chemical vapor deposition (PECVD). In spin-coating, liquid precursors are put onto the substrate which then rotates at high speed. The liquid spreads out due to centrifugal forces, the excess amount of the liquid flies off the substrate and after drying, a thin film is

obtained. At the end, evaporation of the solvent thins the film further out. The thickness of the spin-coated film mainly depends on the viscosity of the initial liquid, concentration of the different components in the solution and the rotation speed. The higher the viscosity, the thicker the film will be. On the other hand, a higher amount of solvent will decrease the thickness and also a higher rotation rate will lead to thinner films.[35]

Two methods can be applied to introduce porosity in spin-on deposited films. The first one is the creation of pores by adjusting the synthesis parameters, thus without using templates (porogens). For instance, when using base catalyzed sol-gel reactions, the density of the films decreases. The most known examples of template free porous silicate materials are aerogels and xerogels. Silica aerogels are prepared by sol-gel via spin-coating in a saturated solvent environment. By adjusting the drying conditions (supercritical, freeze-drying), the solvent can be removed without pore collapse leaving behind a very porous material.[35,36] To reduce the amount of silanol groups an extra thermal and sylilation treatments can be applied. Another way to create porosity is the deposition of silane precursors in the presence of a porogen generator. This method allows to deposit films with good and controllable quality. A majority of works were firstly performed using polymethysilsesquioxane (PMSSQ) as low-k matrix. A review of these works can be found here.[34,36]

Recently, new types of spin-on deposited films, so called Periodic Mesoporous Organosilicates (PMO) have attracted much attention. PMOs were discovered in 1999 by three different groups [37,38,39] and they are similar to ordered mesoporous silica materials but at least one siloxane bond in the matrix is replaced by an organic bridge.[40] From a low-k application perspective, an important feature of PMO materials is their ability to undergo self-hydrophobization - a silanol-consuming transformation of bridging methylene to terminal methyl groups.[41] They are usually amorphous, but their pores and pore walls are arranged in a structural order. Typically, PMO materials are synthesized by hydrolysis and condensation of bridged organosilanes $(R'O)_3Si – R - Si(OR')_3$ in the presence of a surfactant which acts as structure directing and pore generating agent. After an ageing period and soft baking, the surfactant can be removed by an extraction procedure or by a thermal treatment under an inert atmosphere, leaving behind a porous PMO material. Interest to these materials is related to expected improvement of their mechanical properties because of ordered pore structure and higher strength of Si-C bonds in comparison with Si-O bonds in pure silica.[42,43] It has also been demonstrated that the presence of carbon bridge improves their plasma and VUV resistance.[44,45]

PECVD is currently the method of choice in the microelectronic industry, because this technique is more easily integrated in the device manufacturing process.[1,5] In PECVD, precursors are brought in the gas phase and transferred to a vacuum reaction chamber. The heat and plasma deliver the energy which is needed for reaction of the vaporized precursors to produce the desired layer on the substrate. The main advantage of PECVD is that the deposition can occur at relatively low temperatures on large areas. The main parameters to obtain good quality dielectric films are the substrate temperature, pressure, the radio frequency (rf) power and the flow ratios of the reactant gases.

PECVD of ultra-low-k ultra-low-k films were reported for the first time in 2001 by A. Grill and colleagues (IBM). They presented results on a porous SiCOH using a PECVD porogen approach (using tetramethyl-cyclotetrasiloxane (TMCTS) as the matrix precursor).[46] Afterwards, other research groups successfully achieved this porous SiCOH using different precursors (Table II.1): diethoxy-methyl-silane (DEMS),[47] dimethyl-dioxiranyl-silane and diethoxy-methyl-oxiranyl-silane,[48] trimethyl-trivinyl-cyclotrisiloxane [49] decamethyl-cyclopentasiloxane (DMCPS) and diethoxy-methyl-silane.[50] These works have shown that cyclic and linear organo-silicate precursors are suitable to perform porous material. For the porogen precursor, any hydrocarbon source with sufficient volatility to be delivered as a gas to the PECVD reactor could be, in principle, used as a porogen.[5,33] In the literature, many of them were tested and studied, such as unsaturated cycles like terpinene (such as a-terpinene or ATRP) or norbornene [51,52,53,54] or molecules with strained rings like cycloalkene oxide.[50,55] It is necessary to mention that presently new precursors containing carbon bridge between Si atoms are becoming more and more popular.

Table II.1. Examples of matrix and porogen precursors for PECVD low-k manufacturing.

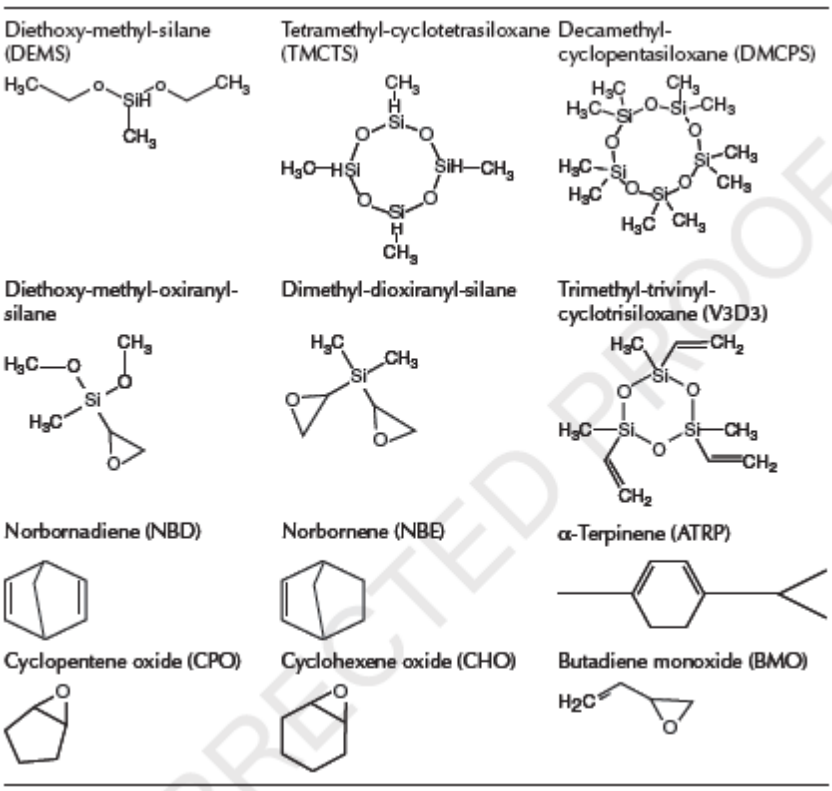

The films with sacrificial porogen deposited by both spin-on and PECVD technologies represent a mixture of matrix material and organic porogen. The matrix material is an organosilicate where the carbon containing groups (methyl) are bonded to Si, to keep the material hydrophobic. The matrix composition depends on the precursor. In the case of spin-on deposition the film composition quite well reproduces composition of the precursor solution.[56] The porogen molecules form agglomerated states that allow formation of porous structure after the curing. The matrix/porogen phase separation was studied for spin-on deposited films polymethysilsesquioxane (PMSSQ) for the low-k matrix and -polymethylmethacrylate-co-dimethylaminoethylacrylate (PMMA-co-DMAEMA) as the porogen, which is volatilized to leave nanopores in the matrix in ref.[57] Using small-angle neutron scattering the kinetics of matrix crosslinking was revealed, while thermal desorption mass spectrometry showed the evolution of gaseous reaction products from porogen and matrix during the complex chemical transformations which occur with thermal cycling from 100 °C to 450 °C. Matrix crosslinking occurs primarily at lower temperatures at 100–225 °C, while porogen diffusion and decomposition begins somewhat above 200°C, leading to the phase separation and formation of the final nanoporous structure (Figure II.1). Since the matrix crosslinking and porogen removal reaction kinetics have some overlap, relative kinetics

can be important: e.g., matrix crosslinking proceeds more rapidly for PMSSQ precursors with high Si–OH content in comparison with low SiOH content, with implications for the morphology of porogen-derived nanostructure. Porogen decomposition is ligand selective, in that the N-containing ligand of DMAEMA is volatilized at considerably lower temperatures (≈200 °C). High temperature anneals (400 °C) is needed for removal of the remaining species such as PMMA ligand.

The first stage of this process which is matrix crosslinking and nanophase separation occurs at relatively low temperature (100-225°C) and normally this step is separated from the final curing and often is termed as “soft bake”. This step is also needed for evaporation of excess solvent and minimizes the risk of structure collapse during the final curing, which normally occurs at 400 – 450°C.

Similar approach is used for preparation of PMO materials. In these processes amphiphilic surfactant molecules form micelles and the silane precursor hydrolyzes and self-assembled around the micelles.[58] In the case of PECVD films, the deposition temperature is usually higher than is required for matrix cross-linking and phase separation. For this reason, PECVD deposited films can go directly to the final curing without soft bake step. To support this statement, Urbanowicz [59] demonstrated that PECVD film before UV curing has already phase separation and the size of porogen agglomerates is not changing during the high temperature curing. He deposited several OSG films. One of them received a standard UV curing.

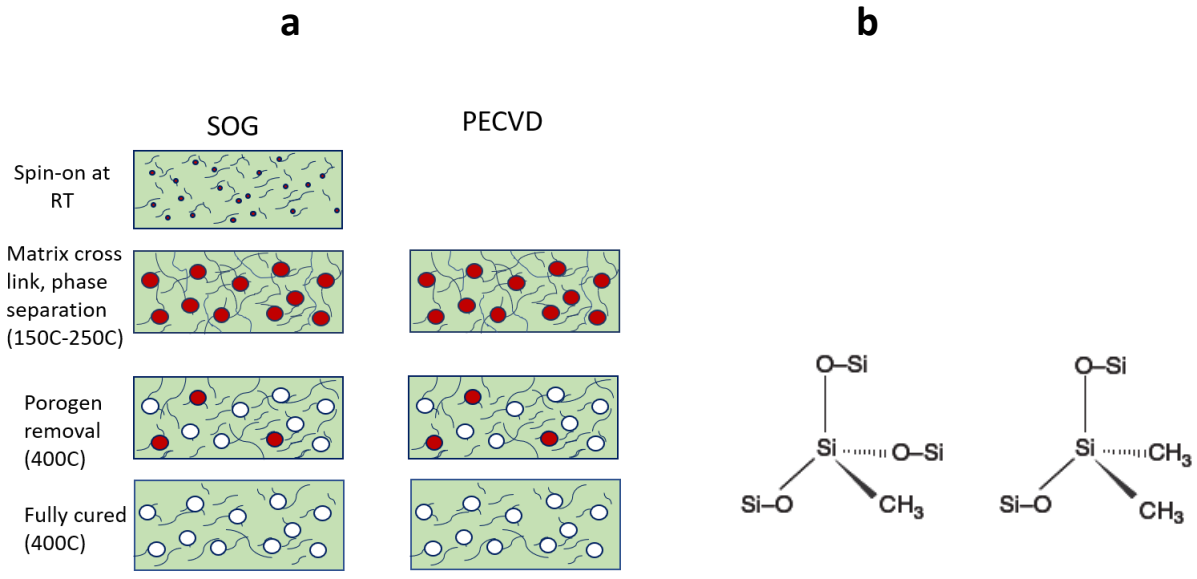

Figure II.1. The consequent steps of porous low-k films formation in PECVD and spin-on technology(a) and skeleton of completely cured OSG glass with 1 (T) and 2 (D) methyl terminal groups.

The second film was exposed to He/H_2 downstream plasma and the third one received UV curing after exposure to He/H_2 downstream plasma. Then all three samples were evaluated by using ellipsometric porosimetry.[60] All three samples showed quite similar pore size distribution. It suggests that the porogen phase has already been separated from matrix materials and formed the pore size defining agglomerates.

II.2. UV Curing.

The deposited OSG films intended for curing (as deposited PECVD films and spin-on deposited and soft baked films) have already certain degree of matrix crosslinking and porogen phase separated from the matrix (Figure II.1). In order to create porosity, the agglomerated porogen phase must be removed with high selectivity in respect to matrix. This step is called curing and it is crucial for the fabrication of porous low-k with sufficiently good mechanical properties and low dielectric constant. The porogen removal occurs through the polymer fragmentation with formation of more volatile species but process should be sufficiently gentle and do not brake $Si\text{-}CH_3$ bonds in the matrix (Figure II.1b). Several methods have been evaluated for porogen removal, making low-k film porous. These techniques include thermal annealing, Electron Beam (EB), by Ultra Violet radiation (UV) assisted thermal curing, H_2 Plasma, and supercritical CO_2.[46,61,62,63,64,65,66,67,68,69,70,71,72,73,74,75] J. Liu et al. proposed curing based on consecutive exposure of OSG low-k film to UV and infrared (IR) radiation. IR radiation delivers thermal energy necessary for cross-linkage of OSG matrix.[76,77] Recently a room temperature curing with consequent treatment by UV (6.2 eV) and VUV (8.8 eV) photons has been proposed.[78] However, although substantial improvement of mechanical properties was demonstrated in the last work, the chemical composition of the cured low-k films was not analyzed.

Thermal curing during several hours at high temperature (≥400°C) in inert atmosphere and vacuum has been widely used for spin-on deposited films.[34,36,79] A thermal curing of PECVD films during 4 hours at 400°C in Helium atmosphere was initially used by A. Grill et al. in order to remove the porogen and produce porous films.[5,80] However, at this temperature and time, this annealing might be not enough to produce stable and residue free porous ULK films. In particular, thermal treatment does not enhance sufficiently the volumetric concentration of Si-O-Si bonds and, then, the film exhibits poor mechanical properties. Actually, thermal annealing even at extreme conditions (high temperature and long time: up to 12 h at 450°C let some uncondensed silanols bonds (SiOH) that are not participating in the cross-

linking mechanisms.[81] Moreover, thermal curing, especially for highly crosslinked as-deposited films, is not able to remove all porogens.[82] Some residues are still present and can deteriorate the low k film properties. Then, curing by thermal annealing requires long times at temperatures at the upper limit of acceptability for BEOL processes and produces porous films with crosslinking and, therefore, insufficient mechanical properties.

To circumvent these limitations, the thermal treatment can be assisted by additional energetic sources. Although different techniques have been evaluated for porogen removal and curing, EB and UV curing found most extensive application because they offered the opportunity to process at temperatures of ~400°C for short durations (few minutes) and to achieve porous films with better mechanical properties.[61,83,84,85] Many similarities have been evidenced with EB and UV treatments: both curing remove efficiently the porogen from the deposited films but they can also react with some skeleton bonds (such as Si-CH_3, Si-H, and (Si-OH)), leading to the increase of the Si-O-Si cross-links concentration.[61] However, because EB cure can induce potential damages of certain types of active devices, it was abandoned by some manufacturers in favor to UV treatment.[86,87,88,89,90,91]

II.2.1. UV absorption of OSG matrix and porogen. Optimal wavelength range.

As already mentioned, the purpose of low-k curing is selective removal of porogen phase and cross-linking (strengthening) of low-k matrix. Ideally, the curing process must completely remove porogen fragments without leaving any carbon containing residues. Concentration of terminal CH_3 groups bonded to Si in low-k matrix should be preserved to ensure film hydrophobicity and low matrix permittivity. Since UV has been adopted as the major process in curing ultra-low-k material, numerous studies have been devoted to fundamental understanding of the mechanisms behind the transformation of OSG films through UV exposure.[63,64,85] To understand mechanisms of UV assisted curing, it is necessary to know optical characteristics of matrix and porogen.

Organosilicate glasses have silica like matrix, in which some bridging oxygen atoms are replaced by terminal alkyl (methyl) groups. Concentration of alkyl groups should be optimized: it must be sufficient to keep OSG low-k film hydrophobic but excess of alkyl concentration reduces degree of matrix cross-linkage and deteriorates mechanical properties. Amorphous silicon dioxide has absorption edge near 8-8.5 eV (150 nm) that can be shifted to lower energy if silica matrix has certain degree of physical disorder. It can be related to high temperature, introduction of some defects and impurities like

vacancies, SiOH, organic groups, etc.[92,93,94,95] VUV photons with energy higher than 8.5 eV are photochemically active in respect to SiO_2 and generate different kind of defects, such as positive charges and E' deep hole trap defects.[96,97,98,99] Therefore VUV light selected for OSG low-k curing certainly should have energy lower than 8 eV. Absorption spectra of OSG low-k films were analyzed in refs.[100,101] Choudhury et al. [101] measured depth of VUV damage of OSG films exposed to synchrotron VUV radiation with energies ranging from 7 to 21 eV. The films density vs. depth profile of the VUV-irradiated films was extracted from the fitting of the XRR (specular X-ray reflectivity) experimental data. Between 7 and 11 eV, the depth of the damaged layer decreases sharply from 110 nm to 60 nm and then gradually increases to 85 nm at 21 eV. The maximum VUV absorption in low-k films occurs between 11 and 15 eV. Similar results were also reported by Rakhimova et al.[102]

Most comprehensive analysis of UV absorption spectra of OSG matrix and porogen in the region important for UV curing was done by Marsik et al.[100] using vacuum UV spectroscopic ellipsometry (Figure II.2). The optical response of the films was measured in the range from 2 eV to 9 eV (wavelengths from 620 nm down to 138 nm) using a variable angle of incidence spectroscopic ellipsometer. The dielectric function ε of the low-k film was modeled by generalized Gauss–Lorentz (G–L) peaks, calculated as rational approximations.

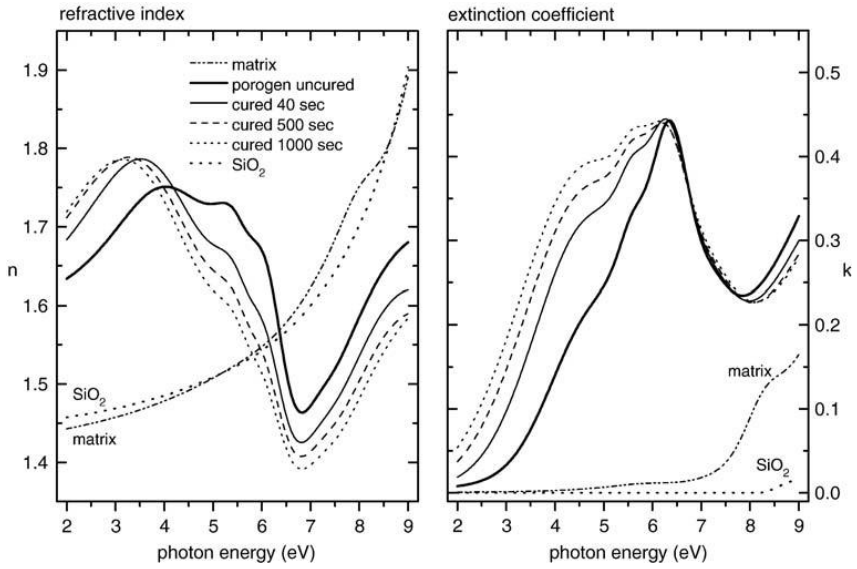

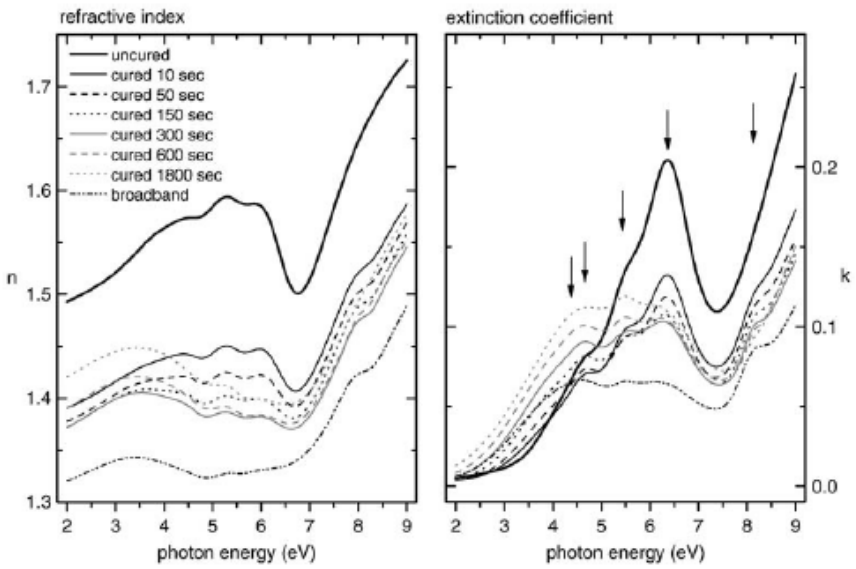

Figure II.2. a) Optical functions of porogen films UV-cured for various curing times from 0 s (solid thick black line) to 1000 s (dotted line) and the optical functions of the matrix material (dash dot line). The optical functions of SiO_2 are plotted for comparison (thicker dotted line). b) Optical functions of hybrid film (OSG matrix/porogen). Solid line represents uncured film, the optical functions of low-k film cured with broadband light with $\lambda > 200$ nm is represented by dotted line (bottom line). Other curves are porogen containing films cured different time with light with λ=172 nm.

The studied samples were prepared by PECVD mixing of the OSG matrix precursor (containing Si–O and $Si–CH_3$ bonds, and the sacrificial CxHy precursor (porogen). Along with hybrid low-k films, reference samples were also studied (depositing either the porogen material itself or the OSG matrix without any additional porogen). The deposited low-k films were heated up to 430 °C in nitrogen atmosphere (pressure 6000 Pa) and exposed to nearly monochromatic UV light with a wavelength of 172 nm from Xe excimer lamps. Under these conditions, the porogen decomposes and the pores are created. An additional sample was exposed by a broadband (λ>200 nm) light source for a moderate curing time (close to the optimum curing time: lowest k-value and highest porosity) to assess the possible effect of the UV light source. The optimal curing time for the studied 172 nm UV-cure is approximately 300 s. The optimal curing time for used broadband lamp is roughly 2–3 times longer. One can see from Figure II.2b that broadband lamp with λ>200 nm forms less sp2 carbon porogen residues (absorption at 4-5 eV) [100] and the cured films have higher porosity (lower index of refraction at 2-5 eV).

Figure II.2a shows the optical functions of the porogen films and the matrix. The porogen material manifests similar features as observed in the hybrid low-k film, while the matrix material shows

dispersion similar to silicon dioxide, with an additional shoulder at 8.5 eV and with slightly lower values of refractive index (RI=1.45 compared to 1.46 of SiO_2). During the 172 nm UV-cure of porogen-only layers, most of the volume was removed in the early stages (60% in 40 sec) and optical properties were changing: an increase of the absorption band at 4.5 eV was observed and the following changes in the refractive index (similar to the case of the low-k hybrid). Additionally, effect of UV wavelength was evaluated. It is shown that the selection of the UV-curing light source has significant impact on the chemical composition of the low-k material and modifies the porogen removal efficiency and subsequently the material porosity. The 172 nm photons induce greater changes to most of the evaluated properties, particularly causing undesired removal of Si-CH_3 groups and their replacement with Si-H. The softer broadband radiation from lamp with broad wavelength λ >200 nm improves the porogen removal efficiency, leaving less porogen residues detected by spectroscopic ellipsometry in UV range.[103] The nature of this difference was studied by Prager et al.[104] From quantum-chemical calculations on model substances such as octamethyl-and tetramethylcyclotetrasiloxane as well as on hexamethyl- and tetramethyldisiloxane, it has been shown that a threshold wavelength exists for the excitation of the molecule into the first excited singlet state of 190 and 198 nm as well as of 189 and 192 nm, respectively (Figure II.3).

After excitation and intersystem crossing in an excited triplet state, the scission of the Si–CH3 bond may occur, gaining an energy benefit of around 50 kcal mol−1. The calculated Si–CH3 bond dissociation energy (about ≈90 kcal mol−1) is in agreement with the experimental data given in Ref.[105] These findings reveal the presumption that only photons with λ < 190-200 nm can generate Si-centered radicals that subsequently attract protons from neighboring methyl groups.

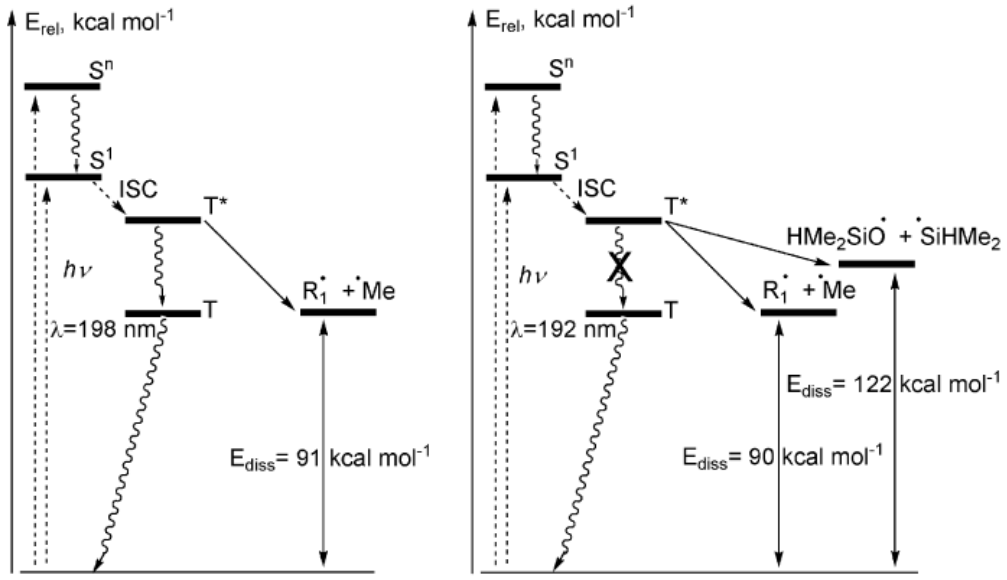

Fig. 3. Results of quantum-chemical calculations on tetramethylcyclotetrasiloxane (left) and tetramethyldisiloxane (right).

Figure II.3. Results of quantum-chemical calculations on tetramethylcyclotetrasiloxane (left) and tetramethyldisiloxane (right).[104]

This is in good agreement with the behavior of the H–SiO peak after irradiation with 172 or 222 nm photons.[103] Moreover, it opens the pathway for cross-linking via Si–Si, Si–O–Si and Si–CH_2–Si bonds. The formation of this kind of defect (Si-centered radicals) has also been demonstrated by Nakao et al. [106] and confirmed by Tajima et al. [107] and Seo et al. [108] as the following:

$$–Si–CH_3 + eV \rightarrow –Si\bullet + CH_2 (H) \qquad (II.2)$$

This defect can easily interact with hydrogen and oxygen atoms to form Si–H and Si–OH bonds. This is the reason why a UV curing with 172 nm light forms more Si–H bonds than broadband light with $\lambda > 200$ nm and this explains the observed anticorrelation between concentration of Si–CH_3 and Si–H groups (Figure II.4). [103] In the case of formation of Si–H bonds, this also leads to generation of less free volume than with Si–CH_3 and contributes to shrinkage of the film.

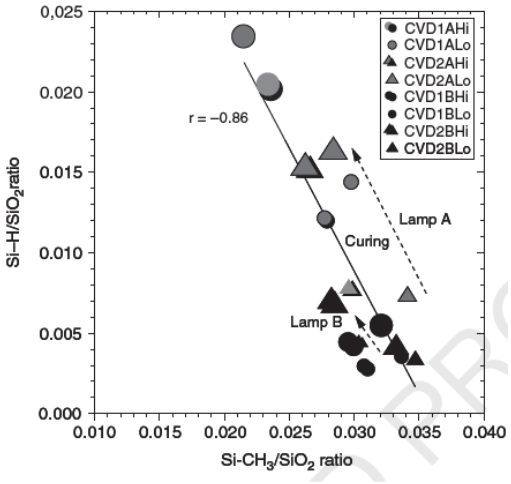

Figure II.4. Anticorrelation between FTIR measured concentrations of Si-CH_3 and Si-H groups observed after curing with a monochromatic light λ=172 nm (lamp A) and broadband light with λ >200 nm (lamp B). One can see that Si-CH_3 reduction is much higher for λ=172 nm. More detailed information about these experiments as well as the samples description can be found in ref.[103]

It is necessary to mention that some loss of methyl groups was observed during the long time exposure of OSG films to UV light with wavelength > 200 nm.[86,109,110] The reason of this contradiction is that the quantum chemical calculations were carried out for several different molecules (particularly tetramethylcyclotetrasiloxane and tetramethyldisiloxane in figure II.3), which are reasonable representatives of OSG fragments. However, it is not possible to exclude that in some cases OSG films can contain different groups absorbing light up to 200 nm. The complex behavior of UV light with λ > 200 nm was also demonstrated by Ming et al.[111] They cured PECVD films by using the different UV radiation wavelengths including quasi single wavelength light emitted from H^+ type bulb (254 nm), dual wavelengths emitted from D type bulb (375 and 385 nm), and dual wavelengths combined with single wavelength. The obtained results indicate that the properties of the porous OSG film treated using the dual wavelength first and then single wavelength were the best among the above three kinds of UV curing conditions. The possible explanation is that porogen removal before matrix strengthening is helpful because it allows to avoid presence of remaining porogen residues embedded into the matrix. Relatively short wave length (254 nm) can form some kind of crust that reduces efficiency of porogen removal.

II.2.2. Chemical composition OSG films before and after curing.

Figure II.5 shows FTIR absorbance spectra of PECVD deposited films: as-deposited matrix material, as-deposited porogen film, as-deposited hybrid film and cured low-k. The inset graph shows the evolution of the peak area around 2900 cm^{-1} attributed to removal of CH_x from the low-k material. One can see from the porogen spectra that the complex CH_x peak located in the region 2700-3000 cm^{-1} is a good representative of porogen (the same CH_x peak in the matrix material is very small and it is only related to presence of $Si-CH_3$ bonds in the matrix). Therefore, uncured hybrid film contains this peak because of presence of porogen. Then this peak almost completely disappears after UV curing.

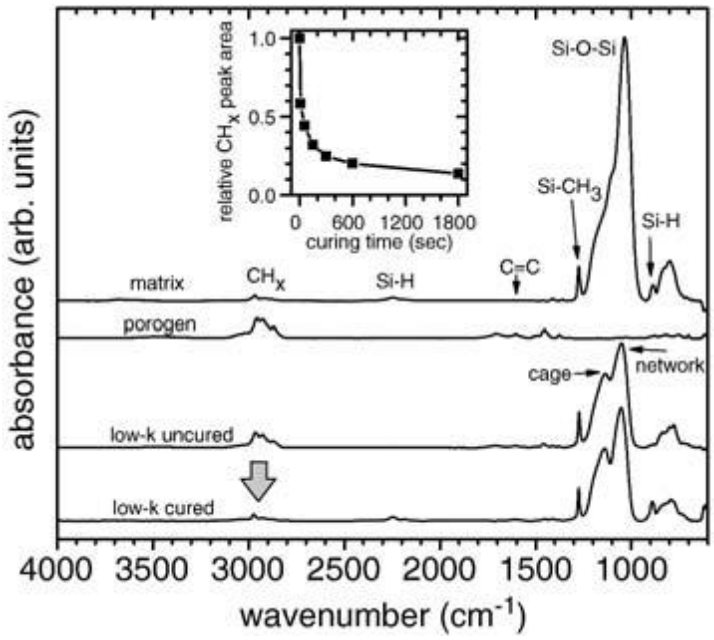

Figure II.5. Infrared absorbance of studied films: as-deposited matrix material, as-deposited porogen film, as-deposited low-k and cured low-k. The inset graph shows the evolution of the peak area around 2900 cm^{-1} attributed to removal of CH_x from the low-k material.[100]

However, the difference in chemical modification of low-k films cured at different wavelengths of UV light can be observed. Figure II.6 displays the transformation occurring during the UV curing. Moreover, a rearrangement of the Si–O–Si structure can be observed as a reduction of suboxides (≈1023 cm^{-1}) and an increase of network concentration (≈1063 cm^{-1}). All these modifications are indicators of the porogen removal and the mechanical properties enhancement.

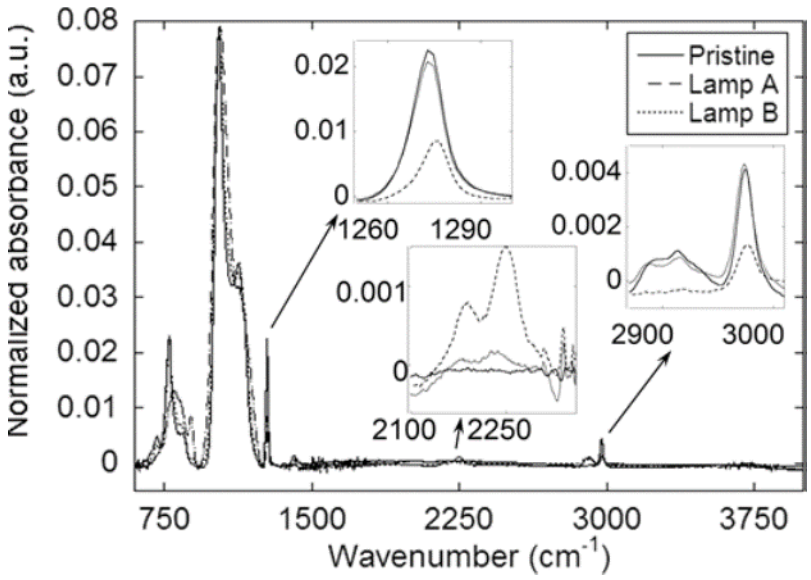

Figure II.6. FTIR spectra of a spin-on deposited low-k film after curing by UV light at 430°C with wavelength 172nm (lamp A) and broadband light with wavelength >200 nm (lamp B).[112]

The light with wavelength >200 nm is almost not depleting concentration of CH_3 groups bonded to Silicon (1260-1290 cm^{-1}). Exposure of the film to the light of 172 nm significantly reduces the concentration of Si-CH_3 groups, the total CH_x concentration (2900–3000 cm^{-1}) mainly linked to porogen organic species, and increases the concentration of Si-H bonds (2100–2300 cm^{-1}).

A valuable information helping to understand formation of OSG low-k films can be obtained by using High-resolution solid-state NMR (Nuclear magnetic resonance). Figure II.7 illustrates the benefit brought by UV curing for porogen removal. A better efficiency in terms of porogen removal is observed for the UV cured sample in comparison to thermal curing with the quasi-disappearance of porogen-related structures (–CH_2O, –CH_2– and –CH_3). The peaks of Si–CH_3 slightly decreases, meaning that there is a substantial effect of UV on the photolysis of methyl groups.

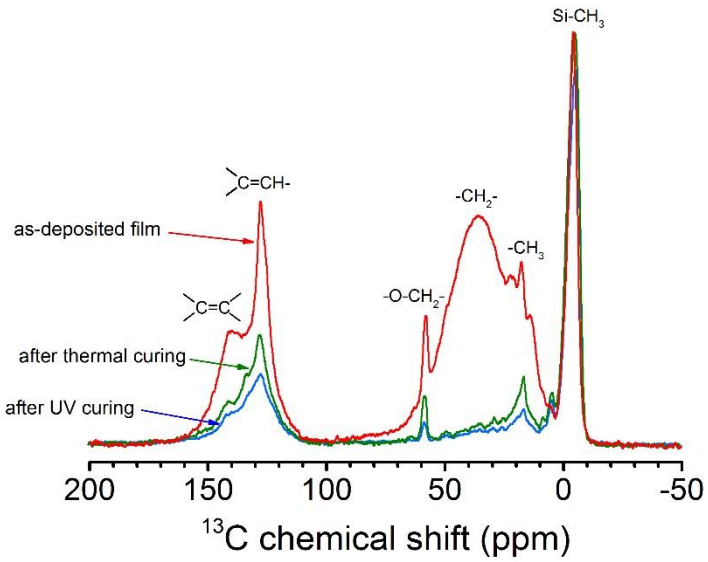

Figure II.7. ^{13}C NMR spectra for the as-deposited SiCOH film (by PECVD using a porogen approach, precursors used were DEMS and NBD), thermally cured film and UV cured film using a broadband UV lamp. [52]

Figure II.8 shows an example of ^{29}Si NMR spectra performed on porous samples deposited by PECVD using a porogen approach after different types of curing. Several papers have already discussed such spectra and have proposed peak assignations.[51,85,113,114,115] The band between –120 and –80 ppm corresponds to Si bonded to four O atoms (SiO_4 denoted as Q); the band between –75 and –40 ppm can be correlated to Si bonded to three O atoms (O_3–Si–R, denoted as T); the band between –25 and –5 ppm is due to Si bonded to two O atoms (O_2–Si–R_2, denoted as D) and the band between 5 and 15 ppm corresponds to Si bonded to only one O atom (O_1–Si–R_3, denoted as M). R is alkyl group. The number corresponds to the -O-Si bonds linked to the Si atoms. The same contributions are observed for all the studied porous films, the main differences being in the T and Q environments, which are linked to film cross-linking. The porous film skeleton is mainly constituted of an Si–O–Si bond network with CH_3 that are directly bounded to silicon and the main difference between all different porous OSG is the amount of terminal bonds (such as Si–CH_3, Si-H and Si-O-CxHy). The other difference comes from the diversity in the Si–O–Si bonding environment. For instance, depending of the deposition conditions, porous SiCOH films deposited using decamethylcyclopentasiloxane as the matrix precursor and cyclopentene oxide as porogen can present various structures such as D_2, M_1 and M_H, even after porogen removal.

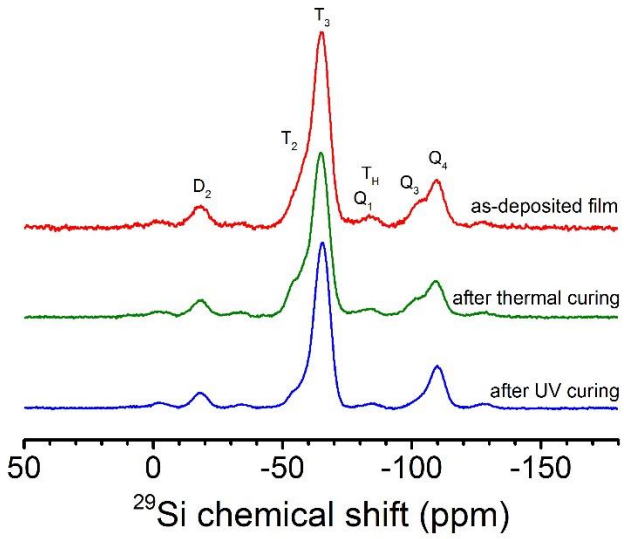

Figure II.8. ^{29}Si NMR spectra of different SiCOH thin films. The thermal treatment was performed at 450°C while the UV cure was performed at 400°C using a broadband UV lamp. The NMR spectrum of the hybrid film is shown for comparison.[52]

The final skeleton structure can be optimized depending on the post-treatment used to cure the film. Normally long curing time reduces concentration of M and D groups and the films is becoming more Q and T rich. These changes happen more intensively if short wavelength (λ<200 nm) is used and lead to significant improvement of Young's modulus. However, the cost of this improvement is normally loss of chemical resistance and deterioration of reliability.

II.2.3. Porogen residue.

The necessary step of porogen phase removal is fragmentation. Fragmentation forms small and more volatile compounds but some fragments might be nonvolatile and stay in the film. These residual impurities are known as porogen residues. The existence of porogen residues after curing was already reported quite long time ago, but their effects on the low-k properties have been studied only recently. Jousseaume et al. have highlighted the presence of C=C bonds in nuclear magnetic resonance spectra after e-beam or UV curing.[51] Gates et al. have also reported their formation after thermal curing.[116] Indeed, Figure II.7 shows the 13C NMR spectra of hybrid and porous SiCOH films. C=C and C=CH bonds

are observed in the spectra with a chemical shift corresponding to graphitic-like structures. Such structures could arise from the degradation of the porogen under energetic conditions in the plasma (during deposition), this signal being observed in the hybrid film and not in a matrix film. These contributions also remain present in the porous film, indicating that the curing treatment does not completely remove these structures. The hypothesis that porogen species can also be partially converted by UV light into nonvolatile graphitized-carbon residues is certainly possible. Although some progress has been made on porogen residues investigations, their detection remains uneasy. Indeed, their quantitative evaluation cannot be performed by Fourier transform infrared spectrometry because it has a limited sensitivity to amorphous carbon, such as C=C and C–C bonds. NMR is a powerful technique used to highlight the presence of residues but it remains costly and difficult to set.[115]

Marsik et al. developed a versatile method based on vacuum UV spectroscopic ellipsometry in order to estimate the amount of residues.[100] They have found that the optical properties of the low-k films between 2 and 9 eV are mostly sensitive to the presence of porogen and its removal during UV curing (Figure II.2). The figure emphasizes that the band at 4.5 eV (in the extinction coefficient curve) is due to a porogen residue: π–π* electronic transitions between the sp2 carbon orbital in the ultraviolet. A following of this band versus the UV curing time shows clearly that few porogens are still kept within the materials and do not disappear, even for long curing times. This carbon fraction could thus be considered as a porogen residue in the low-k material. The amount and the nature of residues are closely dependent on porogen chemistry and composition, deposition and curing conditions.

The porogen residues can seriously impact physical properties of porous thin film. For instance, Gourhant has shown that the presence of porogen residues leads to an increase of the electronic and dipolar contribution of the permittivity. Indeed, the porogen residues are carbon bonds containing graphitic-like phases (C=C–H). These structures hold a permanent dipolar moment and nonlocalized valence electrons. This would explain the negative effect of porogen residues on the electrical properties of porous SiCOH films. Moreover, these graphitic-like structures are more conductive than the SiCOH skeleton. Baklanov et al. have shown a clear correlation between 'porogen residues' and leakage current.[117] Moreover, the presence of porogen residues also impacts the elastic properties of porous SiCOH films. For instance, in the case of very high porogen loading (>60 %), the mechanical strength is lower than those simulated by the foam mechanical model.

In conclusion, the graphitic structures, which are detrimental from the electrical point of view, should also be avoided in order to have the optimal Young's modulus/porosity ratio. Some ideas to limit

the formation of porogen residues are reported in the literature. For instance, Gourhant has shown that a too-high deposition temperature is not appropriate because it favors the graphitic transformation of porogen, which becomes difficult to extract.[118] This leads to an incomplete porogen removal, even for a long curing time. Marsik et al. have also reported that a broadband lamp with $\lambda > 200$ nm is more suitable as it produces less residues.[100] Urbanowicz et al. reported a curing procedure of PECVD SiCOH thin films that allow to avoid the presence of porogen residues in the porous film.[70] They proposed to remove the organic porogen from the PECVD hybrid film before the UV-cure. The removal of the organic porogen was found to be possible by annealing of the low-k film in a H_2-based plasma, by using a remote H_2 plasma source combined with an ions/VUV filter to generate the hydrogen radicals. In such a way, bombardment of the deposited film with hydrogen ions is avoided and no significant damage to the ULK films (such as Si-CH_3 bonds scission) is observed. Material studies effectively confirm that this approach is more effective in the final removal of porogen than the direct UV cure of the as-deposited film. The only limiting factor for porogen removal is the limited penetration depth of the H radicals into porous low-k because of surface recombination. The effective depth of the porogen removal depends on the penetration depth of the active H radicals into the porous SiCOH matrix and it was found to be approximately 160 nm.

II.2.4. Change of structure and mechanical properties of OSG films after curing.

Figure II.9 shows an example of dielectric constant and thickness evolution versus the curing time. The k-value before curing (t=0) represents a double phase system including matrix and porogen. The porogen removal occurs on the primary steps of curing (often limited to 5 min for broadband UV) and leads to the formation of porous structure and reduces dielectric constant. This results in a fast increase of shrinkage (up to 12 % in this example), whereas the k-value falls from 2.7 to 2.4 after 5 min of curing. For short UV curing durations, although the bulk material is impacted by shrinkage (free volume loss), this effect is counter balanced by porogen removal (potential porosity creation), leading to a lower film density. The porosity created within the film increases continuously as a function of the UV curing time and the dielectric constant decreases with the UV curing time.

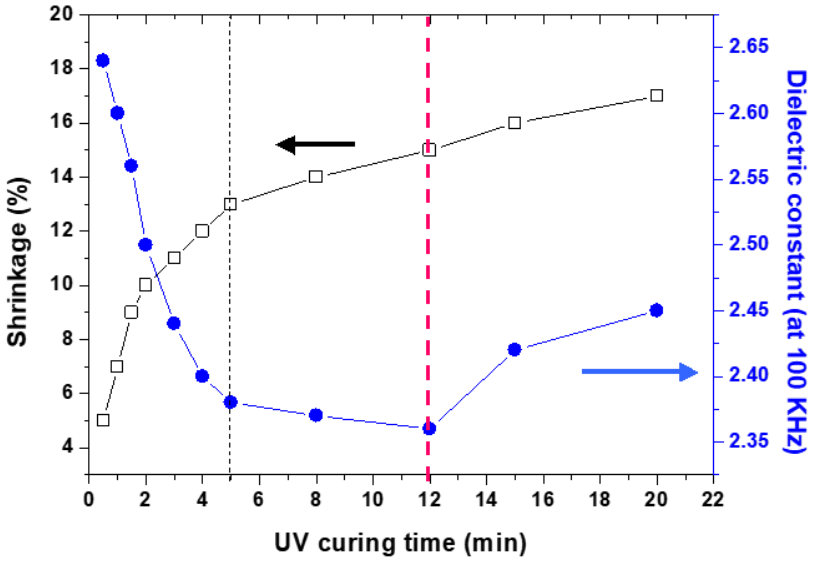

Figure II.9. Film shrinkage and dielectric constant as function of the UV curing time (broadband UV lamp) in case of PECVD SiCOH films.

Then, after 5 minutes curing, the k-value reaches the minimum value corresponding to nearly complete porogen removal and highest porosity. However, additional curing (at t > 12 min in this example) still leads to additional shrinkage. The k-value in this region slowly increases. For long UV curing duration, some remaining porogen that are embedded into the matrix and part of Si-CH_3 bonds are removed. As a result, the shrinkage that continue to increase, can be mainly related to matrix densification. After very long UV curing time (several hours using a broadband UV lamp at 385°C), SiCOH film can be completely converted into SiO_2-like films.[119] Usually, the film corresponding to the min k-value (12 min in Figure II.9) is considered as optimal. It should be noticed that the UV curing time have to be adapted depending on the film thickness and taking into account that physical parameters (such as k) do not necessary varies monotonously with the curing time. [110]

The introduction of porosity into the amorphous matrix induces also strong modifications of elastic properties of thin films. Figure II.10 shows variations of Young's modulus, evaluated by nanoindentation, versus the porosity for different cured films. As expected, a decrease of the elastic properties is observed as a function of the porosity. Several authors have shown that this behavior is compatible with a model typically used for foam [52,120,121] Indeed, classical foam mechanical models predict a linear relation between the modulus of porous materials and their square density, with the

assumption that the material skeleton remains unchanged. However, this model fails to explain the difference between mechanical properties observed on materials cured with different post-treatments, even though they have the same density (porosity).[120]

A typical example is presented in Figure II.10, which evidences that, at equivalent porosity, a thermal curing leads in general to porous films with weaker mechanical properties than those obtained for UV cured films. This result can only be explained by taking into account the chemical structure of the porous film.

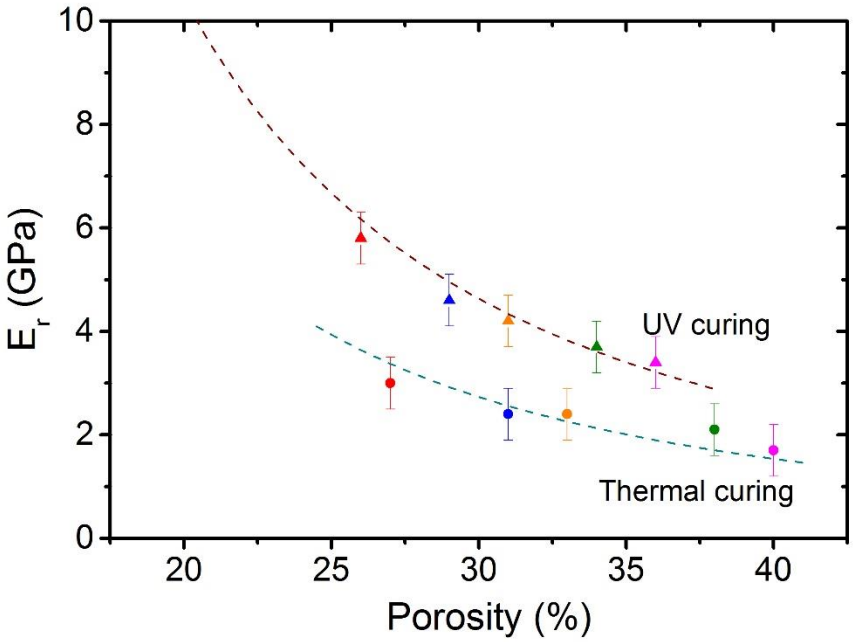

Figure II.10. Reduced modulus (Er) obtained by nanoindentation as a function of the porosity for SiCOH films deposited by PECVD from DEMS and NBD, after UV (at 400°C, using a broadband UV lamp) or thermal curing. [52]

II.2.5. Mechanism of matrix cross linking.

In OSG porous films, the Si–O–Si network constitutes the skeleton that sustains the structure of the film. Mechanical properties enhancement would be logically related to the Si–O–Si structure. Some works have claimed the ability of energetic radiation to improve the skeleton cross-linking, initiated by

silanol condensation.[122] The increase in the amount of Si–O–Si could result from a condensation reaction of two silanol group:

$$Si–OH + HO–Si \rightarrow Si–O–Si + H_2O \qquad (II.3)$$

Reaction (2) is thermally activated and needs enough Si–OH bonds to lead to a closeness of these groups, making the chemical reaction easier. This cross-linking mechanism results in a decrease of the distance between the two atoms of silicon, which leads finally to a film shrinkage. Thus, an aspect that has to be taken into account in the curing process is the deposition conditions and, more specifically, the hydroxyls content –OH. A low deposition temperature favors the appearance of Si–OH bonds into the films.[52,55] During curing, the condensation of abundant Si–OH results in Si–O–Si formation, as estimated by an increase of the FTIR signal. In this case, the mechanical properties can be enhanced thanks to a better cross-linking. At a high PECVD temperature (typically T > 250 °C), there is no evidence of the presence of a high amount of Si–OH in the film, meaning the absence of a significant condensation phenomenon. Reaction (2) does not allow an explanation of the improvement of the thin-film strength (and consequently of the mechanical properties), which is observed after UV curing of PECVD films.

Several works have dealt with the Si–O–Si cross-linking with UV in order to obtain a unified explanation of the UV photon effect and how they can improve the mechanical properties.[63,64 ,85,122] The main studies have maintained that broadband UV serves only as a breaking energy source that cannot be considered to favor any silanols condensation.[63] Indeed, a structural rearrangement of the existing silica bonds into a small-angle Si–O–Si configuration can be initiated by UV radiation at wavelengths above the silica absorption energy (Ed ~ 155 nm). In the UV broadband configuration, there is neither rearrangement occurring in the Si–O–Si network nor a condensation of silanols. Zenasni et al. have shown that, in the case of hybrid films with a low amount of silanols, the increase of the concentration of Si–O–Si bonds, is not due to the creation of new Si–O–Si bonds, but mainly involves a densification of the bulk structure under UV irradiation, leading to an enhancement of the Si-O-Si volume concentration. However, a careful study of the SiOSi band before and after curing in Figure II.6 shows a clear decrease in the peak area in all cases. This densification is at the origin of the enhancement of mechanical properties. When sufficient Si–OH is created, it can cross-link to form an Si–O–Si bond thanks to thermal activation. In this case, an appropriate UV wavelength can eventually compensate for the lack of Si–OH in the initial SiCOH structure. This is the reason why UV curing is efficient only when the wafer temperature is about 400-450°C. UV curing at low temperature normally leads to pore collapse because of not sufficient matrix cross-linkage. It is necessary to mention that room temperature curing was

recently proposed by using consecutive treatment by UV light with λ = 6.2 eV and VUV light with λ = 8.8 eV.[78] Porogen was removed during the first step while the second step provided the matrix cross-linkage. It was shown that this method allows improvement of dielectric properties. However, the lack of detailed analysis of chemical composition makes difficult discussion of precise mechanism. Special worry is related to possibility to keep sufficient concentration of terminal methyl groups that can be broken by VUV photons with energy 8.8 eV.

In the case of matrix precursor containing ethoxy groups, Gourhant et al. have proposed original mechanisms of condensation involving Si–O–C bonds.[52]:

$$Si–OCH_2CH_3 + Si\text{-}CH_3 \rightarrow Si–O–Si + C_xH_y \qquad (II.4)$$

This proposed transformation has a substantially smaller energy barrier and is exothermic.[107] Finally, other cross-linking mechanisms based on the reaction between $Si\text{-}CH_3$ have been also proposed but the presence of $Si–(CH_2)_n–Si$ bridges was never clearly evidenced experimentally in case of methyl terminated matrix.[52,113]

The difference in skeleton cross-linking observed with different deposition techniques or post-treatments can explain the differences of elastic properties. Ciaramella et al. have proposed a way to plot the elastic properties versus the volumetric concentration of Si–O–Si bonds in the film by FTIR ([Si–O–Si] = area of the Si–O–Si band/film thickness; see an example in Figure II.11).[120] A good correlation between the volume concentration of Si–O–Si bonds and the elastic properties is obtained. This result has been confirmed by different groups.[123,124,125,126]

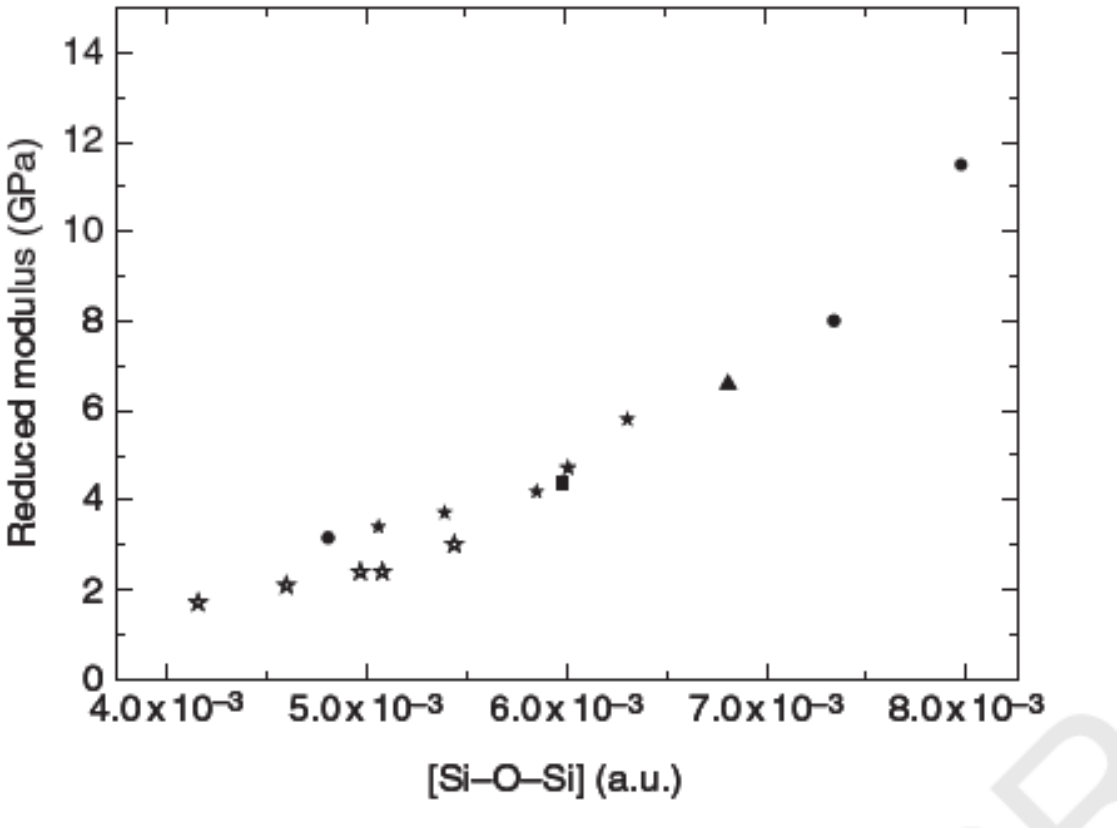

Figure II.11. Variation of the reduced modulus obtained by nanoindentation as a function of the volumetric concentration of Si–O–Si bonds (obtained from FTIR analyses) (from Ref[51,52,123])

The Si–O–Si concentration, which is related both to the film density and the skeleton chemical is the key parameter for the elastic properties of OSG thin films. Then, the enhanced of mechanical properties observed after UV curing is mainly due to a higher concentration of cross-links. Other approaches have also been proposed in order to better take into account the impact of the Si–O–Si bonding environment on the mechanical properties. The Si–O–Si FTIR band is usually decomposed into three peaks corresponding to different Si–O–Si angles.[127,125] Indeed, in fully relaxed stoichiometric thermal silicon oxides, the bonding angle is reported to be 144° with a FTIR absorption around 1080 cm $^{-1}$. For low-temperature stoichiometric silicon oxides, the FTIR stretching frequency decreases from 1080 to 1060 cm^{-1} as the Si–O–Si angle decreases. In SiCOH thin films, a first peak centered at 1135 cm^{-1} is attributed to larger angle Si–O–Si bonds in cage-like structures with a bond angle of approximately 150°.[127] The peak at 1063 cm^{-1} is assigned to the stretching of smaller angle Si–O–Si bonds in a network-like structure. A last peak close to 1023 cm^{-1} is assigned to stretching of a smaller Si–O–Si bond angle, such as might be encountered in a networked silicon suboxide. Based on this decomposition, Grill et al.

have observed that the elastic modulus increases while the mechanical stress decreases with increasing fraction of network oxide.[128] Other authors have also explained the increase of mechanical strength of porous SiCOH film after UV curing by the effect of Si–O–Si suboxide structures and the transformation of broken Si–O–Si cage-like bonds into a Si–O–Si network structure.[125] However, this approach is limited because it does not take into account the concentration of bonds which must be proportional to the elastic properties.

As discussed previously, Gourhant et al. have emphasized that, for hybrid OSG films deposited by PECVD from a matrix precursor containing ethoxy bonds, Si–O–C bonds could be at the origin of a large part of the reorganization observed in the Si–O–Si band.[52] They have suggested that the decrease at the shoulder centered at 1150 cm^{-1} in the FTIR spectra could be explained by the disappearance of Si–O–C bonds. During UV curing, the ethoxy bonds are removed and new Si–O–Si bonds are created which improves the elastic properties of the material.

The elastic properties improvement discussed here is observed both after UV curing using a broadband UV lamp and for single wavelength UV curing. However, a specific behavior is observed when a monochromatic bulb is used. Indeed, the absorption spectra of the material depend on the carbon concentration and type of porogen, and penetration depth of light decreases with decreasing wavelength.[129] This leads to a different depth dependence of the UV curing. For instance, studies using near monochromatic (172 nm) UV radiation, where the depth dependence is significantly higher, indicate UV light interference, which forms a standing wave during the curing process.[129,130,131] The standing waves generate corresponding oscillation of Young's modulus. In the case of a curing system with light of different wavelengths and with an appropriate design, such gradients are not observed. Formation of these gradients also affects the fracture energy, which is important for integration. For instance, it was shown that, while adhesive fracture energies at the top interface can be improved by 200 %, cohesive fracture energies and bottom adhesive fracture energies are improved at best by 20 %, which is clear suggestion of a depth dependence of the UV curing.[130,131]

II.2.6. Alkylene bridged OSG matrix.

Another possible improvement of OSG low-k materials consists in introducing Si–CH_2–Si bonds as replacement of some Si–O–Si bonds in the skeleton chemistry in order to improve the mechanical properties and decrease low-κ sensitivity to plasma induces damage.[132,133 ,134,135,136] Only few papers deals with the impact of UV cure on these Si-CH_x-Si bonds. Volksen reported first on the full crosslinking

of a spin-on oxycarbosilane backbone and the total removal of the porogen, which were obtained by exposing the hybrid film to UV irradiation (from a broad-spectrum lamp with significant intensity in the 200 to 250 nm wavelength range) at 400°C under nitrogen.[137] However, no data was reported about the methylene bridge stability under UV. More recently, Redzheb et al. have studied the UV-assisted thermal cure of spin-on oxycarbosilane films with k ≈ 2.3.[138] They studied the impact of UV wavelength on the material properties and concluded that: i) 254 nm photons do not possess enough energy to cleave C–C bonds; ii) the intensity of the 185 nm line which is one tenth of the overall intensity is too low to contribute significantly to the template removal, iii) On the other hand, 172 nm and 222 nm photons lead to nearly complete template removal for times as short as 1 min to 3 min, respectively. They emphasis that the methylene groups are not significantly affected by the high energy photons probably because they require higher excitation energy or the methyl groups protect them by preferentially absorbing the photons. Nevertheless, the methylene groups can be converted into methyl groups through a self-hydrophobization process which occurs in the presence of proximal Si-OH groups around 400 °C.

Recently, You et al have combined the use of alkylene-briged OSG matrix and optimized porogen removal treatment to perform porous SiCOH by PECVD.[139] They incorporate Si–CH_2–Si bonds in a SiCOH skeleton by adding a carbosilane precursors (containing methylene bonds) to the original precursor mixture (diethoxymethylsilane (DEMS) with bicycloheptadiene (BCHD)) used for the fabrication of the ULK dielectric by PECVD. Then, the as-deposited films were exposed to a remote plasma of 5% H_2 in He. Following the partial porogen removal by the hydrogen radicals, a UV curing process was used for the final crosslinking of the film. They show that the methylene groups are stable and not affected by the treatment with the H radicals but the impact of the UV cure on methylene bridges was not studied. As for more standard SiCOH film, the UV cure of the skeleton after the removal of porogen by the H radical treatment enables an improved crosslinking of the skeleton. As a result, in spite of an increase of porosity by the combination of H radicals with UV cure compared to solely UV cure, the elastic modulus remained essentially the same for the films of the different k values.

In parallel to these works on the porogen approach, several attempts were done for the realization of porous SiCOH thin films by PECVD using a single precursor. In all cases, a thermal treatment at high temperature is necessary to make the films porous. Recent works show that the UV cure of a “dense” SiCOH (without addition of porogens) can also induce porosity in the film. For instance, by UV curing an

octamethylcyclotetrasiloxane (OMCTS) films, Priyadarshini et al. have obtained a porous SiCOH film (porosity of 20%) with a dielectric constant as low as 2.4.[140] The porosity creation was supposed to be related to the removal of some CH_3 groups that act as template agent (like a porogen) and generate pores resulting in an increase in porosity. It is worth noting that in this case also, the use of UV cure allows to improve the mechanical properties of the films. Increasing UV cure time leads to an increase of the modulus of the film, and interpreted by an additional cross-linking that occurs during the curing process. In the case of OMCTS films, Grill also emphasizes the creation of bridging skeleton Si-CH_2-Si bonds due to the removal of -CH_3 and the cross-linking between the remaining Si and Si-CH_2- bonds (due to the removing H from some -CH_3 groups). However, over-cure can result in losing too many Si-Me bonds, thereby resulting in film collapse and higher k value.

Finally, a UV curing process was also used as foaming treatment in order to perform highly porous SiCOH thin films without the use of porogens.[141] In this case, SiCOH deposited by PECVD (without any porogens) was intentionally covered by a dense crust (a very thin SiO_2 film). The porosity generation was obtained through a UV cure (at 400°C) of the stack. This treatment allows to remove some methyl bonds from the skeleton but, contrary to the previous cases, the film thickness increases. This film expansion is at the origin of the creation of porosity. In this approach, it is supposed that a gas resulting from the methyl depletion under UV is trapped in the SiCOH layer due to the presence of the SiO_2 crust, and act as a foaming agent. This concept, which use the properties of the UV cure to remove -CH_3 bonds, allows to obtained highly porous SiCOH thin films (open porosity > 65% are reported).

III. VUV effects during the plasma processing

III.1. Impact of UV/VUV and EUV photons on damage of low-k dielectrics

The first law of photochemistry claims that light has to be adsorbed in order to cause a photochemical reaction. OSG films are SiO_2-based and naturally reproduce features of SiO_2 absorption. Characteristic absorption spectra of crystalline SiO_2, UV-grade amorphous quartz glass and PECVD low-k OSG material of ~30% porosity is shown in Figure III.1. Structural disorder of atoms in amorphous phase leads to red shirt of absorption edge due to appearance of defect states in band gap. Amorphous SiO2 has absorption edge near 8-8.5 eV (150 nm) that can be shifted to lower energy if silica matrix has certain degree of physical disorder.[92,93,94,142] It can be related to high temperature, introduction of some defects and impurities like vacancies, SiOH, organic groups, etc. Strong absorption of OSG below 170 nm reproduces general feature of all silica-based materials and corresponds to absorption of O-Si-O matrix. Above 170 nm absorption is mostly caused by porogen itself and porogen residues. Therefore,

absorption spectrum of OSG low-k films above 170 nm is ultimately related to technology of their fabrication, first of all, curing technology which provides removal of porogen and creation of open pores.

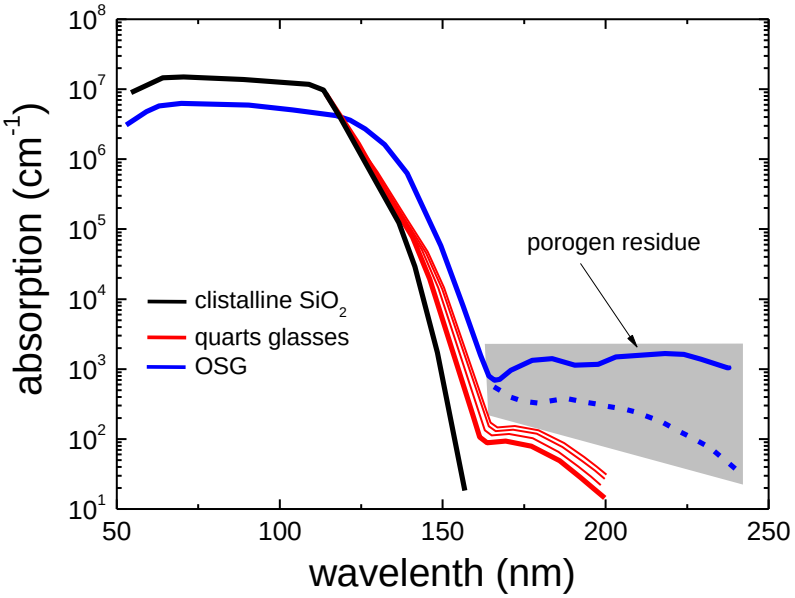

Figure III.1. Characteristic VUV absorption spectra of crystalline SiO2, UV-grade amorphous quarts glass [92,93,94,142] and OSG low-k material. OSG spectrum was estimated from data of [100,104,102,109,101].

UV curing often leaves some porogen residuals containing carbon rich species and even amorphous carbon in -sp and sp2 states. According to ref.[70], H_2 afterglow (AFT) plasma can be used for efficient removal of porogen residuals. The H_2-AFT treatment was performed before UV curing at the wafer temperature of 280 °C using 350 s of the He/H_2 20:1 downstream microwave plasma. The effect of UV-radiation from plasma area was avoided by a special design of the chamber. The following UV-curing was performed in a separate chamber in nitrogen ambient at temperature close to 430 °C by using excimer Xe lamp (172 nm) and broadband UV source with the wavelengths higher than 200 nm. It was shown that porogen removal by H_2-AFT treatment allows to obtain porogen residue low-k films. The obtained films demonstrate improved high Young's Modulus 5 - 9.5 GPa for open porosity in the range of 41%–46% with k-value of 1.8–2.6. Extinction coefficient of low-k films for photon below ~7 eV (above ~180 nm) becomes similar to PECVD silica material or spin-on deposited nanoclustered silica. Nevertheless, some absorption of the matrix is still observed at the lower photon energies up to 4-5 eV. It indicates presence of some defect states in the matrix itself.

In ref.[143] the band gap (Eg) and energy position of sub-gap defect states for both non-porous and porous low dielectric constant (low-k) materials were measured by using the reflection electron energy

loss spectroscopy (REELS). REELS measurements on a porous low-k OSG with k=2.3 conformed a smaller band gap (Eg=7.8 eV) for O-Si-O matrix and a broad distribution of defect states ranging from 2 to 6 eV. These defect states were attributed to a combination of both oxygen vacancies created by the UV curing process and carbon residues left in the film due to incomplete removal of the sacrificial porogen. Similar to ref.[70] it was shown that plasma ash can remove the defect states attributed to carbon residues, but the oxygen vacancy defects remained.

Effect of VUV photons depends also on the way of relaxation of the excitation arising after the photon absorption. Obviously, the higher photon energy, the more relaxation ways are available. One of the ways is generation of charged pairs in OSG bulk (matrix) with producing charged defects like E' color centers.[99] Another way is chemical modification of surface bonds leading to changes of different parameters of OSG low-k films such as, for example, reactivity[144] and dielectric permittivity.[145] Therefore, in addition to absorption coefficients, such parameter as effective quantum yield characterizing probability of photon energy realization in the separate channels of chemical modification is also important. Moreover, degree of VUV impact depends also on photon fluence, i.e. both photon flux and exposure time. Low fluences lead mostly to generation of some charge-related defects in OSG bulk with minimal chemical modification. The higher fluences can cause significant chemical modifications (such as removal and change in CHx bonds covering the pore surface). Further increase of VUV photon fluence can lead to physical transformations (such as reconstruction of surface bonds causing big stresses etc.) up to complete film damage and even cracking.

The impact of EUV and VUV emissions on the chemical modifications of various low-k films have been studied Rakhimova et al.[102,109] by using VUV sources with fixed wavelengths of 13.5 nm, 58 nm, 106 nm, 147 nm and 193 nm and by Choudhury et al.[101] by using the synchrotron VUV radiation with photon energies ranging from 7 to 21 eV (≈ 60-175 nm). In the papers[102,109] the degree of damage versus photon fluences were studied for few OSG low-k films with different porosity and different pore radius. The films characteristics are presented in Table II.2.

TABLE II.2. Characteristics of investigated OSG materials.

Sample	**CVD1**	**CVD3**	**NCS**	**ALK B**	**OP_B**	**SBA 2.2**	**SBA 2.0**	**SBA 1.8**
Type	PECVD	PECVD	Spin-on	PECVD	Organics	Spin-on	Spin-on	Spin-on
Porosity (%)	24	28	35	46	17	40	44	51
Pore radius (nm):	0.8	0.75	1	1.5	0.59	2.1	2.1	2.7
Thickness (nm)	500	185	200	105	205	218	217	214
k-value	2.5	2.3	2.2	2.1	2.3	2.2	2.0	1.8

The research was focused on chemical modification of OSG low-k films due to -CH_3-groups depletion as a function of VUV/EUV photon fluencies. In addition, the depth profiles of C/O ratio were measured by

secondary ion mass spectroscopy (SIMS) and the depth profiles of C, O and Si atoms fractions were measured by Rutherford backscattering spectroscopy (RBS) method. This study allowed estimating penetration depth of photons and correspondingly absorption coefficients for each wavelength and to correlate it with the fraction of the removed -CH_3 and thereby to determine the effective quantum yield. The example of evolution of the -CH_3 depletion with photon fluence at different wavelength is shown in Figure III.2. It can be seen that OSG damage correlates with the photon penetration depth, which can be estimated from saturation by knowing the film thickness. The minimal penetration depth is observed for photons with energies ~21.2 eV (58 nm) and ~11.5 eV (106 nm) that agrees well with the measurements with synchrotron radiation.[101]

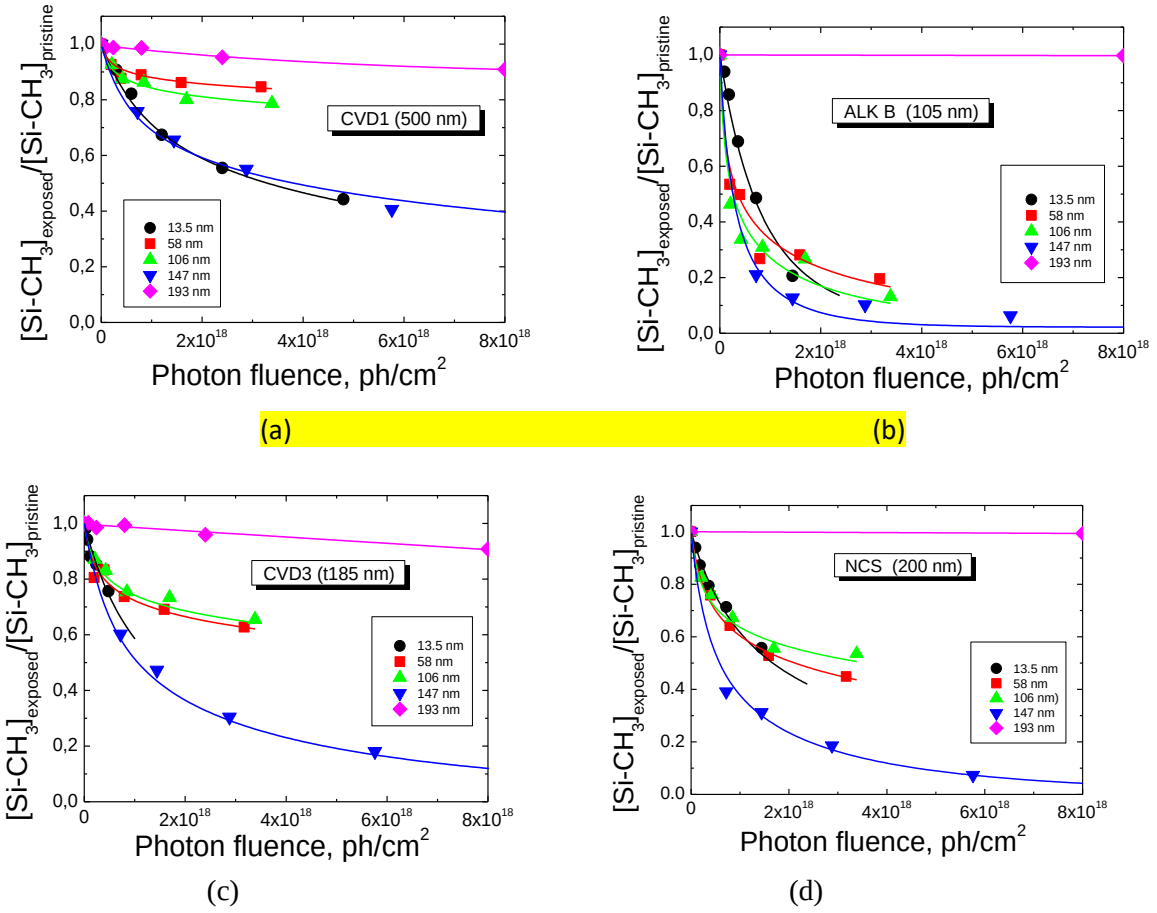

Figure III.2. The fraction of Si-CH_3 bonds remaining after the OSG films exposure to VUV radiation at different wavelengths as a function of the photon fluence: (a) - CVD1, (b) - ALK B, (c) - CVD3, (d) - NCS. Symbols – experimental data, solid lines are model results. The solid line for 193 nm is a fit of the experimental data. Photon fluxes: at 193 nm – 8.10^{15} ph/(cm^2pulse, 20Hz); at 147 nm - $1.6.10^{15}$ ph/(cm^2s); at 106 nm - $4.7.10^{14}$ ph/(cm^2s), at 58 nm -$4.4.10^{14}$ph/(cm^2s), at 13.5 nm – 5.10^{12}ph/(cm^2pulse, 900-1600 Hz)

In the paper [102], the 1D semi-analytical model of photons absorption and OSG film damage (Si–CH_3 bond break) was developed on the base of photo-induced dissociation mechanism similar to [102,109]. The 1D (in the depth direction) model includes photoabsorption by SiO_x and O_xSi-CH_3 complexes (with the same wavelength dependent cross-section $\sigma_{PA}(\lambda)$ for the both ones) and CH_3 group elimination as a result of photo-induced dissociation of the electronically excited $(O_xSi\text{-}CH_3)^*$ complex produced after the photon absorption:

$$O_xSiCH_3 + h\nu \rightarrow (O_xSiCH_3)^* \rightarrow SiO_x + CH_3 \qquad \text{(III.1)}$$

Si-CH_3 bond break was treated in the model as a photodissociation process with cross-section $\sigma_{SiCH3}(\lambda)=\sigma_{PA}(\lambda)$ x $\varphi(\lambda)$, where effective photodissociation quantum yield $0\leq\varphi(\lambda)\leq1$ includes the efficiency of CH_3 escaping from the porous film with a possible re-attachment of -CH_3 radical back to dangling -Si bond. Absorption of EUV emission at 13.5 nm was considered in the same manner as VUV, but EUV photons absorption mechanism can be more complex involving additional channels such as ionizations, excitations and secondary effects of hot photoelectrons.

The described above approach was realized with the appropriate model equations for radiation flux (intensity) I(z) (photons/(cm^2s)) inside the OSG film (0<z<L) and the dynamics of Si-CH_3 depletion with exposure time t and depth z inside the film:

$$dI(z)/dz = -\sigma_{PA}\cdot[Si]xI(z) \qquad \text{(III.2)}$$

$$d[CH_3](t,z)/dt = -I(z)\cdot\sigma_{PA}\cdot\varphi\cdot[CH_3](t,z) \qquad \text{(III.3)}$$

Here z=0 corresponds to the surface of OSG film of thickness L, $I_0=I(z=0)$ is radiation intensity on the sample surface, $[CH_3]$ (in cm^{-3}) is a concentration of Si-CH_3 groups. The model equations (III.2, III.3) can be integrated analytically to obtain the depth profiles of radiation intensity and CH_3 concentration:

$$I(z) = I_0\exp(-\sigma_{PA}\cdot[Si]\cdot z) \qquad \text{(III.4)}$$

$$[CH_3(t,z)] = [CH_3]_0\exp(-t\cdot\sigma_{PA}\cdot\varphi\cdot I_0\cdot\exp(-\sigma_{PA}\cdot[Si]\cdot z)) \qquad \text{(III.5)}$$

Here $[CH_3]_0=[CH_3(t=0)]$ is an initial concentration of Si-CH_3 groups in a pristine film. Column density $\{CH_3(t)\}$ of Si-CH_3 groups was calculated as integral $\{CH3(t)\}=\int[CH3(t,z)]dz$ over film thickness and could be directly compared with the experimentally measured behavior of $\{CH_3(t)\}$. The calculated evolution of Si-CH_3 bonds in OSG films at exposures to various VUV wavelengths are shown by solid lines in Figure III.2. The developed 1D model was capable to describe numerous experimental data for different photon fluences and wavelengths using only two fundamental parameters $\sigma_{PA}(\lambda)$ and $\varphi(\lambda)$ for each OSG film. The obtained photoabsorption cross-sections σ_{PA} and effective quantum yield of Si-CH_3

photodissociation process $\varphi=\sigma SiCH_3/\sigma_{PA}$ for studied OSG films are shown in Figure III.3a and Figure III.3b respectively. Recent measurements of σ_{PA} in the range 140-160 nm together with normalized σ_{PA} from penetration depth measurements in ref. [101] by synchrotron VUV radiation are also shown. The agreement between different studies is quite satisfactory indicating that matrix absorption-excitation-relaxation mechanism is the main source of OSG damage at VUV photon impact.

Lee and Graves[146,147] also developed a one-dimensional (1D) model to predict the -CH_3 removal from OSG low-k films by various VUV radiation (Xe lamp, Ar and O_2 plasma). This 1D model assumes that the total absorption coefficient is determined by the absorption of Si–C and Si–O bonds. For the 147 nm VUV emission they have approximated the measured Si–CH_3 depletion by photodissociation cross-section $\sigma_{SiC} = 8.8\times10^{-18}$ cm^2 with the dominated PA of Si–C bonds $\alpha_{SiO}<<\alpha_{SiC} = 3.6\times10^5$ cm^{-1}.[146]

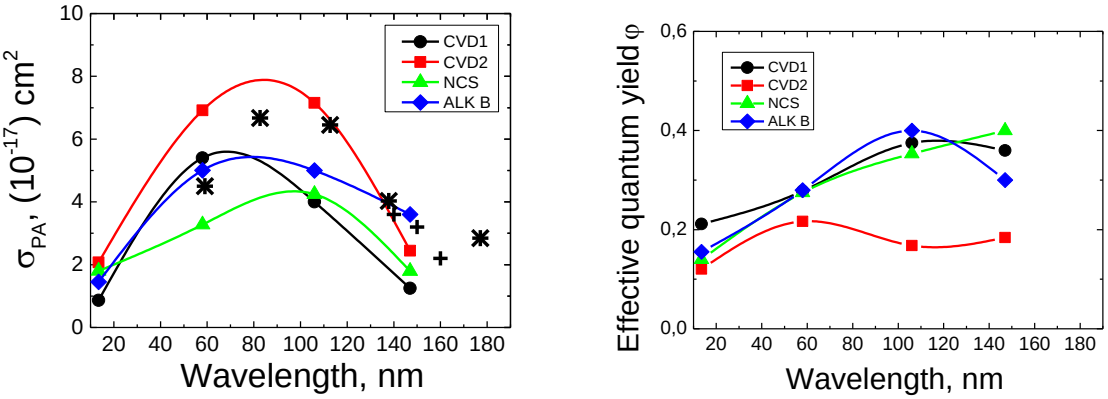

(a) (b)

Figure III.3. (a) - photoabsorption cross-sections (symbols – data of [102], stars – data of [101], crosses – data of [148]) and (b) - effective quantum yield of Si-CH_3 photodissociation for various radiation wavelengths and different OSG films.[102]

Thus, due to higher absorption coefficient at ~50–130 nm, the VUV emission in this range causes most intensive Si–CH_3 depletion in the top part of the OSG films. At the same time, the penetration of this emission is limited and OSG damage in depth occurs at the other wavelengths where PA cross-section is lower. So, the deepest strong damage is observed for 147 nm light when penetration depth corresponds to the film thickness [102,146,149]. As it was shown in [102] for CVD1 films, the penetration depth z_{pp} (if to define z_{pp} by the depth where 95% of initial emission intensity I_0 is absorbed, $I(z>z_1)<0.05<I_0$) is only 50–75 nm for the range 50–120 nm whereas 147 and 13.5 nm emissions can penetrate deeper up to z_{pp}~150-200 nm. Figure III.4 presents example of model evolution of [Si–CH_3](z,t) density profiles in CVD1 (24%

porosity, k=2.5) film with exposure time t for VUV emission at 147 nm (figure III.4a) and 58 nm (figure III.4b). Due to lower absorption the 147 nm emission provides more extensive Si–CH_3 depletion in the film depth in contrast to the 58 nm emission. EUV photons absorption mechanism is more complex involving various channels, (ionizations, excitations and secondary effects of hot photoelectrons) and therefore resulting in decreasing effective quantum yield of Si-CH_3 photodissociation with transfer from VUV to EUV range (Figure III.3b). The typical fluences in EUV lithography are lower by orders of magnitude than the fluences required to introduce strong chemical OSG damage. At the same time some OSG degradation due to charge and field induced defects is possible.

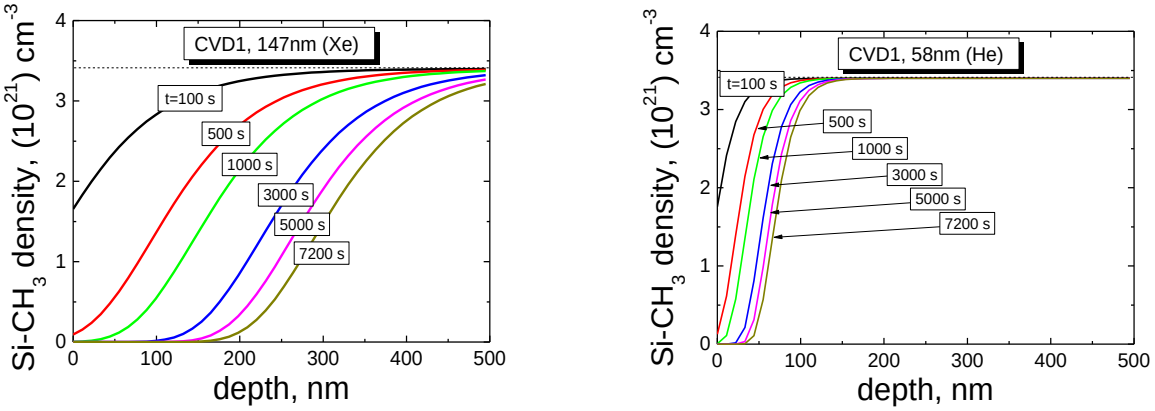

(a) (b)

Figure III.4. Evolution of [Si–CH_3](z,t) density profiles in CVD1 (24% porosity, k=2.5) film with exposure time t for VUV emission at (a) 147 nm and (c) 58 nm.[102] Photon flux at 147 nm is $1.6x10^{15}$ph/(cm^2s)

The similar level of photon-penetration depths (z_{pp}~60-96 nm for photons wavelengths λ~59-138 nm and very low photoabsorption and Si-CH_3 depletion for λ>175 nm) for low-k films recently measured in [101]. 120-nm thick SiCOH films were exposed to synchrotron VUV radiation with energies ranging from 7 to 21 eV, and the electron-density depth profile of the VUV-irradiated films was extracted from the fitting of the X-ray reflectivity experimental data. Between 7 and 11 eV, the depth of the damaged layer decreases sharply from 110 nm to 60 nm and then gradually increases to 85 nm at 21 eV. It was found that the highest photoabsorption occurs between 11 and 15 eV which is the most damaging spectral region for thin 120-nm SiCOH films (when the photon penetration depth and correspondingly the damage depth appear to be correlated with the film thickness). The most damaging region for thicker films will be shifted to lower energy photons e.g. 9-10 eV as it was observed in [102].

To meet ULSI technologies interconnects requirements for advanced technology nodes, new generations of low-k materials with the k-value smaller than 2.3 (porosity up to 45–55%) might be required. In this respect the study of impact of various VUV emissions on ULK films with increasing porosities is of importance. The most correct study of the porosity effects is possible only for ULK films of the same (or similar) chemical composition. Such an experimental and theoretical study was carried out in ref. [102] and also in ref. [101]. In ref. [102] it was done for spin-on films SBA2.2 (k=2.2, porosity=39%), SBA2.0 (k=2.0, 44%), SBA1.8 (k=1.8, 51%). The measured and model evolutions of Si–CH_3 depletions in these films under 58.4 nm, 106 nm and 147 nm VUV radiations are shown in Figures III.5a, III.5b and III.5c, respectively. The degree of Si–CH_3 depletion in SBA films increases with increasing porosity for each VUV wavelength. The obtained PA cross-sections for SBA1.8 and SBA2.0 films are the same (σ_{PA}/(10-17 cm^2) = 3.75, 2.5 and 2.1 for 58.4 nm, 106 nm and 147 nm, respectively) and agrees very well with cross-section for other OSG films. But the effective quantum yield of Si–CH_3 photodissociation increases with porosity especially it happens for the highest porosity films when porosity reaches a certain critical level > 45-47 % as it is shown in Figure III.5. The same trend in the change of damage depth with porosity was also demonstrated in[101] during the experiments with synchrotron VUV radiation. So, the damage depth increases with increasing porosity to 42%.

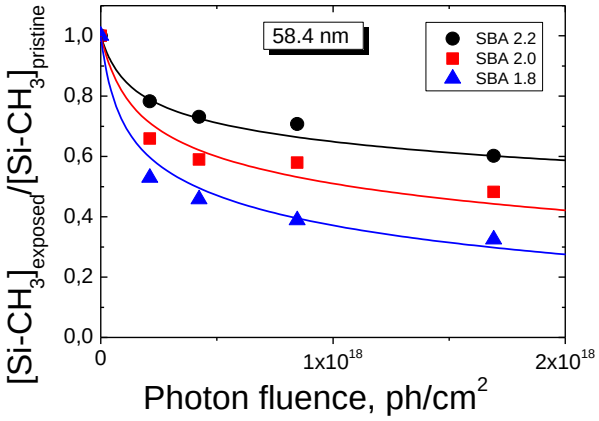

(a)

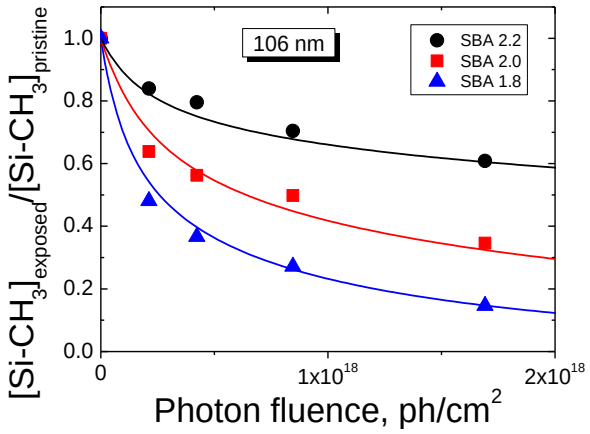

(b)

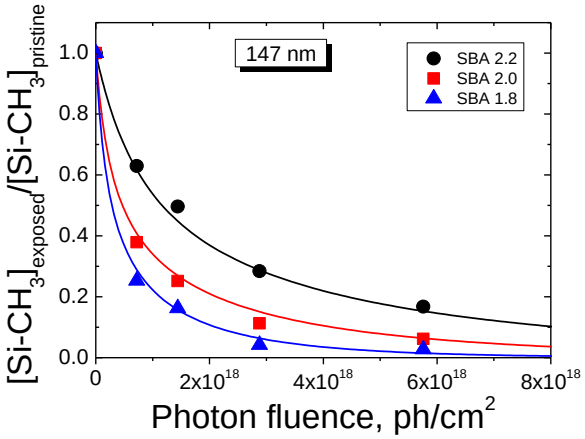

(c)

Figure III.5. The evolution of Si–CH_3 depletion in SBA 2.2, SBA 2.0, and SBA 1.8 films after exposing them to the different photon fluences at wavelengths of 58.4 nm (a), 106 nm (b) and 147 nm (c). Symbols represent experimental data, solid lines are the modeling results[102].

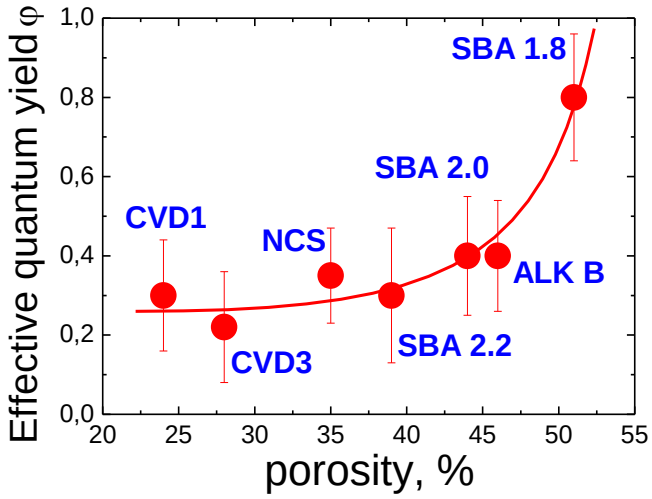

FIG III.6. The effective quantum yield for -CH_3 removal at VUV photon impact (in a range 58 nm-147 nm) on OSG films of different porosity[102].

Thus, VUV photons impact is fully determined by absorption spectrum since energy of absorbed photon can be enough effectively realized in dissociation of surface Si-CH_3 groups. At the same time degree of the impact is also limited by the absorption or the penetration depth of VUV photons. The penetration depth for the different wavelengths estimated by different diagnostics (XRR[101], SIMS[102], RBS[102] and XPS with depth profiling[150]) is shown in Figure III.7. It is clear that VUV damage for radiation in the range 70-120 nm was concentrated on OSG film top even at powerful VUV impact. Radiation of more soft VUV photons can penetrate deeper on the whole depth and cause strong damage in case of the high-intensity VUV emission of during long exposures. Thus, to minimize damage it is necessary to take into account both intensity and spectrum of VUV radiation.

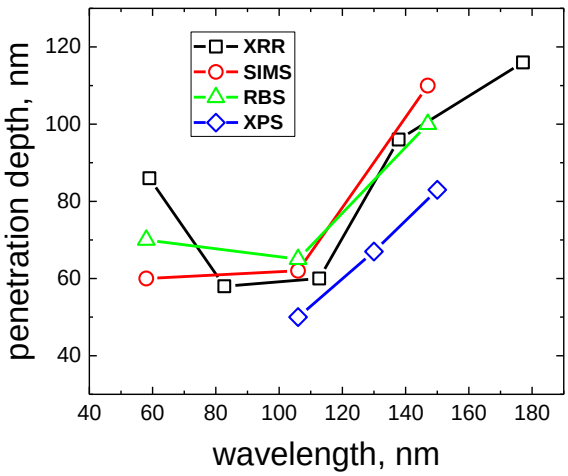

Figure III.7. The penetration depth of VUV photons in porous OSG low-k measured by XRR (X-ray reflectivity)[101], SIMS[102], RBS[102] and XPS with depth profiling[150]. The XPS data was recalculated for the 40%-porosity film.

III.2. VUV/UV radiation in low-k plasma processing

During the integration, low-k films are exposed to plasma in numerous processing steps that all are potentially damaging: e.g. plasma enhanced chemical vapor deposition of dielectric and metal barriers; plasma patterning (anisotropic etch, photoresist strip and surface cleaning); surface treatment (CuO_x reduction and surface functionalization for the adhesion improvement). Plasma damage can be caused by ions bombardment, penetration of radicals and VUV photons emitted during processing.[112] Typical plasma interaction with low-k films results in the films hydrophilization (by removal of methyl group) and/or densification. Such damage can be expanded into the depth of low-k films in dependence on radical's reactivity and fluence. Therefore, a quantitative description of the radical penetration into SiOH films is of importance.

The densification is mainly caused by ion-assisted, VUV-light assisted or chemical assisted cross-linking. Besides densification ion bombardment performs a physical sputtering and stimulates various ion-assisted processes (including hydrophilization, etching) due to the generation of more active sites on the films surface. The damage depth during the low-k interaction with ions depends on ion flux and ion energy and restricted by top layer within 5-10 nm. As a rule, the densification and hydrophilization of low-k films occur at the same time. Most of studies were focused on plasma damage by ion-assisted (ion-induced etching, sputtering, densification) processes to reveal the source of damage under typical plasma conditions[151,152,153,154,155,156,157]. Furthermore, these studies are focused mainly on the role of ion-radical dualism in the film damage[158,159]. However, VUV/UV radiation also can produce different modifications of low-k dielectric, caused by chemical bond dissociation (including CH_3 group removal), or accumulation of trapped charges, caused by electronic excitations. Moreover, VUV radiation with energy higher than 7 eV can generate numerous competing phenomena: photoemission, photoconduction, population or depopulation of electrons from trap states, and photoinjection [160]. The depth of low-k damage by VUV radiation is determined by the wavelength-dependent penetration depth of VUV photons (Figure III.7).

Low-pressure plasmas used in different processing steps produce also a significant vacuum-ultraviolet or ultraviolet (VUV/UV) photon fluxes. VUV radiation is originated primarily via electron impact excitation of neutral atoms and molecules. This radiation can produce damage of low-k materials[145,158,161], or charged species on the surfaces [99], in microelectronics processing. To reduce low-k

films damage it is important to control VUV photons fluxes in modern ultra-large-scale integration (ULSI) technology [162].

The ion and radical modification can be partially controlled by optimized plasma chemistry and plasma reactors. But it is more difficult to control the damage induced by photons because the plasma species can radiate over a wide spectral range. And relative intensities in different spectral ranges are noticeably varied in dependence on the discharge type, input power, gas composition and pressure. The effects of UV radiation on low-k materials have been extensively studied when UV light has been used for the curing of OSG materials [33]. It was revealed that photons with wavelength shorter than 190 nm damage OSG low-k films. In technological processing, low-k films are exposed to various plasmas during the patterning and photoresist removal, barriers deposition, cleaning etc. Along with ions and radicals ultraviolet (UV) and vacuum ultraviolet (VUV) photons are generated in these plasmas. High energy (>7 eV) photons of VUV-EUV range (solely or in combination with active particles) could induce different modifications and damage of low-k materials e.g. reduction of CH_3 groups, generation of trapped charges etc. A fundamental understanding of the damage mechanisms as well as the study of separate contributions (into films degradation) of active particles and photons and their possible synergetic effects are needed in order to reduce the plasma damage.

The following three main types of plasma reactors are used in plasma processing: inductively coupled plasma (ICP with or without bias), single and dual-frequency driven capacitively coupled plasmas (SF CCP, DF CCP) and remote (or downstream plasma, DSP). In the downstream chamber, the plasma region is separated from the wafer area by special grids that neutralize the effect of ions and, partially VUV radiation from the plasma (see for details[112]). In ICP sources, plasma density (typically of ~10^{11}-10^{12} cm^{-3}), electron temperature (T_e) and VUV radiation are higher than plasma density (~10^9-$5 \cdot 10^{10}$ cm^{-3}), T_e and VUV radiation in CCP plasma. Titus et al.[163] have demonstrated that, in general, the VUV flux in argon ICP plasma is approximately one-half of the ion flux. Schematic representation of plasma density and VUV/UV radiation in the different plasma reactors is shown in Figure III.8.

Figure III.8. The red-yellow bar indicates qualitatively the difference in plasma density and VUV/UV radiation interacting with the wafer in three plasma reactors.

Separate control of plasma density and ions energy can be performed in both ICP (with bias) and dual frequency CCP plasmas. The pulsed ICP[164,165] or CCP[166,167] sources provide additional chemistry tuning due to their ability to decrease the average ion energy down to the few eV range during the afterglow period. Besides, pulsed ICP plasmas were suggested by Y. Ichihashi et al.[168] and by Tian and Kushner[169] for VUV emission control.

ICP plasma in O_2/Ar and H_2/(Ar or He) mixtures was used for evaluation of damage mechanisms in strip plasma and for low-k pretreatment in order to generate silanol groups on the hydrophobic pristine surface for deposition of self-assembled monolayers for pore sealing and barrier deposition [170]. Also Cu surface cleaning after CMP (Cu oxide reduction) sometimes are carried out by N_2/H_2 or NH_3/H_2 plasmas that could damage the top surface of the dielectric[171] . Liu et al.[172] also used ICP N_2/H_2 plasma for plasma treatment of interlayer dielectric (ILD) and chemical mechanical polished (CMP) Cu surfaces for two ILD films with different porosities and carbon concentrations and two samples temperatures (380ºC and room temperature). It was obtained that initial N_2 plasma treatment protects the low-k ILD layer by forming a densified surface which provides minimal degradation of the dielectric properties of the films at further treatment in H-containing plasma. The elevated temperature of samples enhances the stability of the low-k ILD layer by inhibiting the formation of polar Si-OH structures and retains the low-k properties in contrast to room temperature processes.

In the DSP reactors, the plasma region is usually separated from the processing region. Charge neutralization is realized due to a grid between the plasma and the substrate. Photon flux can be minimized by special methods. As a result, low-k damage is produced by active radicals mostly. For this reason, DSP reactors could be used for isotropic processes (photoresist stripping or dry cleaning) only. In DSP reactors high substrate temperature (250°C-350°C) is needed to provide acceptably high resist removal rate. H_2 or mixtures of H_2 with noble gases (He and Ar) are usually used. Besides the effects of N_2 addition to H_2-based plasma and pure NH_3 plasma are studied al well[173,174,175]. Thus DSP reactors in H_2, H_2/N_2 gases (and their mixtures with Ar and He) are used in strip processing usually. ICP plasma without bias (steady state or pulsed) in O_2, H_2, H_2/N_2 gases (and their mixtures with Ar and He) is used for surface functionalization, pore sealing, barrier deposition and damage mechanisms studies in strip plasma. Low-k damage is mainly determined by radicals and VUV radiation in these plasmas.

In CCP reactors, the top electrode is usually made from Si, which captures free fluorine from the plasma and increases the C/F ratio. This effect and the presence of high energy molecular CxFy radicals together with high ion energy allow etching of materials with high bond energy (similar to Si-O bond energy) with high etching rate and good selectivity. Therefore, CCP reactors are usually used for anisotropic low-k etch in fluorocarbon-based plasmas with Ar dilution. ICP reactors with fluorine-based

plasmas are used for cryogenic etching of low-k materials[176,177,178,179,180,181,182]. The damage of SiOH films by VUV radiation appears to be critical during the patterning in fluorocarbon-based plasma, when the sidewalls are damaged due to the long exposures to VUV photons and radicals.

So, VUV/UV damage of SiOH films in strip, cleaning and treatment plasmas is originated from VUV radiation in O_2, H_2, H_2/N_2 plasmas (and their mixtures with Ar and He) and from VUV/UV emission of fluorocarbon plasma diluted by Ar. For this reason, we will focus on possible mechanisms of VUV/UV induced processes in these plasmas without detail reference to concrete technological process. As was mentioned above, the damage depth due to radicals is determined by their reactivity, flux and exposition time. And the damage depth by photons depends on wavelength of radiation, extinction coefficient, VUV fluxes and exposition time. The study of combined effect of photons and radicals (photo-induced processes) is a complex task. This effect can be appeared both in new active sites and new reaction channels generation and not studied carefully yet. The effects of VUV fluxes on low-k material and their synergistic effects with radicals VUV fluxes should be measured and calibrated. Compared to the pure gases, various processes could change the respective photon fluxes in the mixtures.

VUV plasma emission is measured by spectrometers that have to operate under vacuum to avoid absorption by ambient gas. To provide relative calibrations of various VUV spectrometer the calibrated light sources with known spectra should be used, e.g. a windowless, rf-excited discharge lamp, a microwave-excited mercury lamp[95] or synchrotron radiation [183]. H_2 discharge spectra can be also used for calibration [184]. Absolute calibration of VUV spectrometer can be performed by using absolutely calibrated detector[95] or by detecting of UV–induced sodium salicylate photoluminescence-broad emission at ~ 420 nm previously calibrated by UV–source with known intensity[185,186]. Absolute fluxes of radiation from resonance lines of Ar (104.8 and 106.7 nm) in ICP plasma were measured in [102,163] and from resonance line of He (58.4 nm). Lee and Graves[146] have measured absolute VUV fluxes from resonance line of atomic O (130 nm) both in pure O_2 and O_2/Ar ICP plasmas used for low-k films treatment (Table III.1).

TABLE III.1. ICP conditions used for exposures of porous-ULK films[146]

Plasma species	Pressure (mT)	Power (W)	VUV flux (104 nm) ($\times 10^{15}$ cm^{-2} s^{-1})	VUV flux (106 nm) ($\times 10^{15}$ cm^{-2} s^{-1})	VUV flux (130 nm) ($\times 10^{15}$ cm^{-2} s^{-1})	Total ion flux ($\times 10^{15}$ cm^{-2} s^{-1})
Ar	10	70	1.07 ± 0.35	2.00 ± 0.14	0	5.41 ± 0.05
Ar/O_2(10%)	10	70	0.74 ± 0.03	1.37 ± 0.07	0.22 ± 0.01	3.87 ± 0.03
Ar/O_2(25%)	10	70	0.58 ± 0.02	1.01 ± 0.04	0.35 ± 0.01	3.57 ± 0.02
Ar/O_2 (50%)	10	70	0.34 ± 0.01	0.49 ± 0.02	0.37 ± 0.01	3.00 ± 0.01
O_2	10	150	0	0	1.11 ± 0.01	5.12 ± 0.01

Fantz et al.[187] have performed comprehensive study on calibrated spectroscopic measurements in ICP plasma in various H_2/N_2 mixtures at the wavelength range of 117 – 800 nm. It was shown that hydrogen

VUV/UV radiation is due to atomic radiation (the Lyman line Lα (121.5 nm)) and radiation of molecular hydrogen: the Lyman (130–170 nm, maximum ~ 160 nm) and Werner (maximum below 130 nm) bands (Figure III.9). As the lower electronic of H_2 state is repulsive, there is broad continuum radiation in range of 190 nm - 300 nm. The VUV part of this continuum overlaps with the Lyman band. Lyman-α line of atomic hydrogen and Lyman band (B-X) of H_2 dominates over other species emissions.

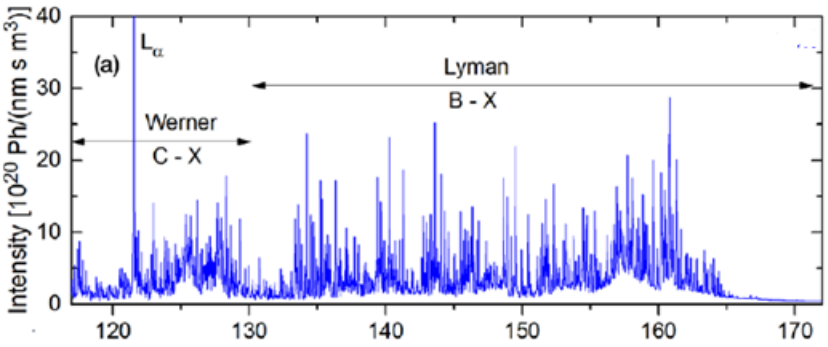

Figure III.9. Spectrum of hydrogen plasma at 3 Pa and 540 W RF power.[187]

In nitrogen plasma the molecular emission of the Lyman–Birge–Hopfield system N_2(a–X) (120–200 nm) is dominant. Dominant emissions in VUV range in H_2/N_2 (50/50) mixture is shown in Figure III.10.

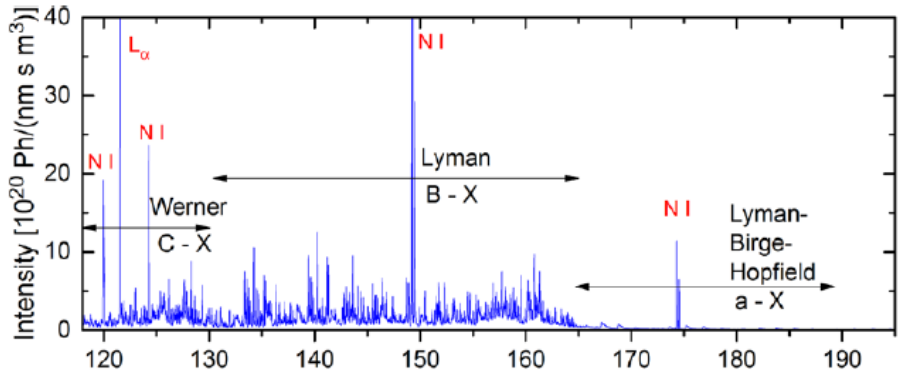

Figure III.10. Spectra of the 50%H_2/50N_2 plasma at 3 Pa and 540 W RF power. [187]

Variation of the nitrogen and hydrogen fractions in the used mixtures reveals a possibility to tune photon fluxes in the respective wavelength intervals (Figure III.11).

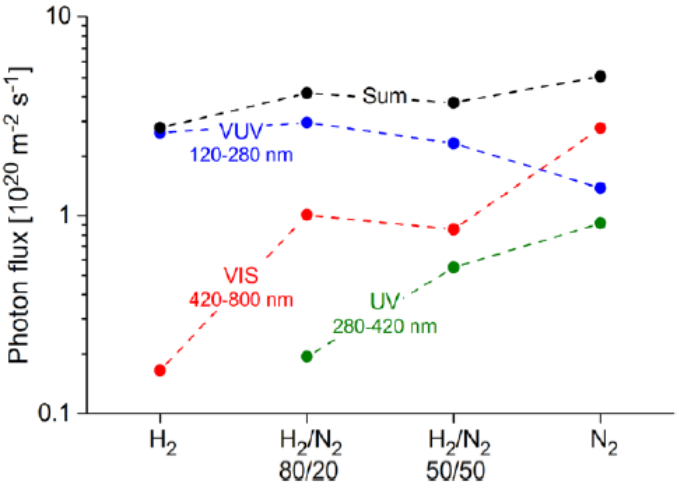

Figure III.11. Photon fluxes for hydrogen and nitrogen plasmas as well as for mixtures at 1 Pa and a RF power of 540 W.[187]

Woodworth et.al.[95] measured VUV fluxes in fluorocarbons (C_2F_6, CHF_3, C_4F_8) and Ar/fluorocarbon gas mixtures in ICP plasma. It was obtained that in fluorocarbon plasma VUV fluxes are in the range of 70 – 140 nm. VUV fluxes in C_4F_8, CHF_3, C_2F_6 plasmas (8.6×10^{14} cm^{-2} s^{-1}, 1.1×10^{15} cm^{-2} s^{-1} and 3.0×10^{15} cm^{-2} s^{-1}, respectively, with dominated resonance lines of atomic C and F) were obtained for a pressure of 10 mTorr and power of 200 W. With Ar dilution, the total VUV flux increases from 1.1×10^{15} cm^{-2} s^{-1} to 1.2×10^{16} cm^{-2} s^{-1} (≈20 mW cm^{-2}) due to argon resonance lines (Figure III.12).

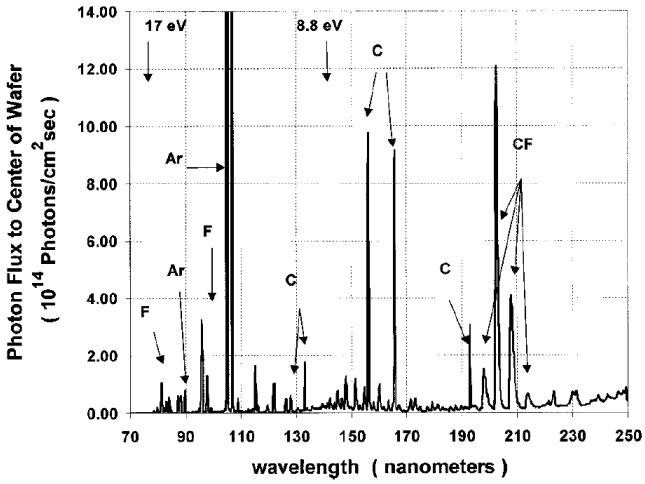

Figure III.12. Spectrum of a 20 mTorr, 200 W discharge plasma in the GEC cell in 50%Ar/50%C_2F_6 mixture.[95]

Jinnai et.al.[188] developed a special original on-wafer monitoring technique with a neural network that was calibrated by a UV spectrometer. The technique allows measurements of the VUV/UV spectra emitted by the ICP plasma and then predicts the type of induced damage. The absolute intensity of VUV photons was about (10^{15}–10^{16} cm^{-2} s^{-1}) in Ar, CF_3I and C_4F_8 ICP plasmas.

An interesting approach was suggested in [184] to calibrate VUV fluxes in industrial reactor in fluorocarbon plasma diluted by Ar. The plasma was generated in a DF-CCP industrial plasma tool (LAM Research 2300® Exelan® FlexTM), which is dedicated for low-k films etching. Experimental conditions are shown in Table III.2.

TABLE III.2. Process parameters of the experiments with 27 MHz RF power source[184]

Gas mixture	Power (W)	Pressure (mTorr)	Gas flow (sccm)
Ar/CF_4	700	50&150	400
Ar/CF_3I	700	50&150	400

The spectra were collected through a pinhole adjusted to a sidewall optical port. The setup and the scheme of light collection are shown in Figure III.13 (a,b). VUV spectrometer was connected via optical port with the chamber separated from the spectrometer system by a pinhole. An absolute calibration of the VUV system was carried out using standard UV + visible light spectrometer that is used as etching endpoint detection and PIC MC model calculations. First, CF_2 concentration was estimated by actinometry method (CF_2 UV ($1B1(0,v',0) \rightarrow 1A1(0,v'',0)$ –230<λ<430 nm and Ar $2p1 \rightarrow 1s2$ 750.4 nm). Actinometry coefficient was taken from the model calculations. When CF_2 concentration is known and taking into account short radiative lifetime of $^1B_1$ state (40 ns), CF_2 emission flux to the electrode center can be calculated as follows:

$$I_{CF_2(230-430nm)} = \int_{d\Omega} [CF_2] \cdot k_{CF_2} \cdot N_e \cdot dV \cdot d\Omega \qquad \text{(III.4)}$$

where k_{CF2} is the excitation rate constant, $[CF_2]$ is CF_2 concentration, dV stands for elementary volume and dΩ is the solid angle of light collection on the wafer center (see Figure 12b). Then CF_2 230 – 430 nm emission was measured by VUV spectrometer and so the last was absolutely calibrated.

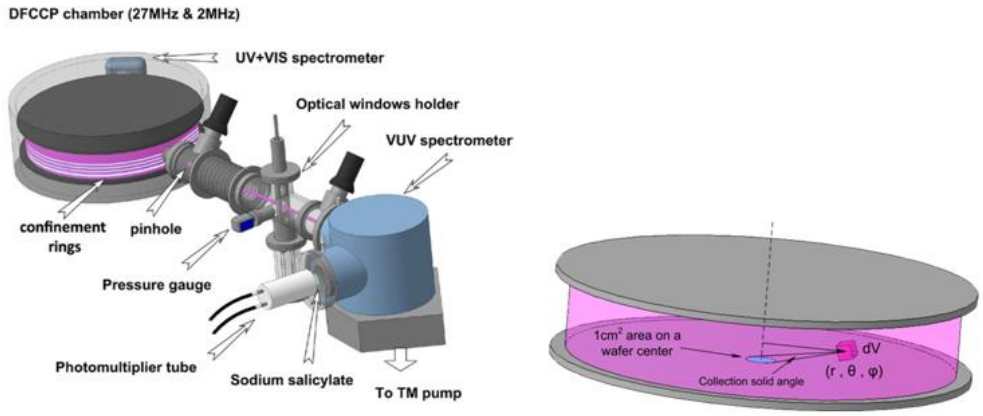

a) b)

Figure III.13. a) Experimental set up, b) principal scheme of calculation of the absolute photon flux at the wafer center.[184]

The measured VUV/UV spectra for various Ar/CF_4 and Ar/CF_3I mixtures are shown in Figure III.14.

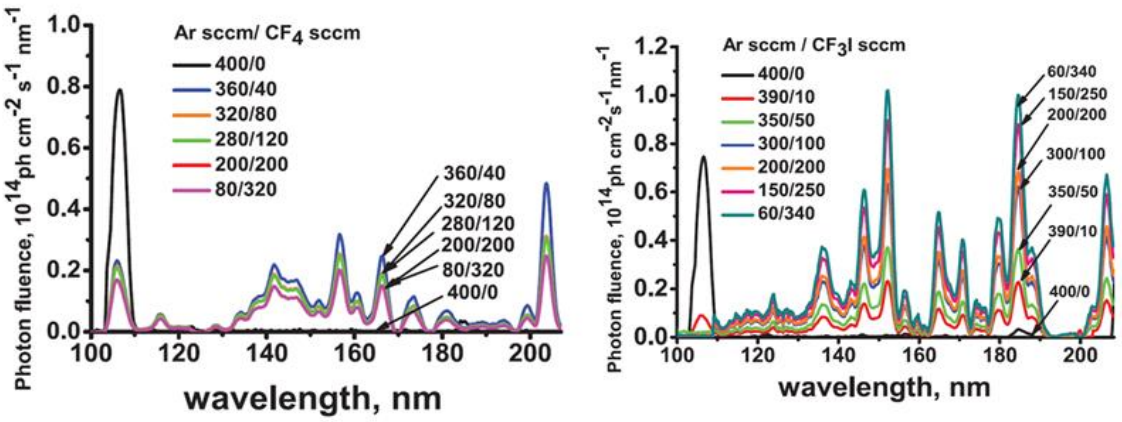

a) b)

Figure III.14. The measured VUV/UV spectra in CCP plasma in various Ar/CF_4 mixtures (a) and Ar/CF_3I mixtures (b) at 150 mTorr. Intensities are given in units of photons/(cm^2s) striking the center of the wafer. Ar resonant line is modified by self-absorption in a) and by self- absorption and CF_3I absorption in b).[184]

It is seen from comparison of Figure III.12 and Figure III.14 that emission spectra from CCP plasma is enriched by radiation of molecular species due to higher gas pressure. Emitting species in Figure III.14 are: are CF_2 (~130 -150 nm), CF molecules (bands maximums 198.1 nm, 202.6 nm, 208 nm and 213.6 nm), C (115.6 nm, 115.8 nm, 119 nm, 126.1 nm, 127.8 nm, 193 nm) and F atoms (95.5 nm, 95.8 nm), H atoms (121.6 nm, 102.6 nm). When CF_3I gas is presented in plasma mixture I atoms emission lines are also seen in VUV spectra (121.8 nm, 125 nm, 130 nm, 145.7 nm, 151 nm, 170.2 nm, 178 nm, 183nm,

184.4 nm). Ar resonant emission at 104.8 nm and 106.6 nm is a very significant part of the plasma VUV emission. Ion fluxes ($\sim 2 \div 3 \cdot 10^{15} cm^{-2} s^{-1}$) were measured by DC pulsed probe which was capable to measure the ion flux despite polymer coating during processing at the same plasma conditions [189]. It was obtained that VUV/UV fluxes in real technological conditions were a half of ion fluxes similar to.[95] This important result can be used for evaluation of VUV induced effects when the measurement of photon fluxes is difficult.

Proshina et al.[190] presented experimental and theoretical study of plasma chemistry in Ar/CF_4 and Ar/CHF_3 CCP plasma used for low-k etching. VUV/UV spectra was measured and calibrated. Density main charged and active neutral species was determined. The self-consistent particle-in cell model with Monte Carlo Collisions (PIC MCC) was applied to reveal mechanism of different species production.

Separate and combined effects of photons, ions and radicals are hardly possible to study in real plasma etch/strip conditions. For this reason, the experimental studies of the low-k films damage by photons and radicals were carried out in the modified commercial plasma reactors (by using special optical filters) and small gap technique. The authors [158,191,192 ,193] used various optical filter, small gap technique[194,195] , and their combination (authors [158,191,192,193] called this technique as pallet for plasma evaluation, PAPE) (Figure III.15) to study a separate and combine effects of VUV/UV and radicals on low-k films.

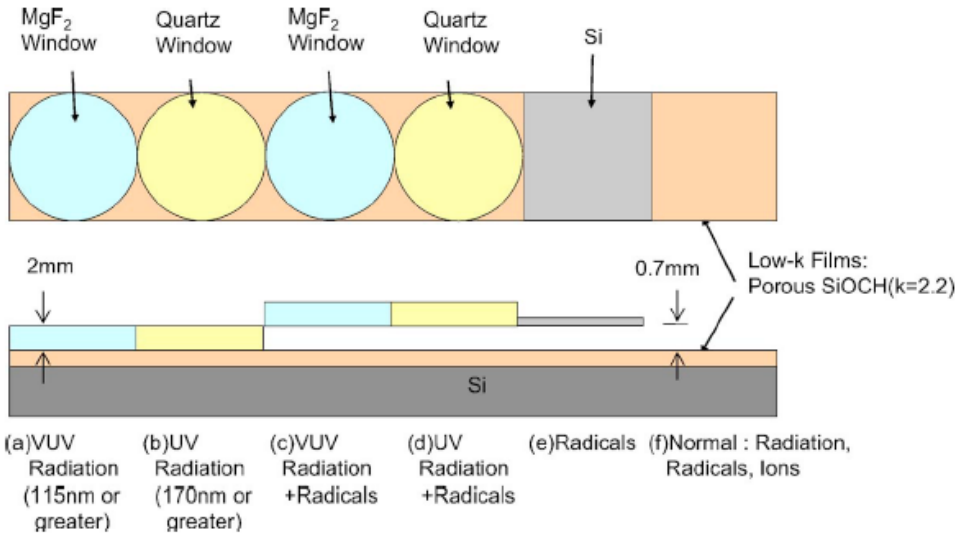

Figure III.15. Schematic diagram of PAPE.[158]

Using PAPE technique and the measured data (calibrated VUV/UV fluxes; densities of radicals and dynamic data of SiCOH films modifications) both separate and synergetic effects of photons and radicals on films damage can be studied.

III.3. VUV- induced processes in plasma treatment in gas mixtures used in strip, cleaning, and surface functionalization processes.

This section is focused on the review possible VUV assisted processes in O_2, H_2, H_2/N_2 plasmas (and their mixtures with Ar and He) which used in different processing steps in low-k material technology. Most attention is paid on the demonstration of synergetic effects of VUV radiation and radicals.

Synergistic interaction of VUV and reactive oxygen species (active oxygen, AO) was observed early in the polymers etching processes[196] . The etch rates induced by AO or by VUV radiation alone are smaller than those observed when both are present simultaneously. This result agrees with theoretical predictions: the "thermal" atomic oxygen etch rates, which are very low, are significantly increased in the presence of VUV. The VUV radiation gives rise to photochemically-induced chain scissions in the polymer surface and subsurface regions (typically a few tens of nm). Depending upon whether O_2 is present or not, volatile fragments and oxidation products are liberated at the surface, and cross-linking reactions induce the formation of a three-dimensional network in the near-surface amorphous layer and thereby reduce the etch rates. This does not occur in the case of simultaneous VUV and AO exposures, where the radicals formed are readily oxidized and do not “organize” the amorphous layer.

Using a vacuum beam apparatus with a calibrated Xe vacuum ultraviolet (VUV) lamp, Lee and Graves[197] showed that 147 nm VUV photons impacting SiCOH (k=2.54, Novellus, Inc) result in post-exposure adsorption and reaction with water vapors from the atmosphere to form silanol bonds, thereby raising the dielectric constant. Interesting synergetic effect was revealed at the addition of a flux of O_2 to this VUV radiation. It was shown that sequential exposure of O_2 after VUV exposure demonstrates the damage similar to a VUV exposed sample. Only simultaneous exposure of VUV photons and O_2 is necessary to observe this synergetic effect. It was estimated also that this effect cannot be explained by O_2 photodissociation. Lee and Graves have proposed that synergetic effect in simultaneous VUV/O_2 exposure is due to the reaction of O_2 with a methyl intermediates desorbing due to broken Si–C bonds by VUV emission. As a result, CO_2 and H_2O molecules are produced within the pores. This mechanism has been validated in the Matsunaga’s experiments[198] with VUV irradiation on SiO_2 hard mask-covered SiCOH low-k film and it is also in good agreement with the results reported by Goldman et al.[159]. However, the direct detection of these species is difficult. The mechanism of direct scission of Si–CH_3 bonds by VUV photons was suggested in [104]. The produced active sites can operate as initial centers for

further reaction with damaging molecules. The mechanism of low-k damage induced by VUV and VUV/O_2 for the same films was also suggested by Kazi and Kelber[199] from in-situ XPS and ex-situ FTIR measurements with Kr lamp (123 nm). It was suggested that carbon loss due to VUV radiation are determined not only by photon-induced Si-C bond scission but also by reverse process of CH_3 attachment on radical Si sites. At VUV/O_2 exposure this CH_3 addition (Si/CH_3 recombination) can be reduced by O_2 reactions with radical Si sites. Besides, a chemical reaction with O_2 results in Si-Ox based bond formation. Behera et al. [200] and Choudhury et al.[201] reported similar synergetic effect of VUV radiation with NH_3 and air, respectively. These results show that photo-induced effects with molecular species can play an important role in SiCOH films damage and should be discussed separately.

The relative drops in the Si–C bonds for Ar and O_2 plasma, were compared with e-beam VUV/O_2 results [197]. It was revealed (Figure III.16) that the loss of methyl groups due to radiation increase with wave length of VUV radiation: 104 and 106 nm (for Ar), 130 nm (for O atoms) and 147 nm (for Xe VUV/O_2). This trend correlates with experimental data [101,102,109].

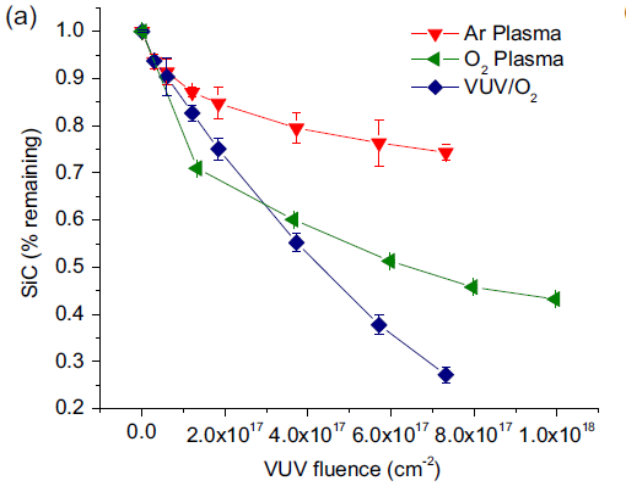

Figure III.16. Integrated FTIR peak values for Si–C content in the porous-ULK material as a function of VUV fluence for Ar plasma, O_2 plasma and VUV/O_2 in the vacuum beam system[146].

It was observed that the VUV/O_2 case causes the biggest modification, while there is the saturation for O_2 and Ar plasmas impact at higher VUV fluencies. Besides the saturation of Si-C group drop in O_2 plasma follows for their fast reducing. The authors have attributed this fast Si-C group drop to combine effect of VUV and atomic oxygen. However, a reason of the saturation is not fully understood.

In further study[147], the authors report the measured films damage induced by VUV photons, by O radicals, and by O_2 plasma in the conditions of the study[146]. In the case of VUV exposition (for O_2 plasma, the main VUV emission is O atoms emission at 130 nm), the sample was placed behind an MgF_2 window. Small gap technique (Teflon cap with a small gap ~1.5 mm) was used for radical exposition only. By examining the depth profile using FTIR and HF strip data, they have observed that VUV photons gradually remove carbon compounds throughout the penetration depth, creating a modified layer that still contains a considerable amount of carbon extracted subsequently at HF stripping stage. It was also observed that the damaged profile caused by VUV photons alone is similar to direct plasma exposure. That is the modified layer during plasma exposure appears to be photon-controlled.
By fitting experimental data the developed 1-D model has allowed to obtain an effective photolysis cross section ($1.4 \cdot 10^{-17}$ cm^2 for VUV photons at 130 nm) that corresponds to a photodissociation quantum yield of ~15% for the known photoabsorption cross section of Si-C bonds ($9.3 \cdot 10^{-17}$ cm2) resulted in attenuation coefficient of $3.7 \cdot 10^5$ cm-1. The higher Si-O photoabsorption cross-sections and quantum yields (~30%) were derived.

In contrast to VUV emission, oxygen radicals remove carbon compounds layer-by-layer, creating a nearly carbon free modified layer. It was shown that O atoms effects could be modeled accurately only by including in the model a less diffusive overlayer that inhibits the radical flux at the surface of the film. This conclusion is supported by XPS data of Kazi and Kelber[199]. The authors[147] also reported that these models (VUV and O exposition) cannot be combined to predict behavior under simultaneous exposures resulted in a large overestimation of carbon removal Figure III.17(a). Figure III.17(a,b) demonstrates also interesting “negative” synergetic VUV + O effect: the presence of both species produces less damage that sum of photons and radicals alone. Similar effects were observed in case of ion bombardment when ions produce a dense SiO_2-like overlayer which inhibits O_2 or O penetration [153,154,202,199,203,204,205] .
It was revealed in [147] that exposition of low-k films to radical flux after VUV pretreatment demonstrate “negative” VUV + O synergism also. Probably this effect can be explained by pore shrinking due to big fluxes of VUV radiation [148,154] and additional oxidation by O atoms.

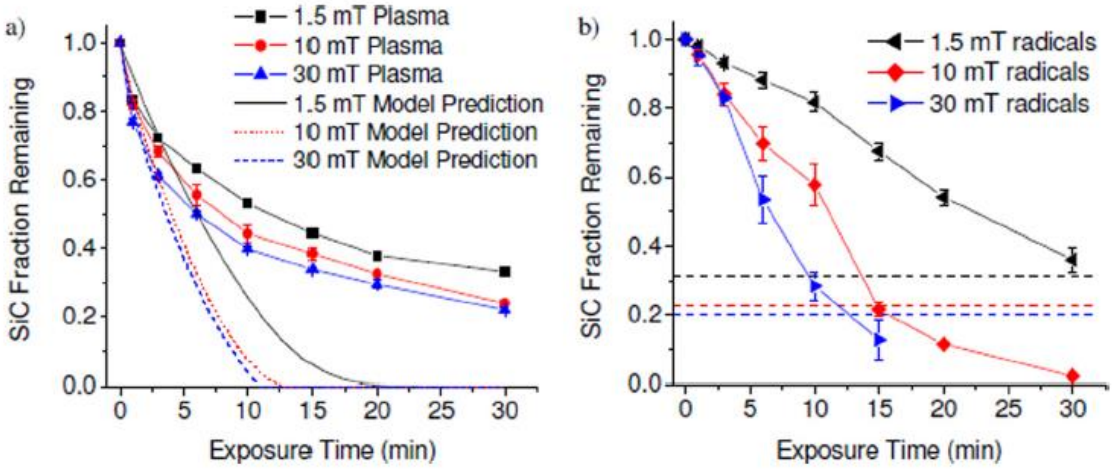

Figure III.17. (Color online) Comparison of carbon loss for (a) plasma exposures and (b) radical exposures as a function of time. Pressure conditions of 1.5, 10, and 30 mTorr and power of 150W were used in each case. Model predictions show a rate of carbon removal that is greatly overestimated compared to experimental results. Horizontal dotted lines show that carbon loss from radicals alone can exceed that of equivalent plasma treatment for longer exposures.[147]

Various optical filter, small gap technique and their combination ("pallet for plasma evaluation" technique, PAPE) were used in [158,191,192,193,194] to study the separate and combined effects of VUV/UV and radicals in DF RF CCP plasma. Takeda et.al. [191] studied effect of O_2 DF CCP plasma (exposition time was 2 min) on damage of SiCOH low-k film (k=2.2, 40% porosity) by using PAPE technique and FTIR data for different cases: a) VUV and UV radiation; b) UV radiation; c) VUV + radicals; d) UV + radicals; e) radicals; f) normal plasma (Figure III.18).

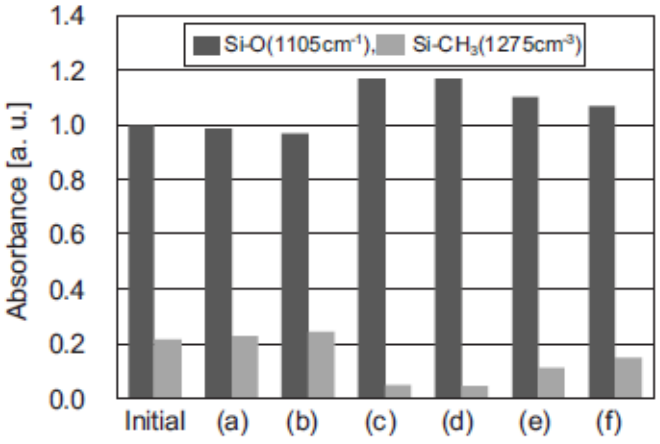

Figure III.18. Absorbance intensity of Si–O (1105 cm−1), Si–CH_3 (1275 cm−1) in the p-SiCOH film. [191]

It was shown that the remarkable modifications of low-k film (decreasing of Si–CH_3 group and increasing of Si-O group) was observed in O_2 plasma only for simultaneous exposure of low-k surface to VUV/UV photons and oxygen atoms (cases c) and d)). It should be noted that the films damage by VUV and UV photons remains small if the low-k film is not exposed to O_2 plasma. This "positive" synergetic effect of VUV radiation and atoms correlates with data of [147] only at small exposition time. In plasma conditions 202, the ions bombardment at high bias power (case f)) suppresses atomic O penetration. Without ion bombardment damaged layers were produced within the film. The increasing of Si-O/Si-CH_3 ratio for cases c) and d) indicates also that the most oxidation is due to O radicals stimulated by VUV/UV radiation. This result is also in an agreement with [147].

The individual and combined effects of light, radicals, and ion bombardment on the SiCOH film (k=2.3, 40% porosity) in H_2 or H_2/N_2 DF CCP plasmas (with floated substrate) was studied by Yamamoto et.al. [192], using PAPE technique and in situ Fourier-transform infrared reflection absorption spectroscopy (IR-RAS). The H and N radical densities in the plasmas were measured by vacuum ultraviolet absorption spectroscopy (VUVAS) [193]. The presence of both hydrogen and NH_x species was revealed by quadruple mass spectroscopy. Four experiments were performed by using PAPE: a) VUV exposition, b) radical exposition, c) VUV + radical exposition and d) plasma exposition.

It was shown that the H_2 plasma treatment during 180 s of all four samples causes more extraction of methyl groups than the H_2/N_2 plasma (Figure III.19). Besides, synergetic effect VUV and radicals was observed for both plasmas.

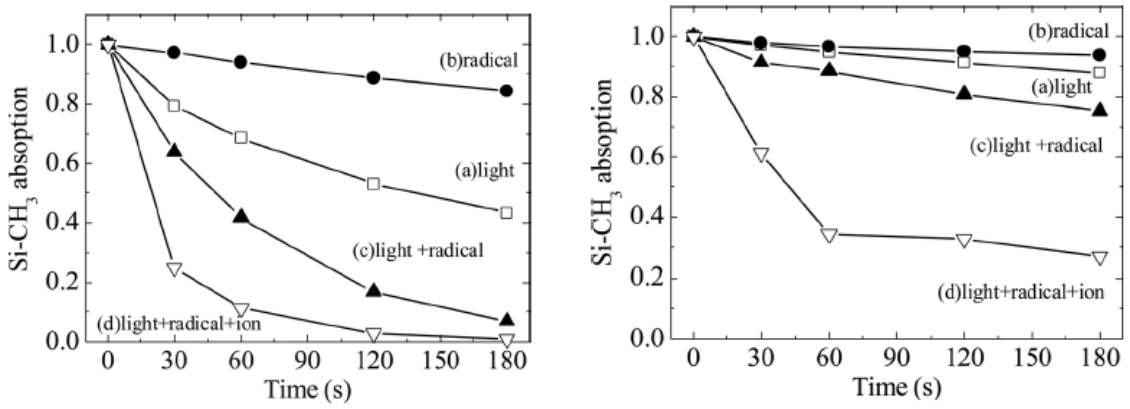

a) b)

Figure III.19. Normalized Si-CH_3 bond absorption of each sample during a) H_2 and b) H_2/N_2 plasma exposure.[193]

In previous study[192] it was revealed that VUV radiation is higher and radicals concentrations is lower in H_2 plasma than in H_2/N_2 plasma. This result and data in Figure III.19 indicate that NH_x radicals in the H_2/N_2 plasma can inhibit atomic H penetration by forming nitride layers on the film surface. This layer production was approved by data of IR-RAS spectra on modification of different structures in low-k film and by XPS and dynamic SIMS measurements.

Interesting results were reported by Grill et al.[206] They observed that the exposure of five ultralow-k porous SiCOH films (with porosity P1 and k=2.0, 2.40, and porosity P2 and k=1.8, 2.05, 2.40) to ICP hydrogen plasmas results in film shrinkage, increase in index of refraction and dielectric constants induced by several factors including molecular rearrangement leading to increased crosslinking and film densification. It was shown that the modifications of film's properties are dependent on the substrate temperature during the plasma treatment, but not on the substrate bias during the room-temperature treatments.

Besides, comparison of the effects of O_2 and H_2/N_2 plasma on refractive index of low-k films [207] reveals that the influence of VUV and UV radiation of the O_2 CCP plasma was lower than that of in the H_2/N_2 CCP plasma. However, the influence of the combination of O radicals and VUV and UV irradiation is higher than H and N radicals. The effect of nitride layer production was studied by numerical simulation for combined He and NH_3 plasma treatment of low-k films.[208] Mechanisms for sealing of SiCOH films were suggested. Effect oxygen and hydrogen containing plasma on low-k damage was studied in ref. [209] on the base of numerical simulation. Shoeb et al. [209] have developed a phenomenological model of OSG film damage during treatment in He/H_2 and Ar/O_2 plasmas to describe the damage induced by photons as well as H and O atoms during the plasma cleaning of the film. Both photons transport and atoms motion in the pores was described on the base of the Monte-Carlo method and two sorts of absorbers were considered in [102,109].

The probabilities of the reactions for surface site modification in Ar/O_2 and He/H_2 plasmas were adjusted using experimental data available in the literature. The values of the reaction probabilities were based on thermodynamic properties and reactions enthalpies. It was obtained that He/H_2 plasmas remove $–CH_3$ groups slower than O_2 containing plasmas due to the higher threshold energies for these reactions involving H atoms. This result is in accordance with data of [158,202]. It was obtained also that due to the less reactive nature of H radicals with $–SiO_2–CH_x$ groups. Si–C bond scission by photons from He/H_2 plasmas has more pronounced synergetic effect than oxygen containing plasmas. This result is in a qualitative agreement with data of [193] in H_2 plasma and with data of [147] in O_2 at low exposition time.

It is necessary to note that the results of plasma treatment are highly sensitive to the pristine films structures. As it was pointed in [210,211] the films with backbone carbon (Si-R-Si) demonstrate the enhanced

resistance to carbon loss upon exposure to either atomic oxygen or VUV radiation in the presence of O_2 (VUV+O_2). Also, Yasuhara et al.[150] have shown that a linear Si–O structure in low-k films was less affected by plasma exposure than network/cage Si–O structures because of the small amount of stress in the O–Si–O structure. A reduced rate of methyl removal from linear Si–O structures was observed during plasma exposure to TCP biased plasma in three gases (O_2, Ar and Ar/H_2). It was demonstrated by XPS depth measurements that damaged layer of low-k SiCOH films prepared by neutral-beam enhanced chemical-vapor-deposition (NBECVD) is thinner than that of for usual PECVD films.

Besides, a shorter plasma exposure time can reduce the damage[102,147,192,212]. Control of VUV emission from plasma and the ratio of VUV fluxes to those of other reactive species is one of the most important challenges in low-k integration technology [162].

III.4. VUV induced effects in etch plasma.

Etching of SiO_2 (and Si) materials by fluorine atoms was studied more than 40 years (see detailed review [213] and references therein). It was shown that the etch rate of SiO_2 by F atoms is very slow at room temperature and the temperature dependence is described by reaction probability $\gamma \sim 0.016 \times \exp(-0.163\ eV/kT)$. The final reaction product is SiF_4 [214]. OSG low-k films are less resistance to F atoms [215,216,217] but also show low etch rate and reduced damage at lower films temperatures [176,186]. Etching of OSG low-k materials is usually performed in fluorocarbon plasma diluted by Ar. One of the possible approaches to reduce/avoid damage caused by VUV/UV radiation is the screening of alternative plasma forming gas chemistries with low intensity of VUV emission. For instance, plasma of CF_3I was examined in several studies [218,219] as a potential replacement of other fluorocarbon gases. The author of the paper [218] compared porous SiCOH low-k (k = 2.6) etching in CF_4, C_4F_6 and CF_3I in a (DF-CCP) discharge. OSG low-k films damage was studied in conditions when discharge was operated at only high frequency (160 MHz) powered at 300 W and pressure of 10 mTorr. At these conditions, CF_3I was found to provide the lowest damage compared to the other gases. The authors have attributed these results to low UV emission intensity at 200–300 nm. However, it is already known [102,104] that only radiation with $\lambda<190$ nm can induce damage in low-k films. The emission spectra of CF_3I plasma within this range were not collected in ref. [218]. Assuming that the low-k films damage in these plasma conditions is mainly caused by F radicals one can conclude that the F atoms flux is high in CF_4 plasma and very low in CF_3I plasma. The same conclusion can be found in ref. [220] where VUV-emission spectra in the conditions of ref.[168] were studied together with low-k plasma damage and etch performance. It was found that the low-k damage is similar for both gas mixtures. VUV spectra were measured in Ar/CF_4 and Ar/CF_3I plasmas ignited in the industrial CCP chamber [184]. It was shown that substitution of CF_4 gas by CF_3I gas results in the increasing

VUV emission of fluorocarbon components mainly due to the presence of I* emission (Figure III.20). Besides, Ar emission plays the dominant role in the VUV- caused damage of low-k material in the conditions under study [184] (Figure III.21). It is a big challenge for industry to perform homogeneous etching in CCP plasma without a diluter gas such as Ar.

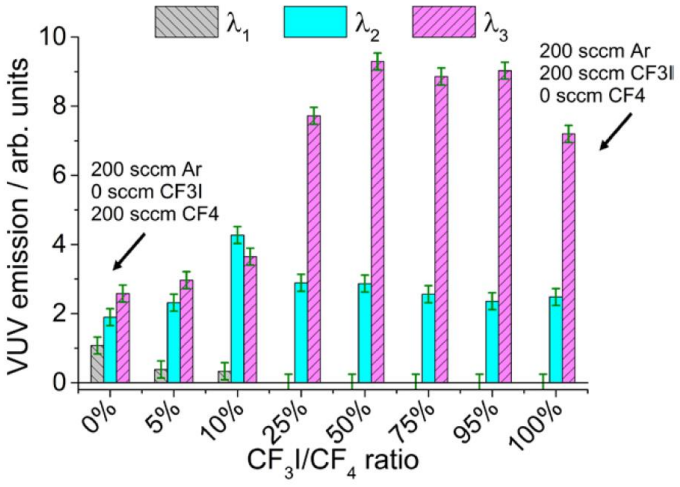

Figure III.20. The effect of replacing CF_4 by CF_3I on the VUV emission. The integrated VUV emission from Ar, Ar/CF_4¬ and Ar/CF_4/ CF_3I discharges is shown for 80 < λ1<120 (grey), 120 < λ2<160 (light cayenne) and 160 < λ3< 200 (magenta). [219]

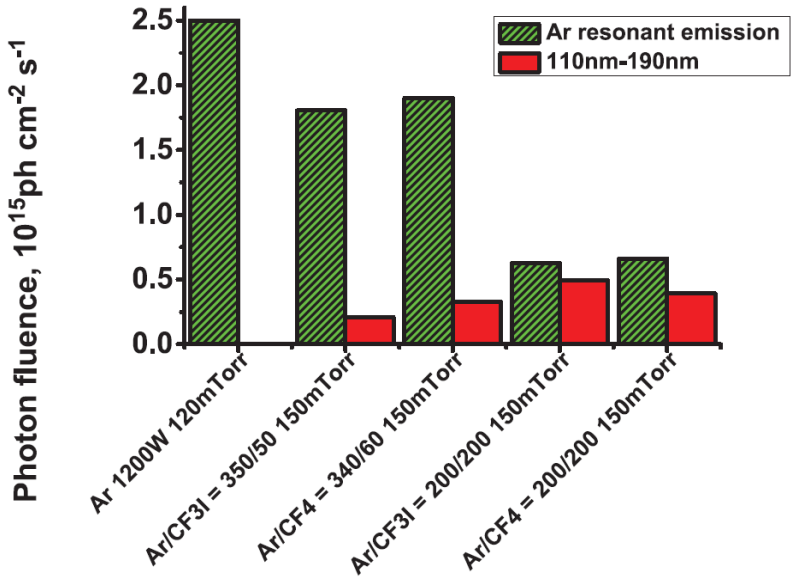

Figure III.21. Integrated VUV flux from Ar resonant lines and the rest of the VUV spectra (noted as 110 nm–190 nm) for pure Ar, Ar/ CF_3I and Ar/CF_4 mixtures with low addition of fluorocarbon gases and the ones with equivalent percentage of CF_4 or CF_3I and Ar.[184]

As it was shown in [184] the main VUV emission is originated from resonance lines of Ar. In ref. [221] , the etching and damage of low-k films were studied in ICP plasma using CF_4, CHF_3 and their mixtures with Ar at room and cryogenic temperatures. Significant slowing down of the films degradation under F atoms flux at decreasing temperature was shown. Also, high contribution of Ar VUV photons into low-k films damage in Ar containing mixtures was demonstrated. However up to now there is no detail data on combined effects of atomic fluorine and VUV emission. VUV emission can break Si–CH_3 bonds deeply in SiCOH films [102,147,213,217] and enhance the films damage and etching by F atoms especially at low films temperatures.[186]

The temperature dependence and reduced stability of OSG films (in comparison with SiO_2) under F atoms impacts were obtained by the detailed study of multi-step mechanism developed in refs. [222,223,] on the base of experimental data and DFT modeling. The mechanism involves fast fluorination stage with quasi-chemisorption of F atoms on surface Si atoms (appeared as pentavalent Si states) as well as successive exothermic (but with small activation energy of about 0.1 eV) reactions of hydrogen abstraction from $SiCH_xF_y$ (x=1-3, y=3-x) by F atoms followed by F atoms addition to radical groups $SiCH_{x-1}F_y$ (HAFA reactions). The volatile products appearing at this HAFA stage (Hydrogen Abstraction Fluorine Addition) are CF_2 and CF_3 radicals rather than CF_4 molecules [222,223,224]. The processes of these two stages result in a heavy fluorinated Si/O/F material with enhanced reactivity and capability of a facilitated breaking of Si–O bonds in the reactions with F atoms. The difference between dense SiO_2 (with quasi-chemisorbed F atoms at the top surface) and fluorinated SiO_x porous films (with quasi-chemisorbed F atoms and, in addition, with ordinary Si–F bonds appeared instead of the initial CH_3 groups) could be responsible for the observed significant difference in radical etching rates of SiO_2 and OSG low-κ films.

The low temperature effects and synergistic effects of VUV photons and F atoms in both damage and etching of various OSG low-k films were studied in [186]. OSG samples were treated in downstream of 13.56 MHz ICP plasma (RF power = 200 W) in Xe/SF_6 = 1/1 mixture (pressure = 100 mTorr). Xenon atoms in the mixture provide powerful VUV emission of 147 nm resonant line with the derived photons flux of $2 \cdot 10^{14}$ ph/(cm^2 s) while SF_6 dissociation provides fluorine atoms with the measured F atoms flux on the film surface of ~$1.6 \cdot 10^{17}$ atoms/(cm^2 s). All the samples were located on a holder which temperature was varied from +15 °C down to −60 °C by two-stage Peltier module. Five types of low-k films were treated separately by VUV light and F atoms and jointly by VUV and F atoms for films temperatures +15 °C, -30 °C and −60 °C (Figure III.22).

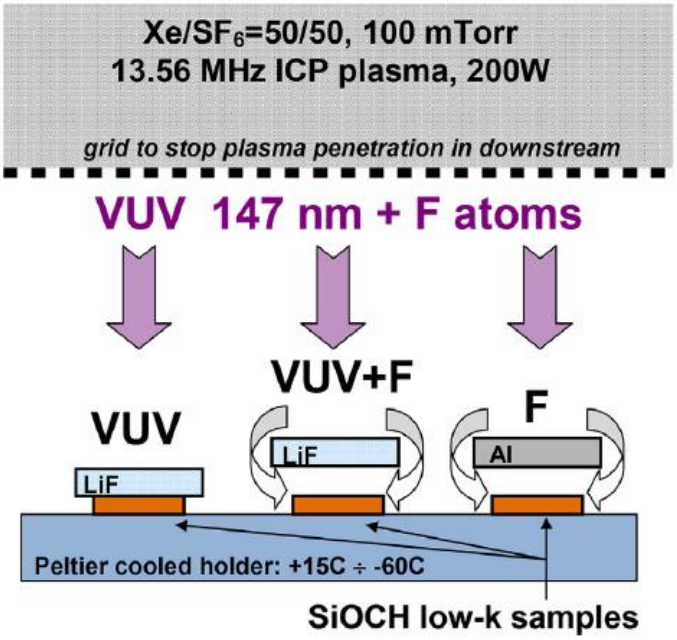

Figure III.22. The experimental scheme. [186]

It was shown that the rate of damage (starting with H abstraction from CH_3 groups) and SiO_x etching by F atoms notably drops at low temperatures due to activation barriers for the both processes [181]. As might be expected, the damage by VUV photons are not sensitive to the films temperature. The simultaneous exposure to VUV photons and F atoms at low temperatures (T = −30 and −60 °C) shows effects significantly exceeding the sum of the separate effects of VUV photons and F atoms (Figure III.23). The rates of CH_3 groups elimination by VUV photons and F atoms are comparable at T = −60 °C. As a result, the synergistic enhancement at joint exposes is more pronounced at this low T. The observed synergistic effects are almost ceased at higher temperature T=15 °C.

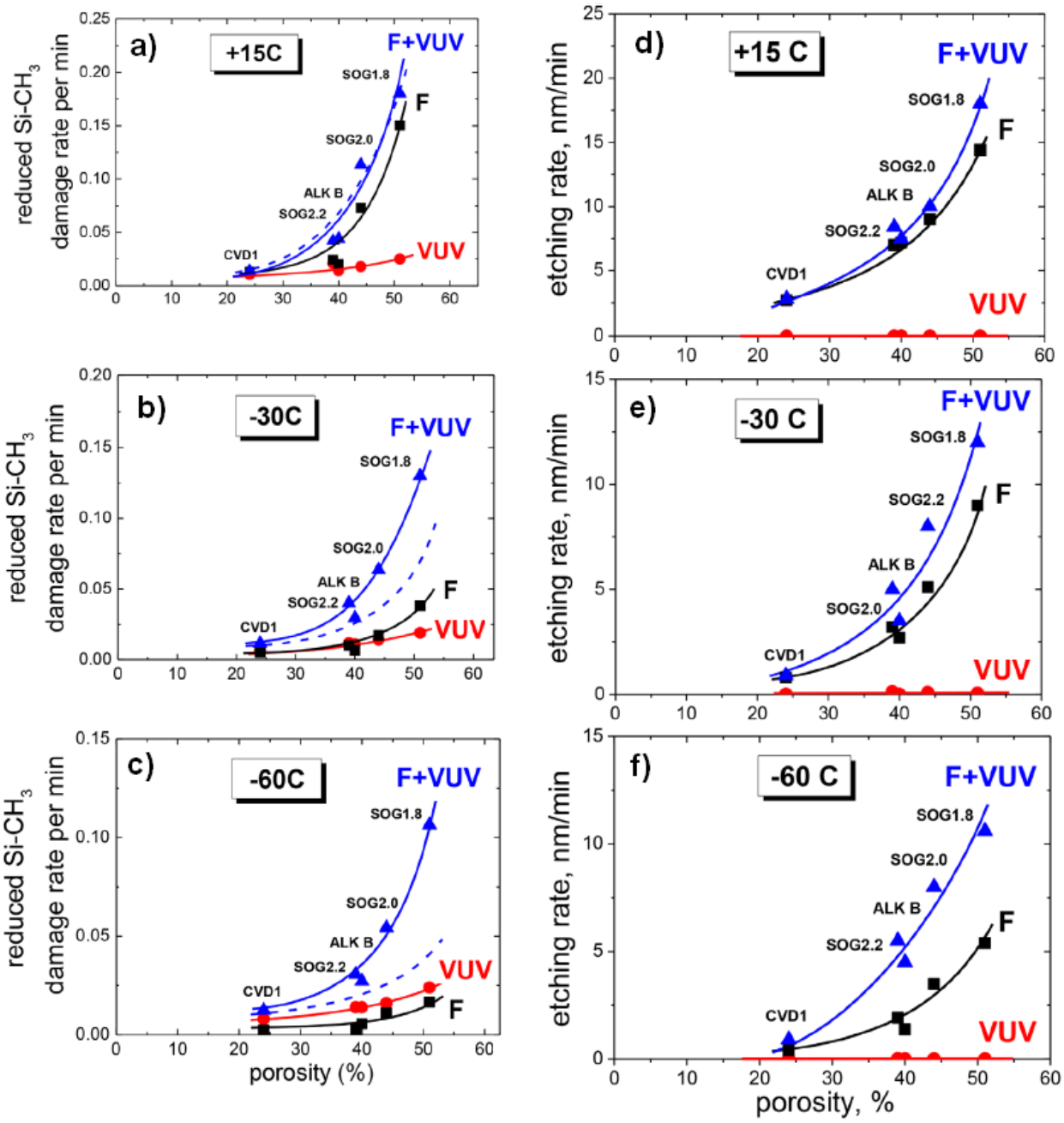

Figure III.23. The rates of [Si–CH_3]treated/[Si–CH_3]pristine damage (a-c) and etching (d-f) as functions of the film's porosities and temperatures T= +15 °C, −30 °C and −60 °C. The types of the treated OSG films are shown near the respective experimental points. Solid curves are the fits of the measured results. The dashed curves are the sum of the separate effects of F atoms and VUV emissions.[186]

III.5. Reduction of VUV induced damage.

The damage of OSG low-k films caused by VUV photons can be reduced by using two obvious strategies:

i) reduction of VUV radiation itself during plasma processing or

ii) protection of OSG from VUV exposure.

In the first case, selection of appropriate plasma reactor and plasma chemistries is the obvious strategy. It is necessary to optimize gas composition and plasma characteristics to provide the required etch characteristics at reduced intensity of VUV radiation. Application of multi-frequency CCP reactors is preferable choice because they provide more opportunities to control the etch processes. A damage-free resist strip processing with using high temperature He/H_2 downstream plasma provides sufficiently high resist strip rate is another example.[70]

The second strategy is more popular in this respect. First of all, it is obvious that the VUV impact on OSG films is sensitive to the film structure. As it was pointed out in [210,211] the films containing backbone carbon (Si-R-Si) in their structure demonstrate the enhanced resistance to carbon loss upon exposure to both atomic oxygen and VUV radiation. However, plasma and VUV resistance of these materials with different types of bridging groups and benchmarking with traditional low-k materials with terminal CH_3 groups needs more comprehensive study.[225]

The most popular approaches are based on densification. Densification and pore sealing by ion bombardment promote significant reduction of radical's diffusion into OSG bulk and VUV damage [202,199,226,227.] Therefore, the main approaches are based on temporary densification of low-k dielectrics by filling of the open pores with sacrificial materials. Three different approaches have been developed for this purpose. The first one is known as Post Integration Porogen Removal (PIPR) when porogen is removed after the complete patterning and metallization [228,229,230]. The second approach was proposed by Frot et al. (IBM) and it was termed as Post Porosity Plasma Protection (P4) when the pores in completely cured low-k film are filled with sacrificial materials [231,232,233,234] . The third approach is based on cryogenic (low temperature) etching when the low-k dielectric is protected against the plasma damage by reaction products condensed in the pores [235,236,237,238] or also filled by condensed sacrificial materials having the melting temperature much lower than the polymers used in P4 approach. These methods have been targeted to avoid penetration of radicals into low-k dielectrics through the interconnected pores. At the same time penetration of VUV radiation and correspondingly VUV induced damage can also be reduced.

The Post Integration Porogen Removal approach was proposed by Calvert and Gallagher[228] about 15 years ago and it is historically the oldest one. The etching (patterning) is performed before complete low-k curing. Critical process steps such as etching, resist removal, metal deposition and CMP are performed on a nonporous film and the porosity is created after integration by using an appropriate porogen removal treatment. The PIPR integration strategy is able to solve major issues of porous

dielectric integration but requires the development of a specific hybrid film with defined characteristics. In particular, the porogen thermal stability should be improved towards a high temperature (typically above 325 °C) to allow the use of conventional BEOL integration processes. Obviously, this should be operated without any porogen degradation. Afterwards, the porogen removal treatment should allow the creation of porosity with minimum film shrinkage at the standard curing temperature (typically 400 °C). Despite extensive research and significant efforts in 2003 – 2010 and demonstrated advantages, most of integration problems were not solved.

The proposed by IBM P4 approach (also known as pore stuffing) is fundamentally similar to PIPR but uses sacrificial polymer filled the pores after complete curing. If to compare with PIPR, it gives 2 important advantages. The first advantage is possibility to use different sacrificial materials (not only materials that can be used as porogen). The second advantage is the degree of matrix shrinkage during the polymer removal is much smaller than in PIPR because the low-k films was already completely cured. The efficiency of shielding the pores with an organic polymer was first demonstrated on ULK 2.0 blanket films, with up to 77% reduction of plasma induced damage. This protective effect depends on both the polymer nature and level of porosity fill.

The detailed study of VUV induced damage in low-k films filled by sacrificial polymers (P4) was carried out by De Marneffe et al.[149] Loss in Si-CH_3 bond due to 60 s VUV exposure, for pristine OSG low-k (Porous) and various filling polymers: Polyethylene glycol (PEG), Polymethylmethacrylate (PMMA), Polystyrene (PS), and an improved Polystyrene (PS-pro) is shown in Figure III.23. Xe plasma exposure tests were carried out in a 300 mm Lam Research Excelan Flex CCP chamber, at a pressure of 120 mT and powered at 1500 W by a 27 MHz generator coupled through the electrostatic chuck. In order to separate the effect of VUV photons from other plasma species (ions mainly for such discharge), a 50 mm diameter MgF_2 optical filter was positioned on top of the samples. Such filter has a cutting wavelength of 120 nm, and therefore transmits the Xe line emission, emitted at 147 nm. It was shown that the low-k damage by VUV light cannot be completely avoided even when the pores completely filled with the sacrificial polymer.

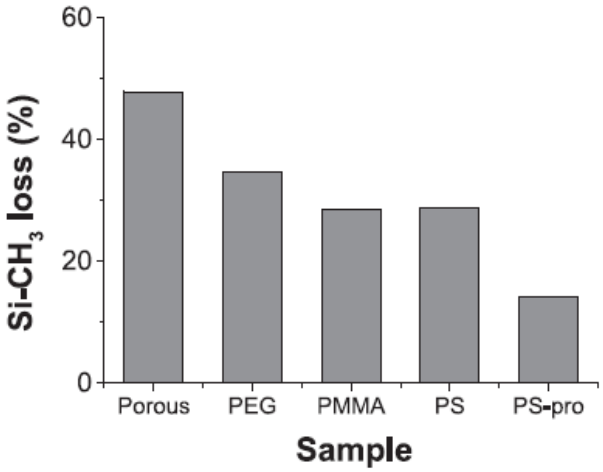

Figure III.23. Loss in Si-CH_3 bond due to 60 s VUV exposure, for pristine OSG low-k (Porous) and various filling polymers: Polyethylene glycol (PEG), Polymethylmethacrylate (PMMA), Polystyrene (PS), and an improved Polystyrene (PS-pro).[149]

The patterning of low-k materials often requires the use of a non-organic hard-mask (HM) having high etch selectivity to low-k. Selection of HM is crucial for the whole process and is usually based on morphological criteria, i.e., favoring a good final profile without post-etch residues. The hard mask must show good selectivity towards low-k etch and resist strip plasmas, low intrinsic roughness, good thermal stability up to 400 C, low stress so as to guarantee the absence of line wiggling, as little as possible post etch residues, wet cleanable with selective chemistries, and easy to remove with chemical-mechanical polishing. HM also acts as a protective layer against the VUV radiation. Detailed study of such opportunity was carried out in [149] where OSG samples were exposed to Xe plasma (147nm). Thin layers of metal oxides and nitrides were investigated as HM. All hard-masks were deposited on a 15 nm non-damaging SiCN/SiCO pore sealing layer, with a thickness of ~25 nm, which was deposited on k=2.05 OSG films with various thicknesses. For the films used in this study, showing an average pore radius of ~1.7 nm, a minimum thickness of 5 nm SiCN allows sealing the low-k. Figure III.24 represents the evolution of VUV-induced damage for different SiCN barrier thicknesses.

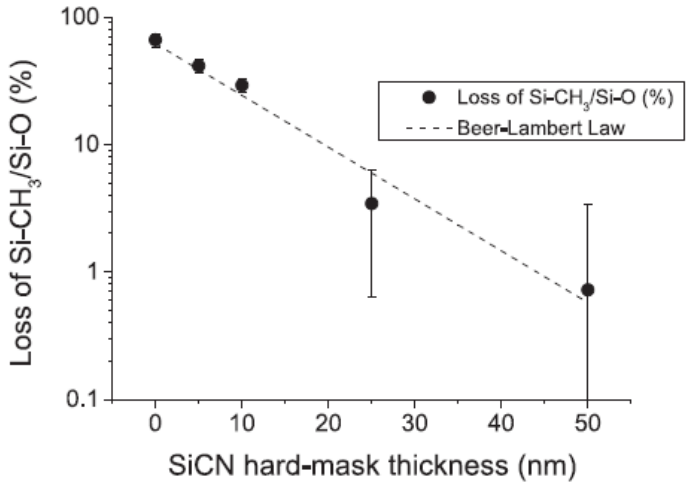

Figure III.24. Impact of SiCN hard mask thickness on Si-CH_3 loss after 120 s Xe VUV irradiation. Dotted line: fit using the Beer-Lambert law.[149]

Figure III.25 shows the Si-CH_3 loss for the different hard masks. 15 nm SiCN/SiCO allows reducing the VUV damage by half. The addition of a supplementary masking layer made of SiTiOx, a-C, or TaO_2 brings little improvement. However, the presence of TiN, TiO_2, ZrO_2, or AlN helps reducing significantly the impact of VUV under the mask. For comparison, Figure III.23 shows also the effect of pore stuffing with the best absorbing polymer without any mask. It is clear seen that, although stuffing helps protecting, the largest VUV protection results from the selection of an appropriate hard-mask.

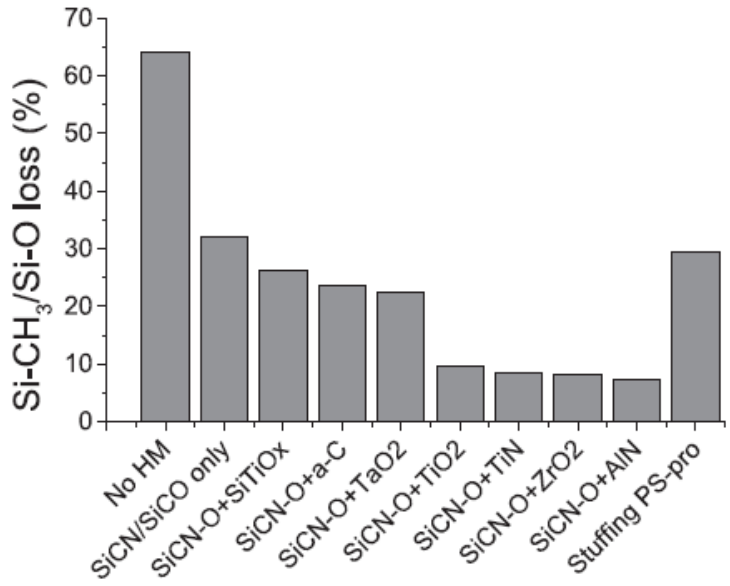

Figure III.25. Effect of various hard masks on Si-CH_3 loss after 120 s Xe VUV irradiation (147 nm or 8.4 eV). [149]

The cryogenic (cryo) protection effect is based either on condensation of the etch products or sacrificial materials having higher boiling temperature that the etch products. Both approaches allow reduction of plasma damage by mechanisms similar to PIPR and P4 (reduced permeability of reactants). The advantages are the possibility to remove the etch products or sacrificial fillers at much lower temperature (ideally, at room temperature) than in PIPR and P4, and also the possibility to reduce plasma damage by suppressing of activated damaging reactions.[176,186]

Condensation of the etch products provides very low degradation of porous OSG and the lowest integrated k-value was achieved by using this approach.[238] In the blanked studies,[176,177,178,179] OSG low-k damage in both SF_6 and SF_4/O_2 mixture is significantly reduced with decreasing temperature. In the ref. [178] SF_6/C_4F_8 plasma, the complete pore filling is achieved at −110 °C and negligible plasma-induced damage is demonstrated on both blanket and patterned low-k films. Figure III.26 demonstrates typical reduction of OSG damage with decreasing temperature. The main drawback for this approach is that very low temperatures are required down to -120° C (provided by liquid nitrogen cooling) that is technically complex because of lack of industrial etch equipment. As an alternative approach, it was proposed to use sacrificial chemical compounds able to be condensed at the temperatures higher that the condensation temperature of reaction products.[239] One example[240] is a recent study of the damage reduction by using a condensed organic compound in low-k films with k=2.3 and porosity=34% and SF_6-based ICP plasma at temperatures T > −50°C. It was shown that negligible damage can be achieved at −50 °C with acceptable etch rates. The evolution of the damage depth observed on 96 implies the Si-CH_3 loss due to Si-C dissociation by VUV photons and directly emphasizes an importance of VUV photon-induced damage even in these special conditions.

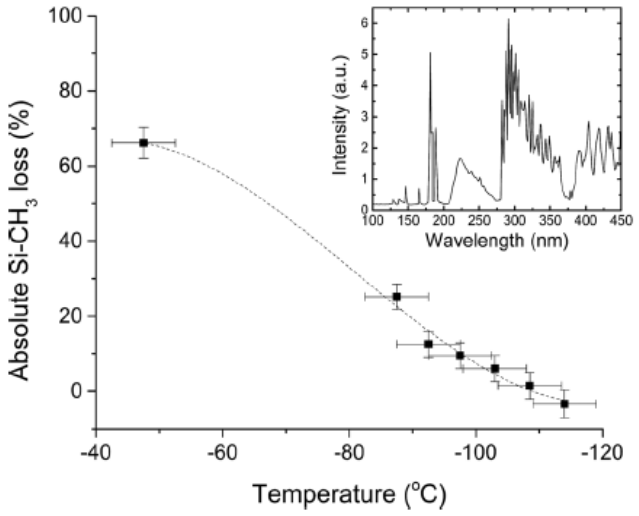

Figure III.26. Change in Si-CH_3 content of p-OSG 2.0 low-k films, during SF6-based etch following C_4F_8 condensation; target thickness after etch is ~110 nm (pristine thickness is 270 nm). Dotted line is a guide to the eye. Inset: emission spectrum of a SF6 plasma recorded in a 300mm ICP chamber (11.75 mTorr, 1 kW ICP power)[149].

One alternative approach is based on the pore wall protection by porogen residues[241,242] or pore surface grafting by organic molecules.[243, 244,180] Some reduction of plasma and VUV damage has also been demonstrated but generally these methods have been less efficient that the above discussed PIPR, P4 and cryogenic etching.

IV. IMPACT OF UV/VUV PHOTONS ON ELECTRICAL PROPERTIES OF SiO_2 AND LOW-k DIELECTRICS

Exposure of low-k dielectrics to high-energy UV/VUV photons can hardly be avoided during their synthesis and subsequent processing because heterogeneous nature of these materials limits applicability of traditional wet chemical treatments. In this section we will attempt to overview the impact of UV/VUV photons on the most essential electrical characteristics of low-k dielectrics: permittivity, built-in charges, leakage currents, and breakdown behavior. At first sight it seems logical to benchmark these effects to well-studied behavior of amorphous (a-) SiO_2 insulators used for decades as gate and field dielectrics. Indeed, the SiO_2-like skeleton represents the essential part of the low-k materials and its electrical response can hardly be ignored. However, the presence of significant amounts of other than Si and O atoms (H, C, etc.) in low-k films resulting from organic residues as well as porosity of some of the low-k matrices bring numerous novel aspects to the UV/VUV response of these layers. For example, UV exposure is shown to cause efficient demethylation of SiOCH films in the presence of active gases (O_2, NH_3)[245] or at elevated temperature[246] leading to changes in dielectric permittivity, leakage current, and breakdown voltage. Therefore, this section will first address the SiO_2-like aspects of radiation response of low-k insulators and then turn attention to the effects specific for porous low-k matrices and reflecting peculiarities of their composition and transport properties.

The most pronounced effect of UV/VUV exposure of a-SiO_2 insulators consists in build-up of a fixed charge. This process is routinely associated with trapping of photogenerated (or injected from electrodes) mobile charge carriers –electrons and holes – on the pre-existing oxide defects. In the case of VUV irradiation with photon energies exceeding the bandgap width of the oxide (8.9 eV for SiO_2 thermally grown on silicon [247,248], positive charging caused by hole trapping is dominant [249,250,251,252]. Negative charge buildup can also be observed upon electron photoinjection and trapping in a-SiO_2 [251,252]

but with much lower trapping rate than positive charging upon hole injection [253]. Though the electric field induced by the trapped oxide charges critically influences operation of active semiconductor devices, this field is unlikely to affect significantly electron transport in metallic conductor elements which are the only ones in direct contact with low-k insulation. The only imaginable effect concerns electrical behavior of perspective graphene interconnects [254], which resistivity might increase significantly would the charge-induced field cause a shift of the graphene Fermi level close to the Dirac point in graphene. What seems to be more relevant for the low-k insulator degradation is generation of energetically deep states in the oxide bandgap facilitating leakage current end eventually leading to the dielectric breakdown.

IV.1. Physics and chemistry of light-induced damage of amorphous SiO_2

Generation of additional charge traps in a-SiO_2 caused electron injection has initially been seen as a kind of radiation damage caused by energy dissipation by high-energy electrons in the oxide network [255,256,257,258]. However, later experiments using exposure of differently prepared SiO_2 films to VUV photons (10 eV) also revealed universal appearance of additional deep electron traps [252,259,260]. Considering that this photon energy is only by ≈1 eV exceeds the oxide gap width thus setting upper limit for kinetic energy of electrons or holes in the oxide, the "knock-off" effects can firmly be excluded. Rather, clear correlation of trap generation with hole trapping and atomic hydrogen presence in the oxide film points towards electrochemical process as the dominant mechanism of oxide damage [259]. Furthermore, the VUV-induced oxide degradation in terms of additional traps appears to correlate with development of leakage currents observed both in thick [261,262] and ultra-thin [263,264] SiO_2 layers. Current-voltage curves measured before (black symbols) and after exposure to 10-eV photons (red symbols) shown in Figure IV.1 for SiO_2 layers of three different thicknesses indicate that irradiation leads to an increase of low-field leakage current by several orders of magnitude. Only in the thinnest oxide sample (2.9 nm) the effect of VUV illumination can be termed as "marginal" because of the high initial leakage dominated by direct electron tunneling from silicon to the metal gate electrode.

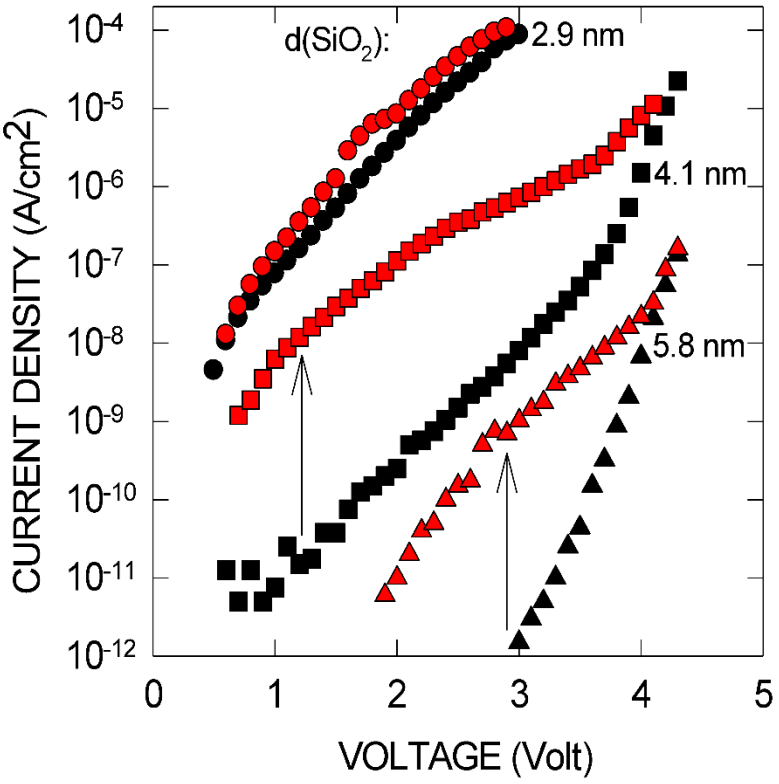
d(SiO2):
2.9 nm
4.1 nm
5.8 nm
CURRENT DENSITY (A/cm2)
VOLTAGE (Volt)
10-4
10-5
10-6
10-7
10-8
10-9
10-10
10-11
10-12
0
1
2
3
4
5

Figure IV.1. Current-voltage curves measured on n-Si/SiO2/Al capacitors with different oxide thickness d(SiO2) prior (black) and after irradiation (red) by 10-eV photons with a dose of ≈3x1017cm-2 absorbed under semitransparent metal layer. Data are re-plotted from Ref. [263].

Interestingly, relationship between generation of neutral electron traps in a-SiO_2 and development of leakage current was also inferred from the systematic analysis of charge injection-induced degradation of thin SiO_2 layers on silicon under electrical stress [265,266,267,268,269,270]. Experimental results also indicate the importance of anode hole injection and hydrogen liberation in the oxide-based gate stack which appear to "trigger" the damage process [267,270]. Eventually, generation of electron traps and development of the stress-induced leakage current correlate with dielectric breakdown of the oxide layer [270]. This striking similarity between the stress-induced degradation and the effects of VUV exposure points towards common mechanisms of the oxide damage. Importantly, during VUV irradiation the strength of electric field in the oxide layer remains low suggesting that the presence of high field during electrical stress is not necessary to damage the oxide network. Rather, injection of some hydrogenic species seems to suffice to generate defects in a-SiO_2 [270]. To get further insight into the origin of the VUV and injection-induced degradation of amorphous SiO_2, one can follow two different routes. First, using the fact that large area oxide surfaces can be exposed to VUV light with good uniformity one may try to use defect spectroscopy methods to identify the damage mechanism. Second, thanks to recent advances in theoretical modeling of amorphous oxides, atomic mechanisms of hydrogen interactions with a-SiO_2 network can be explored in great detail.

Combination of trap cross-section spectroscopy [271] with electron spin resonance (ESR) to analyze the effects of exposure of SiO_2 to VUV (10-eV) photons [259] suggests formation of protons through interaction of photogenerated holes with atomic hydrogen released from the top gate electrode [272]. In its turn, interaction of protons and charge carriers with SiO_2 matrix leads to rupture of Si-O-Si bridges and formation of hydroxyl groups (Si-OH) which represent well-known electron traps in SiO_2 [273,274].With increasing dose of VUV exposure, the density of hydroxyls first increases and then starts to decrease indicating Si-O bonds break while the electron trap spectrum becomes dominated by interstitial H_2O molecules. At the same VUV dose range, hole trapping is enhanced in correlation with intensity of ESR signal stemming from Si dangling bonds in a-SiO_2 (E'-centers) corresponding to formation of oxygen vacancies [259]. As a whole, the VUV-induced damage of SiO_2 can be represented as the proton-assisted electrochemical reduction of the oxide resulting in formation of (partially H-passivated) Frenkel pairs of oxygen vacancies and interstitial oxygen in the form of water molecules. Furthermore, ESR data reveal that rupture of the second Si-O bond of the same silicon atom in the $O_3{\equiv}Si\bullet$ center (dot symbolizes an unpaired electron) occurs with significantly higher probability than the initial break of the Si-O-Si bridge.

This would mean that the damage will cluster eventually leading to formation of well-defined oxygen-deficient regions which would explain local character of the oxide breakdown in the case of electrical stress. Worth of adding here is that similar pattern of SiO_2 degradation is observed if protons are supplied externally from a low-energy ion gun [275]. The proton-driven SiO_2 damage mechanism would also explain formation of Frenkel defects reported in the case of proton implantation into the wet synthetic glass [276] underlining the universality of this effect.

It becomes clear from the above discussion that supply of atomic hydrogen and formation of protons represent the key factors governing damage of a-SiO_2 network. Therefore, it is worth of addressing both the potential sources of hydrogen and the mechanism(s) of its ionization. The most relevant experimental results obtained by using nuclear reaction analysis indicate that hydrogen is abundant at the interfaces of SiO_2 and in the electrode materials [277,278]. Under conditions of UV/VUV illumination hydrogen can be dissociated by direct photolysis, or due to interaction with photo-generated mobile charge carries. Photo-dissociation of H bonds at the surface of silicon [279,280] as well as inside silica glass [281] is observed under 7.9-eV photon excitation, however the glass appears to be nearly immune to the 6.4-eV photon damage [282]. Alternatively, hydrogen can be released by hot photo-electron impact: The threshold of trap creation of about 2.3 eV for electron in the a-SiO_2 conduction band inferred from the electrical stress experiments [265] probably corresponds to the energy onset of H liberation [268]. Another mechanism concerns hole trapping from the oxide valence band on O3≡Si-H bonds leading to release of a proton with neutral O_3≡Si• defect (seen by ESR as paramagnetic E' center) left behind [283,284]. This process represents the most efficient proton generation mechanism when the UV photon energy exceeds the oxide bandgap width [285]. It should be added that the E'-centers can also serve as the cracking sites for H_2 molecules at room temperature [286] and will in this way 'recycle" hydrogen available in the oxide subsequently converting it into the most damaging protonic form when trapping a hole [283]. The latter process accounts both for the a-SiO2 network damage and for the buildup of trapped positive charge [287,288].

Next experimental issue concerns energy level positions of the defects generated by VUV photons. The defect photoexcitation current at photon energy of 2.79 eV is found to decrease after VUV-induced degradation while the photocurrent increase is found for the probing photon energy of 3.81 eV indicating that the defect density becomes higher after VUV exposure [263]. This result suggests that the VUV damage oxide network leads to generation of gap states with energy levels in the range 3-4 eV below the SiO_2 conduction band bottom edge. Another important observation consists in partial "annealing" of the VUV-induced leakage current at relatively low temperature (150 °C in Ref. [26], cf. Fig. 4) in close correlation with donor-like Si/SiO_2 interface states which are ascribed to hydrogen atoms bonded to bridging oxygen atoms in SiO_2 network in a hydronium-like configuration $(Si\text{-}HO\text{-}Si)^+$ [289].

Generation rate of these donor states is largely determined by supply of atomic hydrogen to the Si/SiO_2 interface [290]. These centers exhibit slow anneal already at room temperature [291], particularly if they are filled up with electrons [289]. These interface donors provide well distinguishable peak in the interface trap energy spectrum with maximum at about 0.35 eV above the silicon midgap [292], i.e., approximately 0.9 eV above the silicon valence band top edge. If referenced to the SiO_2 conduction band bottom, this energy corresponds to 3.35 eV, in good agreement with results of photoionization experiments [263].

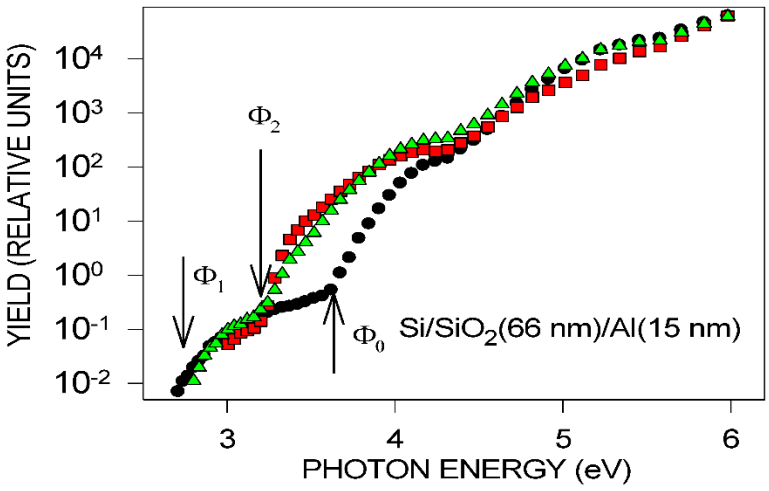

Figure IV.2. Photocurrent quantum yield as a function of photon energy in the Si/SiO2(66 nm)/Al samples prior (black) and after (red) exposure to ≈1x1019cm-2 10-eV photons as measured at the electric

field strength in the oxide of 4 MV/cm under positive metal bias. Green symbols show results for the VUV-exposed sample after subsequent annealing in H2 (1.1 atm) at 400 °C for 30 min. The arrows indicate the spectral thresholds. See Ref. 261 for more detail.

In another experiment intended to estimate the energy of VUV-irradiation generated gap states in SiO_2 the photocurrent spectral distributions were analyzed [261]. On these photocurrent yield (photocurrent normalized to the incident photon flux) spectral curves of the control (non-irradiated) sample shown in Figure IV.2 by filled symbols one can see two spectral thresholds of photocurrent excitation: In addition to the onset of internal photoemission of electrons from the silicon valence band into the oxide conduction band Φ_0, there is a lower threshold $\Phi_1 \approx 2.8$ eV corresponding to excitation of intrinsic oxide traps [293,294]. After VUV-induced degradation additional photocurrent spectral band with threshold $\Phi_2=3.1$ eV becomes clearly visible indicating the energy level of the degradation-induced gap states. An interesting aspect of these states is revealed by exploring the effect of post-irradiation hydrogen annealing at 400 °C routinely used to eliminate radiation-induced damage in Si/a-SiO_2 entities: This anneal does not eliminate these states but clearly affects the spectral distribution of the excited photocurrent, i.e., hydrogen definitely affects the trapped electron states. At the same time, ESR signal from $O_3{\equiv}Si\bullet$ defects (paramagnetic E' centers) disappears entirely after annealing in hydrogen suggesting the silicon dangling bonds to be passivated by H atoms [261]. Therefore, the corresponding energy level has been associated with negatively charged state of H-passivated oxygen vacancies in a-SiO_2 generated during VUV exposure.

Summarizing experimental observations concerning effects of irradiation of amorphous SiO_2 by VUV photons with energy exceeding the oxide bandgap width one may conclude that two types of electron states are generated in the oxide gap due to interaction with protonic hydrogen species: First, due to hydrogen bonding to bridging oxygen the hydronium-like donor states are produced. These states are thermally unstable and account for recoverable fraction of the defects as well as for the associated with them leakage current. Second, at higher VUV exposures protons can break Si-O-Si bridges in the oxide matrix resulting in permanent damage due to O-vacancy formation. Furthermore, subsequent bond rupture events appear to be more probable in vicinity of the already generated O vacancy resulting in clustering of the damage and eventually leading to formation of a breakdown channel.

Now let's address theoretical results which may provide a clue regarding atomic mechanisms of SiO_2 degradation at photon energies lower than the oxide gap (8.9 eV). These considerations include injection of atomic hydrogen (not in protonic form) and electrons since the barrier for hole injection into SiO_2 from an electrode is usually much higher. First, it appears that the presence of strained Si-O bonds in a-SiO_2 gives rise to an additional channel of interaction of H atoms with the oxide networks, predicting the formation of a hydroxyl E_0 center [295]. Hence, atomic H is not always can be seen as a benign agent in

defect-free silica networks. In the contrary, it can produce thermodynamically stable defects in a-SiO_2, adding to the density of dangling bond defects, such as E_0 centers, which are implicated in reliability issues. This result may be of particular relevance for the low-k a-SiO_2-based matrices since they are expected to contain considerable concentration of bonding configurations characterized by extreme angles because the typical low temperature budget (<400 °C for back-end of the line processing) makes structural relaxation impossible. Furthermore, other stable bonding configurations of hydrogen have been predicted including formation of a hydrogen bridge defect at the O-vacancy site [296]. Second, it appears that Si-O-Si bridges with wide bond angle can act as deep traps and accommodate up to two electrons [297]. The latter event results in weakening of a Si-O bond [298] and creates an efficient bond breaking pathway to generate neutral O vacancies and O^{-2}-interstitial ions characterized by low transition barriers. This Frenkel defect formation mechanism is subsequently used to explain intrinsic dielectric breakdown of a-SiO_2 insulators [299]. Again, due to abundance of "abnormal" bonding angles in un-relaxed low-temperature silica matrices this electron injection induced damage mechanism may be of particular importance for low-k insulators irradiated with UV/VUV photons of sub-bandgap energies.

IV.2 Illumination-induced damage of SiO_2 skeleton in low-k insulators.

With the knowledge of radiation response of amorphous SiO_2 matrices discussed in the previous section we can now address the main subject of this paper and start considering effects of UV/VUV illumination on low-k insulators. Since the SiO_2-like skeleton represents the essential part of these materials enabling one to attain sufficient rigidity and the required mechanical properties, there are at least three additional factors which can make the response of low-k insulators to UV/VUV exposure significantly different from that of a-SiO_2. First, the a-SiO_2 matrices discussed above represent high-temperature versions of a-SiO_2 synthesized by thermal oxidation of silicon or by from a synthetic silica molt. These materials have sufficiently relaxed network structure with relatively narrow statistical distribution of Si-O-Si bridge angles around average value of $\approx$144°. However, in the case of low-k insulators the processing temperature is limited by the back-end-of-the-line requirements (<400 °C) which is way too low to allow the network to relax. This factor results in high concentration of network configurations with extreme bonding angles which are expected to be more prone to chemical reactions [295] including those with hydrogen released under UV/VUV illumination conditions from electrodes of the low-k material itself. Second, the low-temperature a-SiO_2 matrices prepared in the presence of organic templates, porogen precursors, or by using spin coating are usually OH-rich as opposed to the a-SiO_2 films thermally grown on silicon or fabricated by O-ion implantation into Si crystal. The latter are usually O-deficient and exhibit characteristic ESR signature of this deficiency – the well-known E'-centers [300,301,302,303,304]. This

difference can clearly be seen from the ESR spectra (Figure IV.3) taken from the "conventional" plasma-enhanced chemical vapor deposited (CVD) a-SiO_2 [k≈4, trace (a)] and two low-k SiO_2-based dielectrics: nano-crystalline silica (NCS) [traces (b)] and porous UV-cured CVD-processed "black diamond" © (BD, labeled as CVD1 through this paper) insulator prior [trace (c)] and after He ion bombardment [trace(d)]) [305]. While the CVD-SiO_2 shows not only the E_γ'-line at g=2.0005 with characteristic powder pattern stemming from dangling bonds of silicon atoms in a-SiO_2 matrix but, also, the 72.5 Gauss doublet associated with the presence of one hydrogen atom in the back-bond of the kernel Si atom, neither NCS nor BD (CVD1) materials exhibit these O-deficiency features. Even after extended VUV (hν=10 eV) exposure no detectable E_γ'-signal can be traced in these samples. Similar observations were also made on other low-k insulators ranging from spin-on glass to self-assembled dielectric layers [306,307]. Only after ion sputtering a "new" ESR signal at g= 2.00247 which can be identified as EX-center representing Si vacancy in a-SiO_2 matrix [308,309] clearly pointing towards O-enrichment in the low-k oxide case. Later high-resolution ESR analysis [310,311] revealed the additional component of the ion-bombardment induced signal tentatively associated with formation of dangling bond defects in oxycarbide clusters since similar signal has also been found in a-SiOC matrices [312].

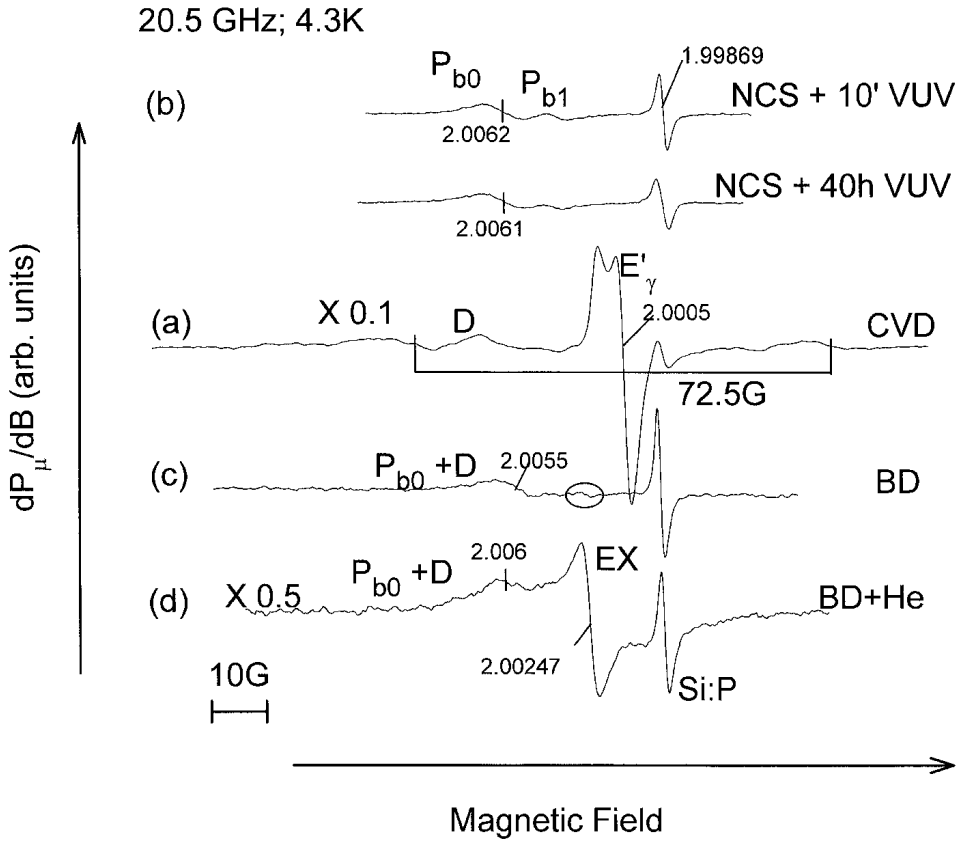

Figure IV.3. Representative K-band ESR spectra measured at 4.3 K on p-Si(100) crystal substrates with 200-nm thick layers of CVD-grown a-SiO2 (k≈4.2) (a), nano-crystalline silica (NCS, k≈2.3, porosity ≈30 %, pore size ≈2 nm) prepared by spin-on coating methyl-silsesquioxane, and CVD-grown carbon-doped oxide (BD, k≈3.0 and ≈7 % porosity, pore size ≈1.8 nm) without (c) and with The plasma surface treatment (d). After initial ESR observations, failing to reveal any signal from the samples (not shown), the samples were exposed to ≈5x10^{17} VUV photons/cm^2 (10 min exposure time) at hν=10 eV to dissociate H from potentially passivated dangling bond defects. The signal at g= 1.99869 stems from a co-mounted Sip marker. See Ref. [305] for more detail.

Finally, it is worth of indicate the third factor which may critically influence properties of the insulating material, i. e., the presence of carbon in the film in various forms ranging from methyl groups (-CH_3) to clusters of elemental carbon originating from porogen or template residuals. In particular, the latter may give rise to deep energy levels in the insulator bandgap causing low-field leakage currents [310,313]. Furthermore, VUV irradiation efficiently modifies the carbon-containing elements of the low-k insulator matrix which is shown to degrade insulating properties of the dielectric film [149,314]. The amount of carbon present in the low-k matrix strongly depends on the fabrication and processing conditions: While the SiO_2-like skeleton exhibits well reproducible bonding features as revealed by X-ray absorption spectroscopy, the amount of carbon present in the organosilicate glass fabricated by self-assembly method appears to be significantly lower than that in the porous films prepared by plasma-enhanced CVD followed by thermal/UV curing [315].

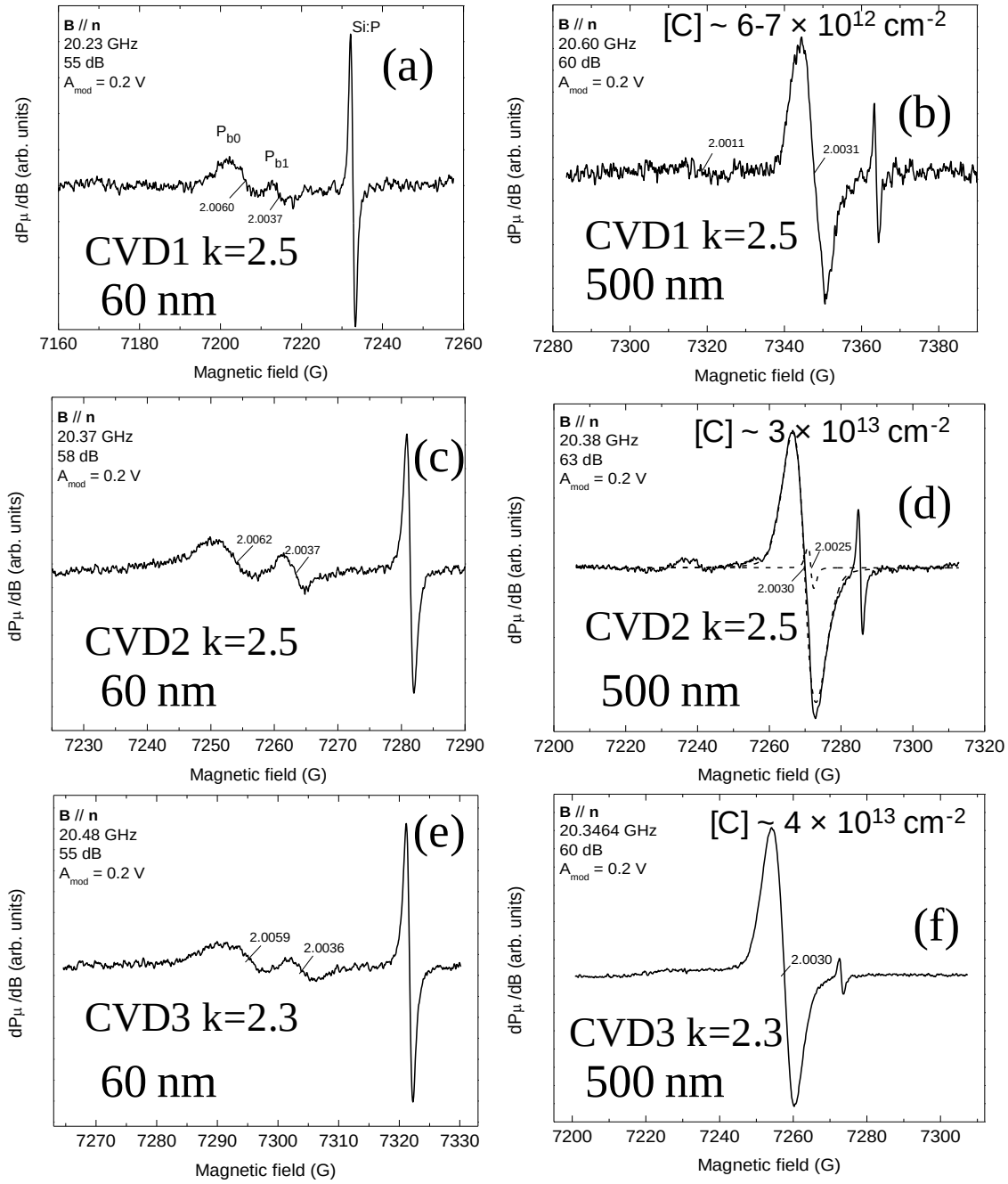

Figure IV.4. K-band ESR spectra observed at 4.2 K on VUV-exposed (≈10^{17} cm^{-2} of 10-eV photons) samples with 60-nm thick CVD1 (k≈2.5) (a, b), CVD2 (k≈2.5) (c, d), and CVD3 (k≈2.3) (e, f) insulators of 60 (a, c, e) and 500-nm (b, d, f) layer thickness. The narrow signal at g= 1.99869, labeled Si:P, stems from a co-mounted marker sample. For more sample details see Ref. [305].

The most dramatic effect is seen, however, in the processing induced variations of the elemental carbon content as revealed by ESR observations of carbon dangling bond defects. This carbon dangling bond

signal at characteristic g≈2.003 has been reported in many studies addressing a broad variety of low-k dielectrics [306,307,316,317,318,319,320,321] and can be considered as qualitative indicator of the carbon presence in the dielectric matrix. The K-band ESR absorption-derivative spectra shown in Figure IV.4 illustrate how significantly several processing factors affect the intensity of the g≈2.003 ESR line in CVD-grown porous low-k materials. First, the simple increase of the film thickness from 60 nm [panels (a, c, e)] to 500 nm [panels (b, d, f)] leads to appearance of the carbon signal suggesting incomplete removal of carbon-containing residuals during UV curing step [308]. Second, changing the UV curing photon spectrum from a broadband [λ>200 nm, sample CVD_1 in panel (b)] to deep UV [λ≈172 nm, sample CVD_2 in panel (d)] while keeping nearly the same porosity of 24-26% leads to many-fold carbon signal enhancement. Next, for the same curing λ=172 nm, further increase of the carbon content is observed when porosity increases from 24 % in sample CVD_2 to 30% in sample CVD_3 [panel (f)]. Taking into account that the intensity of the discussed ESR signal increases even further upon VUV (10 eV) exposure due to hydrogen dissociation from the "passivated" C-H bonds [317], one may conclude that interaction of carbon residuals with radiation should provide significant contribution to the low-k dielectric response to UV/VUV illumination.

Similarly to the case of a-SiO_2, UV/VUV irradiation of low-k dielectrics affects their properties through several physical mechanisms. First, photo-generation [317] or photo-injection [322] of mobile charge carriers results in their trapping leading to formation of built-in charges. High hydrogen content, particularly in porous low-k materials, makes formation of protons even more probable than in the case of thermal a-SiO2 layers explaining dominance of positive protonic charges after irradiation [317,323,324] or electrical stress of low-k insulating layers [314,325]. Upon UV exposure the trapped positive charges can be neutralized by injected electrons [326]. Electron photo-injection experiments also reveal the presence of shallow traps which are absent in a-SiO_2 films thermally grown on silicon [322]. It is also worth of mentioning here that VUV exposure in the presence of oxygen is shown to enrich the layer by silanol (SiOH) groups [197] which, as already mentioned above, represent deep electron traps in a-SiO_2 [273,274].One also may expect that demethylation of a low-k network accompanied with incorporation of polar OH fragments will increase dielectric constant [197]. This effect will be in competition with UV-curing induced increase of porosity by removing organic porogen [327]. Therefore, one may expect that SiO_2-like matrix in low-k dielectrics will become more prone to trapping of both electrons and holes as well as to protonic instabilities after exposure to UV/VUV photons. However, these effects are mostly related to low resistance of C-containing groups against interaction with UV/VUV photons and active gases [245,326,327]. Below we will specifically address the impact of VUV irradiation on a ultra-low-k matrix (CVD1, k≈2.5) which contains no ESR traceable carbon [cf. Figure IV.4, panel (a)].

This experiment has been done using the same approach as in the case of a-SiO_2 thermally grown on Si [259] with close thickness of the CVD_1 low-k dielectric (target k≈2.5) of about 60 nm. ESR spectra taken from the as-deposited film [Figure IV.4, panel (a)] reveal only signals from silicon dangling bond defects (P_{b0} and P_{b1} centers) at the substrate side of the (100)Si/low-k interface. The same spectrum is found after extended exposure (≈106 s) to VUV (hν=10 eV photons, flux ≈$1x10^{15}cm^{-2}s^{-1}$) generated byresonantly-excited Kr discharge and transferred to the sample surface through MgF_2 window and a 0.2-mm air gap. The absence of any measurable oxide defect density even after such high-dose irradiation is consistent with results obtained on other low-k materials, see, e.g., panel (b) in Figure IV.3 for VUV-exposed nano-crystalline silica sample. The picture is changed dramatically if the surface of low-k oxide is covered by semitransparent (15-nm thick) layer of aluminum thermo-resistively evaporated in vacuum on unheated samples surface. The presence of such Al "blanket" dramatically increases concentration of atomic hydrogen released by VUV photons [259] by (probably) preventing it out-diffusion. In the Al-covered CVD1 low k films after 106 s exposure to 10-eV photons several effects are observed:

- Low-field (1 MV/cm) leakage current increases by a factor of ~10^2, i.e., from ≈$4x10^{-12}A/cm^2$ to $(5\text{-}6)x10^{-10}A/cm^2$ suggesting generation of deep gap states;
- Indeed, comparison of the photocurrent spectra (positive metal bias) measured prior and after VUV exposure and shown in Figure IV.5 reveals the increase of the yield by several orders of magnitude in spectral bands with thresholds of 3.1 and 4.2 eV, i.e., the same as found VUV-degraded thermally-grown a-SiO2 on Si [261];
- Supporting this picture, ESR measurements on samples exposed to VUV photons for extended time (106 s) succeeded in revealing generation of previously not observed in low-k dielectrics E'-enters (g≈2.0005) with areal density ≈$6x10^{11}cm^{-2}$.
- Capacitance-voltage (CV) curves (Figure IV.6) reveal significant increase of low-frequency capacitance which might be due to irradiation-induced formation of highly polarizable species in the low-k matrix. Interestingly, at 1 MHz the CV traces show virtually no capacitance change after VUV exposure suggesting that the frequency dispersion in accumulation capacitance is caused by series resistance of 15-nm thin Al electrode which is unaffected by irradiation. Then, the observed large increase in the low-frequency accumulation capacitance should be due to water (or similar) species formed by O atoms removed from the bridging positions in the SiO_2 skeleton matrix by the mechanism similar to that encountered in VUV-exposed a-SiO_2 [259].

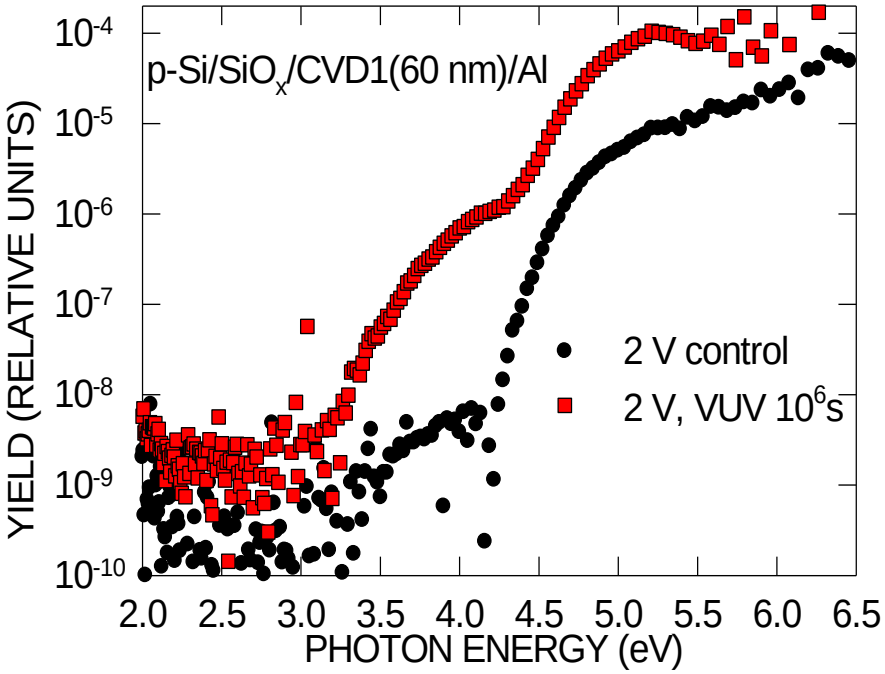

Figure IV.5. Photocurrent quantum yield as a function of photon energy in the Si/CVD1 (60 nm)/Al samples prior (black) and after (red) 106 s exposure to 10-eV photons (external flux $\approx 1 \times 10^{15} cm^{-2} s^{-1}$) as measured at 2 V positive bias voltage applied to the top Al electrode.

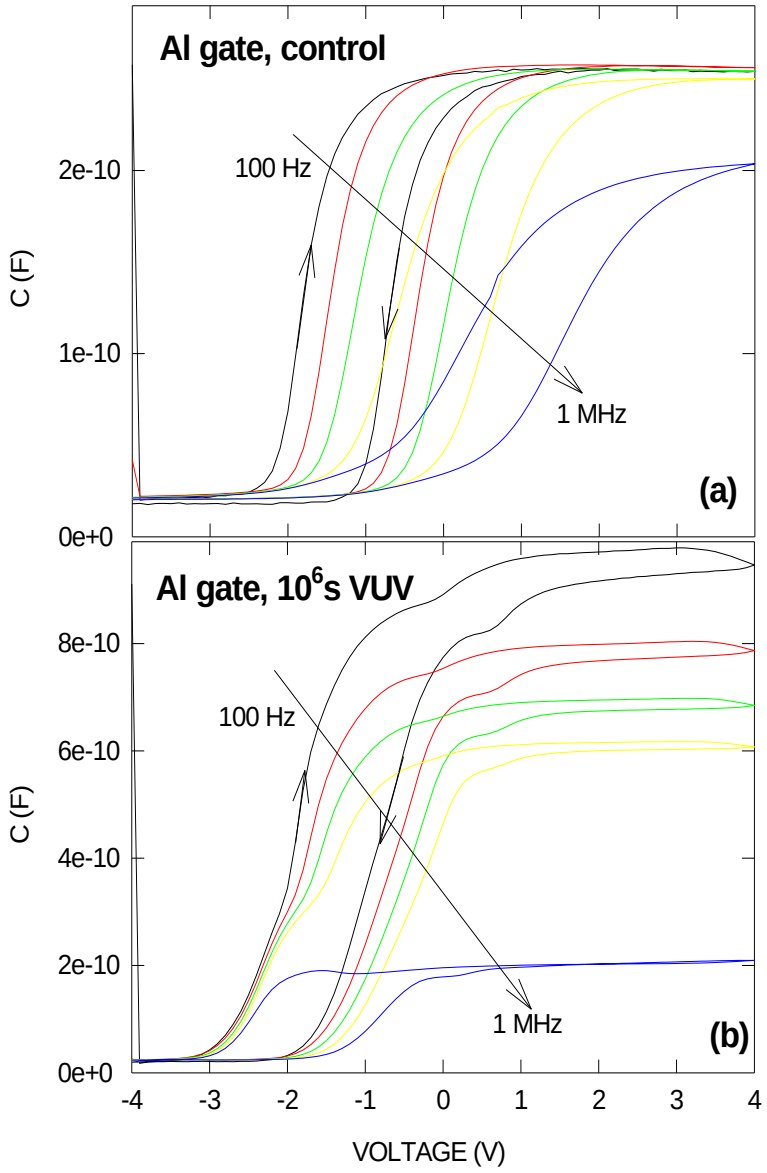

Figure IV.6. Bidirectional multi-frequency capacitance-voltage traces as measured on the Si/CVD1 (60 nm)/Al samples prior (a) and after (b) 106 s exposure to 10-eV photons (external flux ≈1x10^{15}cm^{-2}s^{-1}). Are of top Al electrode is ≈0.5 mm^2. Notice different capacitance axis scales in panels (a) and (b).

All in one, these observations suggest that exposure to VUV can damage the SiO_2 skeleton of porous low-k insulator under conditions of sufficient hydrogen supply. This process looks very similar to the VUV-induced damage of thermally-grown a-SiO_2 films [259] which can be understood as photon-

assisted electrochemical reduction of the oxide. Importantly, however, is that the density of the Si dangling bond defects detected by ESR as E' signal in thermal SiO_2 [259] exceeds that in the porous low-k oxide by three orders in magnitude despite the total (external) dose of 10-eV photons approaching 10^{21} cm^{-2} in the last case. As a hypothetical explanation one can suggest an enhancement of geminate recombination probability of photo-generated electrons and holes due to their spatial confinement in nanometer-sized SiO_2 skeleton fragments. As a result, the concentration of free charge carriers which are needed for network damage will be dramatically reduced. In any case, we may conclude that substantial degradation of low-k insulators experimentally observed at much lower exposures to UV/VUV light is probably caused by impact of radiation on other than SiO_2 skeleton fragments of the material network, e.g., on the carbonaceous fragments.

Strong spectroscopic hint in this direction has been provided by observation that in SiCN diffusion barrier layers development of leakage current upon exposure to UV photons ($h\nu$= 4.9 eV) correlates with generation of ESR-active defects with characteristic $g\approx2.003$ and line-width of 11^{-12} Gauss [328,329].Though, based on the g-value, these centers were initially assigned to dangling bonds of silicon atoms similar to K-center in N-rich silicon nitrides [328], the use of PECVD synthesis at 400 °C from $Si(CH_3)_4$ and NH_3 precursors makes possible incorporation of elemental carbon in the SiCN matrix. Indeed, if applying similar precursor chemistry [$Al(CH_3)_3$ and NH_3] to synthesize AlN films, one can find the same ESR signal (not shown here) though no silicon is present in the material at all. Taking into account the absence of significant hyperfine splitting (or line broadening) expected for paramagnetic centers with Al or N atom in the kernel, in the latter case one can firmly assign the center at $g\approx2.003$ to the dangling bonds of carbon atoms. Worth of adding here is that similar ESR signal has also been observed in porous nitrogen-free SiOCH films after UV exposure ($\lambda\approx200$ nm) and then assigned to carbon-containing defect configurations [330]. Therefore, in the coming sections we will address the impact of carbonaceous species and porosity on VUV-induced damage of low-k insulators.

IV.3. Illumination-induced charging of low-k dielectrics

A critical challenge in plasma processing of porous OSG low-k materials is their sensitivity to charging, chemical and physical damage and time-dependent dielectric breakdown (TDDB) failure as a result of plasma exposure.[331,332,333,88] During plasma processing, ion bombardment, VUV irradiation, and free-radical flux can occur.[334,335, 95 ,158] These are of concern because the critical dimensions are now the same size as the penetration depth of particles and photons.

VUV radiation has been found to introduce photoconductive effects[336,337] which govern the density and location of trapped charges within the dielectric.[338,339,340] In addition, trapped charges generated by VUV irradiation of low-*k* dielectrics have been shown to adversely affect the capacitance,[341] breakdown voltage,[342] and leakage currents[343,344] without any chemical or structural change in SiCOH. This section demonstrates how VUV irradiation causes generation of trapped charges in SiCOH and how it can be reduced. In describing ways to reduce trapped charges, we also describe methods to determine the number of trapped charges in the dielectric.[345]

VUV irradiation of dielectrics can cause electron-hole pair generation, photoconduction, photoemission and photoinjection of electrons from the substrate into the dielectric.[346, 347] These processes depend on the incident photon energy and the dielectric composition and thickness. Electron-hole pairs will be formed if electrons are excited into the conduction band from the valence band or from defect states within the dielectric. The behavior of photoconduction, photoemitted and photoinjected electrons will then depend on the energy of the generated electron. That is, depending on their energy, the electrons and holes can travel in the dielectric, *i.e*, photoconduction or remain trapped at a fixed location. It is expected that electrons will dominate photoconduction, photoemission and photoinjection, because the mobility of electrons is much larger than the mobility of holes.[348]

When the energy supplied by irradiation is greater than the sum of the bandgap energy and the electron affinity (*i.e.*, photoemission threshold), photoemission can occur from the valence band of the dielectric and/or the defect states in the bulk of the dielectric.[349] An electron with energy lower than the photoemission threshold could gain additional energy from another process and be photoemitted. Thus, photoemission from the defect states leads to depopulation of electrons from the dielectric. Therefore, after photoemission, a dielectric develops a net positive charge.

Photons with energies greater than the bandgap energy but lower than the photoemission threshold, will create electron-hole pairs, which remain within the dielectric layer. The electrons

and holes may separate due to their initial energies and/or the presence of an electric field within the dielectric layer resulting in a photoconduction current.

In addition to VUV photons being absorbed in the dielectric, they can also be absorbed in the substrate. For this to occur, the photons must penetrate through the dielectric. Photoabsorption in the substrate can thus result in electron-hole pairs begin created in the substrate. Similarly to the dielectric, electrons in the substrate can photoconduct. In addition, these electrons can be photoinjected into the dielectric. For photoinjection to occur, the substrate-dielectric interface-energy barrier should be less than the energy of the electrons. For example, the Si-SiCOH interface has an energy barrier of 4±0.5eV.[341] As a result, only electrons in silicon with energies greater than 4.5eV can be injected into SiCOH from Si. A reverse process whereby electrons are injected from the dielectric into the substrate can also occur. However, the probability of an electron being injected from the substrate into the dielectric is higher since the electrons generated in the substrate tend to have a higher energy than the ones in the dielectric because the bandgap of Si is smaller than that for SiCOH. Photoinjection can be further enhanced by the presence of trapped charges in SiCOH at the interface that reduces the interface energy barrier by acting as a low-energy conduction pathway.[350]

It is plausible that photoinjected electrons generate a drift/diffusion current from the substrate-dielectric interface to the dielectric-vacuum interface, where electrons can be photoemitted.[351,352] Thus, at any given time during VUV irradiation, photoemitted electrons are the result of 1) depopulated electrons from the defect states and 2) photoinjected electrons. Trapped charges from the depopulation of defect states will continue to be created until a steady state is achieved. At this point, no more net trapped charge will be generated in the dielectric and the photoemitted electron flux will then be equal to the flux of the photoinjected electrons. In order to have a complete circuit, charge conservation dictates that when the substrate is connected to ground, the photoemitted electrons are returned to the substrate. Thus, under these conditions in steady state, the photoemission current is equal to the substrate current.

Each of the three primary processes (photoemission, photoinjection, and photoconduction) competes with the others to influence charge accumulation during VUV irradiation. Photoemission of electrons from defect states *depopulates* these states of electrons, resulting in accumulation of net positive charge. Conversely, photoinjection can *repopulate* vacant defect

states in the dielectric with electrons from the substrate, resulting in a net depletion of trapped positive charge.[353,354,355,356,357]

IV.4. Effect of UV Curing on Charge Trapping

In device fabrication, chemical-vapor deposited SiCOH glass is often cured with ultraviolet (UV) irradiation.[358] UV curing is advantageous, yielding the benefits of improved hardness and corrosive strength of the dielectric.[359,360] However, by comparing the photoemission currents and surface-potential measurements for pristine SiCOH and UV-cured SiCOH, it is seen that more positively charged traps are generated in the UV-cured SiCOH compared to pristine SiCOH.[361] Furthermore, although UV curing reduces the number of defect states, we find that it also increases both the intrinsic and photoconductivities of SiCOH.

In most cases, photoemitted electrons are collected and returned to the grounded substrate and then injected back into the dielectric. These electrons can travel to the vacant states in the valence band.[362] As these electrons flow back to the substrate, during steady state, the magnitude of the surface potential across the dielectric will depend on the parallel combination of the intrinsic and photo conductivities of the dielectric.[362,363] By finding the combined conductivity in this way and then finding the intrinsic conductivity as described below, the photoconductivity can be determined.

The intrinsic conductivity can be computed from the trapped-charge decay rate after VUV irradiation.[364,365] The trapped positive charges recombine with free electrons under influence of the self-consistent electric field.[365] In the absence of VUV photons, the drift motion of electrons under the influence of the self-consistent electric field in the dielectric is determined by the intrinsic conductivity. Since the surface potential is a measure of the amount of trapped charge in the dielectric, then from the decay rate of the surface potential the intrinsic conductivities and photoconductivities of both pristine and UV-cured SiCOH can be found and compared.[366]

Then, by comparing the surface potential as a function of time after irradiation, we find that trapped charges in the UV-cured sample decay faster. Thus, the charge-decay time constant for a UV-cured sample can be as much as five times that of the pristine sample. Typically, a UV-cured sample has only a few percentage more trapped charges after VUV irradiation. However, the time taken for the trapped charges in the UV-cured SiCOH to decay can be up to one third of that for

pristine SiCOH. Thus, we can infer that the UV-cured dielectric films have a higher intrinsic conductivity.

After VUV irradiation, VUV photoemission spectroscopy was measured for comparison with the pristine samples. The spectroscopy showed two important differences. First, for photon energies less than 8.5 eV as shown in Figure IV.7, the photoemission/substrate current measured during VUV photoemission spectroscopy for pristine SiCOH is larger than the corresponding current for UV-cured SiCOH. This occurs because, for photon energies less than 8.5eV, photoemission can occur only from the defect states in the bandgap. Since the photoemission current will then be proportional to the number of defect states, we can conclude that pristine SiCOH has more defect states in the bandgap as compared to UV-cured SiOCH. On the other hand, for photon energies higher than 8.5 eV, the photoemission current for UV-cured SiCOH is larger than that for pristine SiCOH. This is because for energies greater than 8.5eV, photoemission can occur directly from the valence band in addition to the photoemission from the defect states. In steady state, the photoemitted electrons are replaced with photoinjected electrons. These photoinjected electrons have to drift/diffuse to the surface of the dielectric to be photoemitted. Therefore, in steady state, the drift/diffusion current will be equal to the photoinjection current that in turn is equal to the photoemission/substrate current. Thus, as described above, the surface potential measured in steady state is determined by the parallel combination of the intrinsic and photoconductivities since the photoinjected current may be considered as a current source. Since the intrinsic conductivity can be calculated as described above, the photoconductivities for pristine and UV cured samples can easily be extracted from the surface potential and the steady-state current.

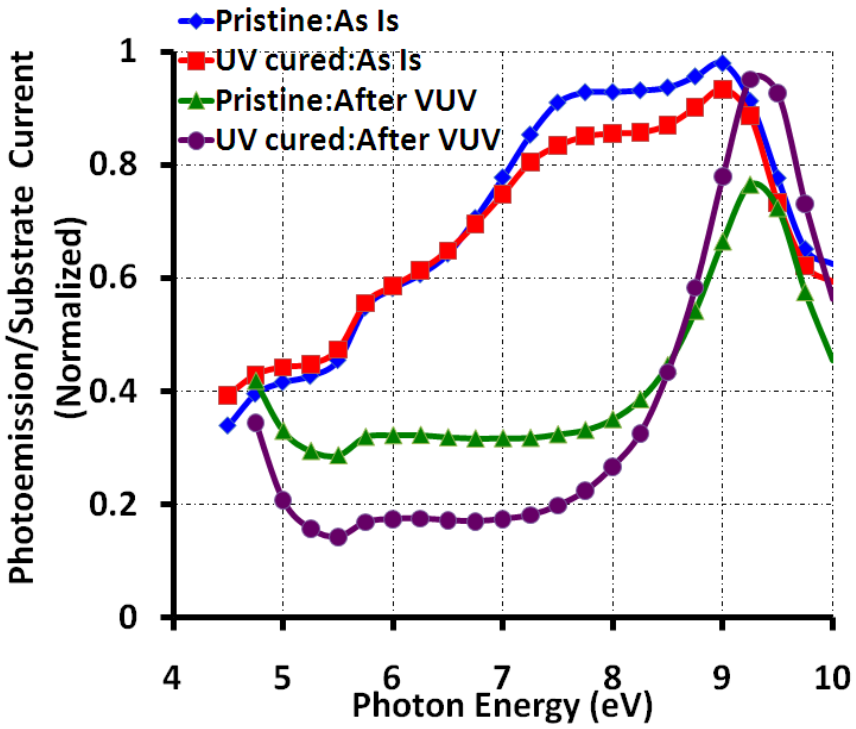

Figure IV.7. VUV spectroscopy at 4.5-10 eV for pristine and UV cured SiCOH before and after 8-eV VUV irradiation.

Hence, we can conclude that UV-cured SiCOH has fewer defect states than pristine SiCOH, especially if the comparison is made after VUV irradiation. In addition, the UV-cured SiCOH has a higher photoconductivity. From calculations of the trapped charge, we find that UV-curing increases the number of trapped charges generated in SiCOH under VUV irradiation for the same photon dose and energy.

IV.5. Effect of Dielectric-Substrate Interface on Charge Trapping

In BEOL processing, a SiCOH/SiCN stack is typically deposited on an exposed Cu/SiCOH following CMP, whereas the work reported in the previous section was for simple stacks of SiCOH/Si. The purpose of this section is to indicate what differences in VUV response are observed for industrially relevant SiCN/SiCOH/SiCN/Cu stacks exposed to plasma etch, as compared to samples on Si with or without native oxide.[364,367,368] Here, dielectric films deposited on Cu and, for comparison, model Si/SiO_2 films, were irradiated with VUV photons having

energies and fluxes typically generated during plasma processing. It was found that the nature of the dielectric-substrate interface changes the number of trapped charges in the dielectric.

To investigate the effect of different dielectric-substrate interfaces on charge trapping, a dielectric stack consisting of 15 nm SiCN (k=5)/ 175nm SiCOH (k=2.4)/ 15 nm SiCN (k=5) was deposited with plasma-enhanced chemical vapor deposition on the following substrates. (1) Si, (2) Si with 5-nm of thermally grown oxide, (3) Cu/ Ta/NiSi deposited on Si. SiCN forms an interface with these three substrates.

All of the samples have the same dielectric stack but have different dielectric-substrate interfaces. The dielectric stack deposited on silicon was used as a reference and compared with the other two. In comparison to the reference sample, the presence of a thin thermally grown oxide layer reduces the density of interface defect states.[356] This occurs because the dangling bonds from the silicon-crystal termination are reduced in the presence of the oxide.[369]

The reduced interfacial states result in a smaller Fowler-Nordheim tunneling current. Fowler-Nordheim tunneling is associated with electrons tunneling from the semiconductor Fermi level into the dielectric conduction band. Under Fowler-Nordheim conditions, it is possible for charge to tunnel from the valence band of the substrate into a trap/defect state in the bandgap of the dielectric. Thus, the number of interface states controls the tunneling current. Hence, the net injection current into the dielectric from the substrate will be smaller when there are fewer interface states. A lower injection current means less repopulation of the depopulated defect states, since, as stated previously, the steady-state condition is the result of a balance between depopulation by photon excitation and repopulation by injection. Hence, more positively charged traps remain in the sample deposited on Si with the interfacial thermal oxide as compared with the reference sample.

Figure IV.8 shows the photoemission/substrate current measured during the 8-eV irradiation. As expected, the substrate current decreases with increasing photon dose for the three samples. The current is found to be same for all three samples at the lower doses. This is because the samples are fabricated with the same dielectric stack and hence, they are likely to generate the same number of photoemitted electrons from depopulation of the dielectric. This will occur until the dose increases so that the self-consistent electric field created by the trapped positive charges builds up to a sufficiently high level to change the photoemission/substrate currents.

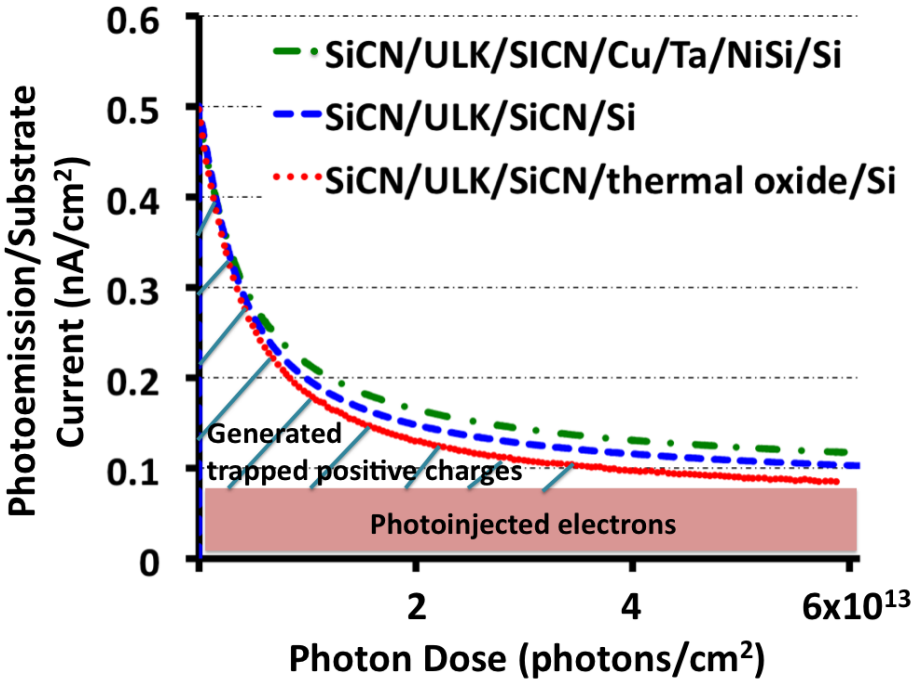

Figure IV.8. Photoemission flux of SiCN/SiCOH/SiCN deposited on Cu, Si, and Si with thermal oxide as a function of dose of 8-eV VUV photons.

In steady state, we find that the dielectric deposited on copper has the largest photoemission current, whereas the dielectric deposited on Si with the interfacial thermal oxide has the lowest steady-state photoemission current. This occurs because the SiCN-Cu interface has a lower energy barrier (0.9 eV) in comparison to SiCN-Si (1.7eV).[370,371,372] On the other hand, the interface energy barrier between SiCN and Si with thermally grown oxide is higher than SiCN-Si because of reduced dangling bonds in the presence of the oxide.[359]

The number of trapped charges per unit area generated as a function of photon fluence per unit area can be calculated from the photoemission current measurements, as described previously. The calculated value of trapped charges for the three samples after a VUV photon dose of 5.9×10^{13} photons/cm^2 is shown in Table IV.1. The injection current, which is sum of the photoinjection and Fowler-Nordheim tunneling currents, is also listed in Table IV.1. From the tabulated data, the inverse relation between the number of trapped charges in the dielectric and the magnitude of the injection current is verified. The dielectric deposited on Si with an interfacial thermal oxide had

the most trapped charges per unit area, followed by the dielectric stack on Si. The dielectric stack on Cu had the smallest number of trapped charges per unit area.

Table IV.1. Comparison of trapped charges generated by 8-eV VUV photons and photoinjection flux for SiCN/SiCOH/SiCN deposited on Cu, Si and Si with thermal oxide. The percentage increase or decrease in the trapped charge compared with the reference (top line) sample is indicated in the left-hand column.

	Trapped Charges (#/cm^2)	**Photoinjection Current (pA/cm^2)**
Stack/Si	2.25×10^{11}	103.4
Stack/oxide/Si	2.49×10^{11} (+10.7%)	84.6
Stack/Cu	2.00×10^{11} (-11.1%)	118.2

The results obtained from the substrate-current measurements were validated with VUV spectroscopy measurements between 4.5-12 eV. These are shown in Figure IV.9. We observe that the VUV spectroscopy curves for the three samples before irradiation are similar. These variations in the VUV spectroscopy curves are again likely the result of the low-level but unavoidable irradiation during VUV spectroscopy. The photon flux was made as small as possible. However, after 8-eV VUV irradiation, the dielectric stack on Cu had the largest VUV spectroscopy current while the dielectric stack on Si with thermally grown interfacial oxide had the lowest VUV spectroscopy current. This result is true for any photon energy between 4.5 and 12 eV and is consistent with the substrate/photoemission measurements discussed earlier.

Thus, we find that the nature of the dielectric-substrate interface changes the number of trapped charges generated in the dielectric under VUV irradiation. As stated earlier, this is because a lower dielectric-substrate interface energy barrier increases the photoinjection current, thereby reducing the number of trapped charges generated in the dielectric. Inversely, a lower photoinjection current due to a higher dielectric-substrate interface barrier energy increases the number of trapped charges generated in the dielectric. Also, the higher Fowler-Nordheim tunneling currents due to the

increased number of interface defect states increases the injection current and reduces the number of trapped charges generated in the dielectric during VUV irradiation.

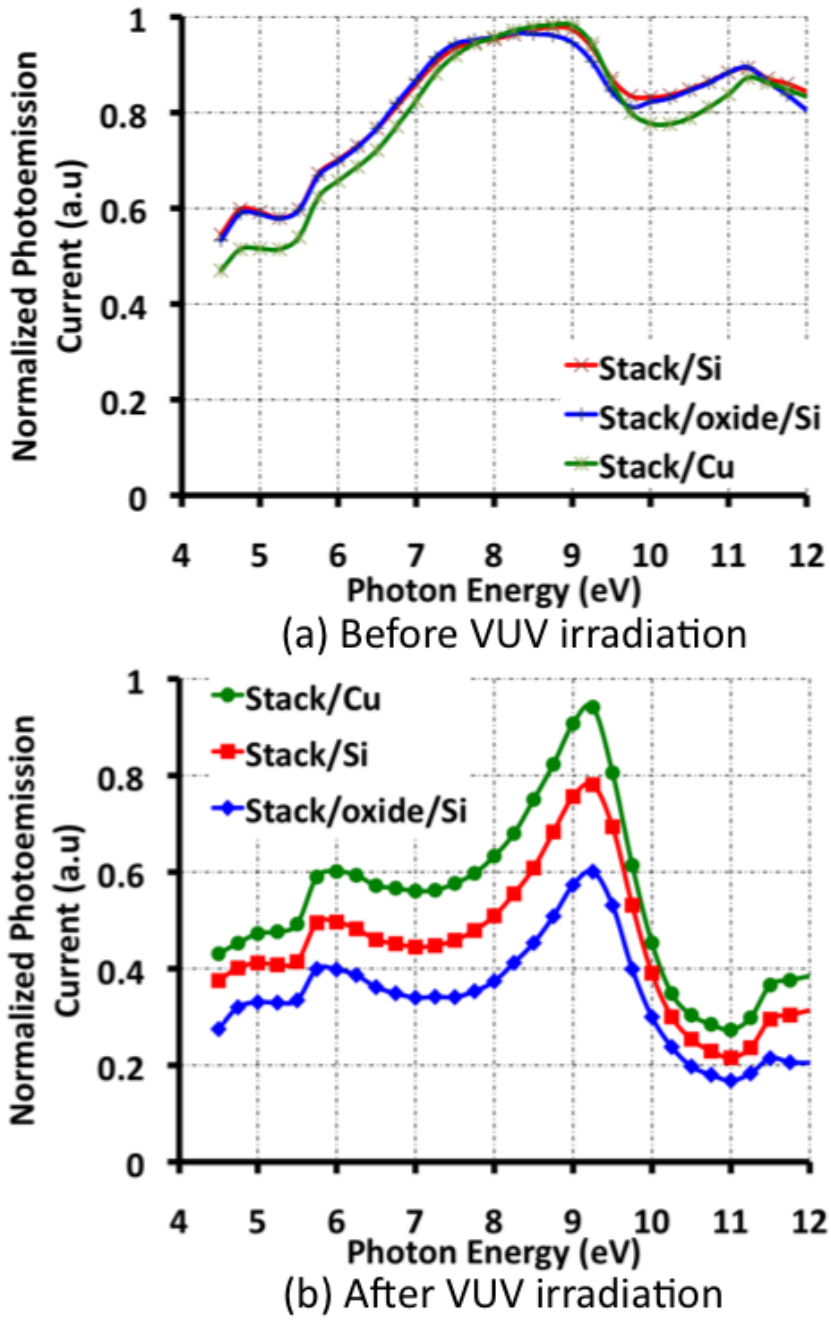

Figure IV.9. VUV spectroscopy at 4.5-12 eV for SiCN/SiCOH/SiCN deposited on Cu, Si and Si with thermal oxide (a) before VUV irradiation (b) after 8-eV VUV irradiation.

IV.6. Effect of Porosity on Charge Trapping

The dielectric constant of SiCOH can often be reduced by introducing porosity.[359,80] However, higher porosities show an increase in the number of trapped charges generated from incident VUV irradiation.[373,374] VUV photoemission spectroscopy, photoemission current, capacitance-voltage characteristics and surface potential measurements are used to determine number of trapped charges generated for the three cases.

Typically, nanopores of size 2.5nm or less are introduced in SiCOH to reduce the dielectric constant.[80] However, the nanopores can act as charge-trapping centers.[363] That is, charges aggregate along the boundaries of pores and remain trapped. Thus, the number of trapped charges in SiCOH will change as the porosity increases.

The number of trapped charges generated per unit dose of VUV irradiation depends on the photoabsorption coefficient of the dielectric. The higher the photoabsorption coefficient, the more charges will be trapped. It has been reported that VUV photoabsorption increases with increasing porosity of SiCOH. Thus, it is indeed plausible that for the same dose of VUV photons, higher porosity (lower dielectric constant) SiCOH will have more trapped charges in comparison to lower porosity (higher dielectric constant) SiCOH.

To investigate the effect of porosity on charge trapping, SiCOH with dielectric constants of 3.0 and 2.65 were deposited with thicknesses of 458nm and 444nm, respectively, on Si followed by UV curing. After UV curing, surface-potential measurements and C-V measurements were made. The samples were then exposed to a fluence of $7x10^{13}$ photons/cm^2 of 8 eV VUV photons. The photoemission/substrate current was measured as a function of time/dose during irradiation. After VUV irradiation, the surface potential and C-V measurements were repeated.

Figure IV.10 shows the photoemission/substrate current of SiCOH for k=2.65 and k=3.0 as a function of the 8-eV VUV photon dose. Both measurements were made during the same synchrotron beam-current condition. The sample with k=2.65 shows a higher photoemission/substrate current for the same VUV irradiation flux rate. This means that a higher percentage of photons was absorbed in the k=2.65 dielectric film. This is validated by a VUV reflectance measurement for the two samples, which is shown in Figure IV.11. The reflectance shows that the film with k=2.65 has a lower reflectance, *i.e.*, a higher photoabsorption.

The photoemission/substrate currents for the films with k=2.65 and k=3.0 as a function of photon dose can also be compared. With increasing VUV photon dose, more trapped charges are

generated, which results in a higher self-consistent electric field. The self-consistent electric field reduces photoemission. As shown in Figure IV.4, the slope of the photoemission/substrate current curve as photon dose increases changes rapidly for the film with *k*=2.65 in comparison to the film with *k*=3.0. This is likely because a larger self-consistent electric field builds up in the *k*=2.65 dielectric in comparison to the *k*=3.0 dielectric for the same VUV photon dose. Hence, we infer that more trapped charges are generated in the SiCOH with *k*=2.65 for the same VUV photon dose.

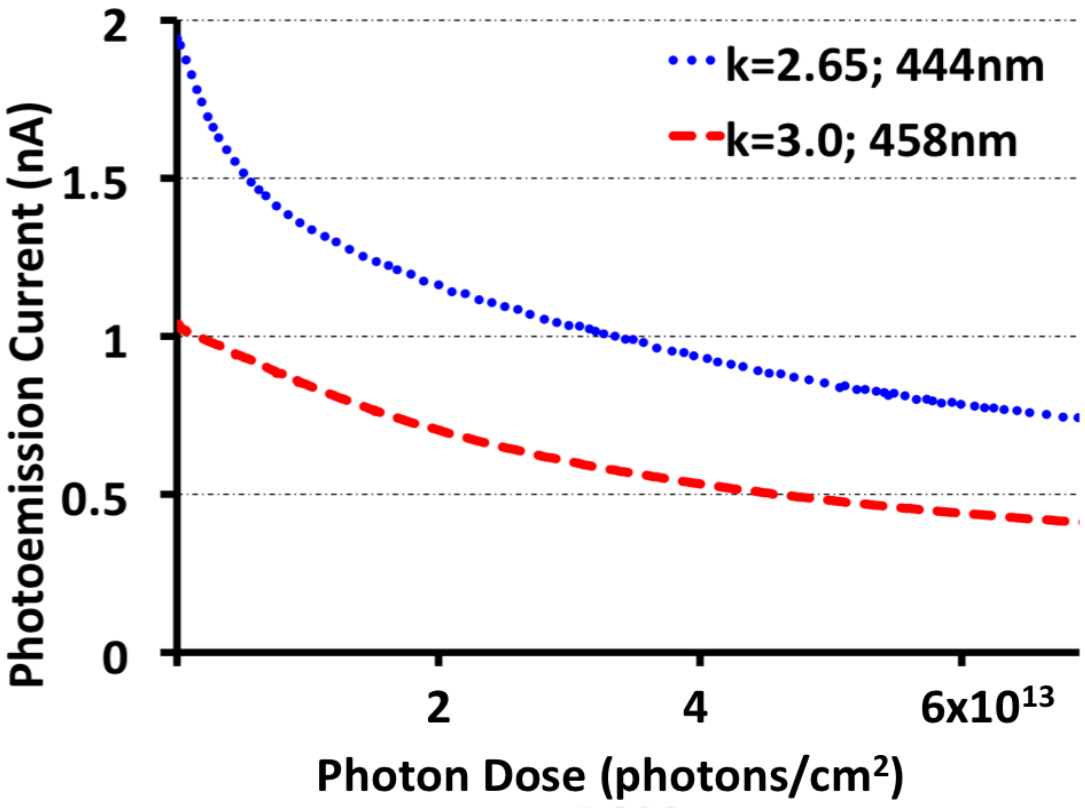

Figure IV.10. Photoemission/substrate current of k=2.65 444nm and k=3.0 458nm SiCOH as a function of increasing 8-eV VUV photon dose.

The number of trapped charges generated from VUV irradiation is calculated from the photoemission/substrate current as was shown previously. For the *k*=2.65 dielectric, a photon dose of $7x10^{13}$ photons/cm^2 generated 3.7 $x10^{11}$ trapped charges per square cm of the irradiated sample whereas for the *k*=3.0 dielectric, only 2.3 $x10^{11}$ trapped charges per square cm were generated. This result can also be confirmed with surface-potential measurements. The surface potential increased by 5.4 V for the *k* = 2.65 dielectric, but increased only by 3.7 V for the *k* = 3.0 dielectric.

This is consistent with the shift in the flat-band voltage of the C-V characteristics as was shown previously. A summary of these results is shown in Table IV.2.

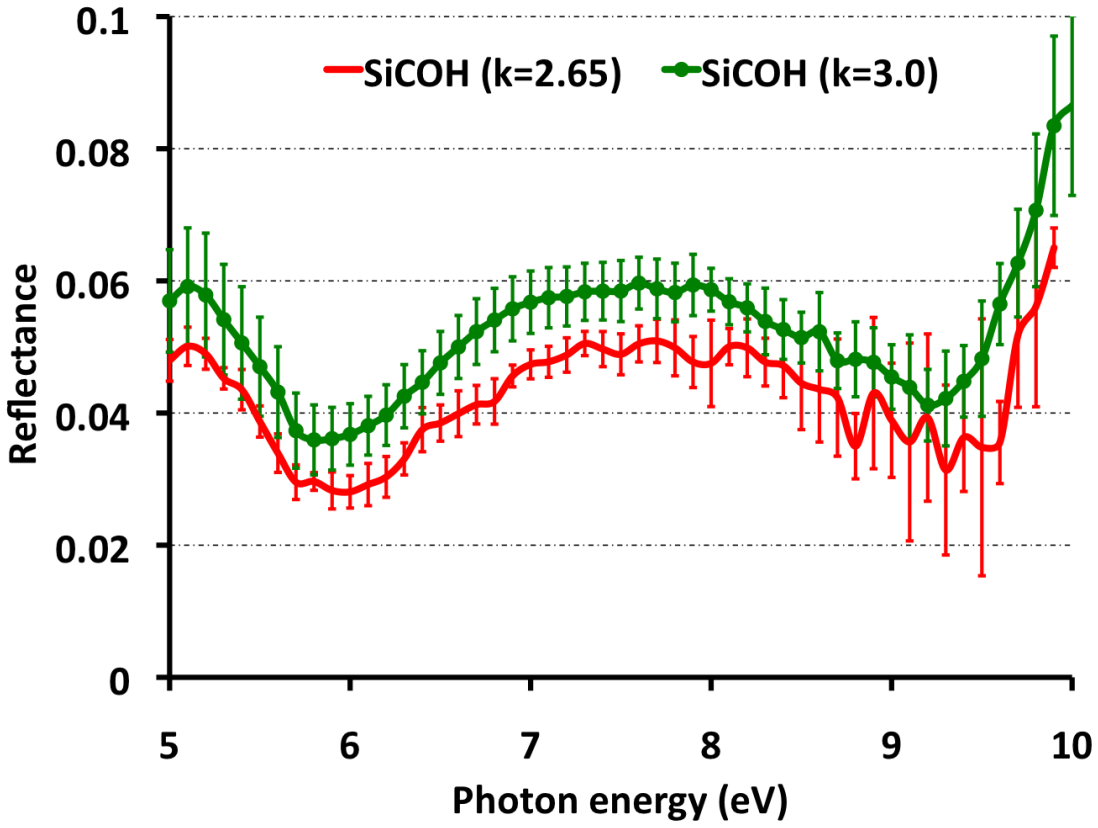

Figure IV.5. Measured reflectance for k=2.65 and k=3.0 SiCOH for 5^{-10} eV photon energies.

Table IV.2. Trapped charges, surface potential and C-V characteristic flat-band voltage shift for k=2.65 444 nm and k=3.0 458 nm SiCOH after 8-eV VUV irradiation.

	k=2.65,444nm	**k=3.0,458nm**
Trapped Charges (#/cm2)	3.65×10^{11}	2.29×10^{11}
Surface Potential(V)	5.4	3.7
C-V flat-band voltage shift (V)	(-) 5.9	(-) 4.2
Photoinjection Current (pA)	0.739	0.41

Thus, it can be concluded that trapped charges in SiCOH due to VUV irradiation during processing are dependent on the porosity of the dielectric. More trapped charges are generated in higher porosity SiCOH for the same photon dose. By analyzing measurements of photoemission currents and VUV spectroscopy, C-V characteristics and surface potential measurements, it was found that VUV irradiation depopulates electrons in the defect states leaving the trapped positive charges in the dielectric. The number of positively charged traps generated by VUV irradiation during processing is altered by the material properties of SiCOH. More trapped charges per unit photon dose are generated in UV-cured SiOCH than in pristine SiCOH during VUV irradiation. Although there are major advantages to UV curing of low-*k* dielectrics, there are thus some deleterious effects on its intrinsic and photo conductivities as well as enhanced charge trapping that are of importance in plasma processing of low-*k* SiCOH. In addition, changing the dielectric-substrate interface can change the number of positively charged traps generated in the dielectric during processing. Higher porosity in SiCOH has the advantage of a lower dielectric constant, but has the disadvantage of more positively charged traps being generated during VUV irradiation. It is likely that the increase in trapped charge is ascribed to higher photoabsorption and charge trapping around the nanopores. Consequently, modifications of the porosity, the dielectric-substrate interface and the UV curing process can be used as parameters to reduce positive charge accumulation during processing of low-*k* SiCOH.

V. Applications of UV and VUV Light in Nanofabrication

In this section we'll review current, potential near term, and longer term applications of UV- and VUV-assisted processing with a focus on low-k materials. Since UV processing for low-k dielectrics also affects other films we also review those as well. We also review learning from other areas that aids our understanding of photon-induced effects in low-k films and because low-k film usage can require gentler processing of other materials. Current applications are those now used in high volume manufacturing, HVM, or for which HVM capable tools are available. Potential near term applications are those in development on HVM-capable tools. Potential longer term applications are those in various stages of research. Applications have been mostly limited to UV light. Commercial UV systems were more readily available, and UV has a deeper penetration depth than VUV in most materials.

V.1. Current Applications

UV curing of pSiCOH low-κ films is the most widely used application of photon-assisted processing. This was covered in depth in Section II and will not be discussed here. Other current applications of photon-assisted processing are UV-assisted repair of plasma damaged pSiCOH and film stress engineering.

V.1.1. UV-assisted Low-κ damage Repair

pSiCOH low-κ films contain both carbon and porosity to lower their dielectric constants. Incorporating carbon, primarily in the form of Si-CH_3 groups, lowers the density of the SiO_x network by reducing Si-O-Si crosslinks.[2] Adding carbon also makes the film more hydrophobic, which lowers κ by reducing the moisture content. Also, moisture can break strained surface Si-O-Si bonds, such as on pore surfaces, to form SiOH, which is polar and increases the film's κ and makes the film hydrophilic resulting higher interconnect wire capacitance. Plasma damage to pSiCOH removes the $SiCH_3$ bonds forming dangling bonds, SiH, $SiNH_x$, or other bonds (depending on plasma chemistry), which are mostly converted to SiOH upon air exposure, Equations V.1 and V.2.[375,112]

$$SiCH_3 \xrightarrow{plasma} SiOH + defects + other\ chemical\ modifications \quad \text{(V.1)}$$

$$Ion\ bombardment \longrightarrow densification \quad \text{(2)}$$

Reactions 3 and 4 show an example of how an NH_3-based plasma damages pSiCOH.[203]

$$\equiv SiCH_3 + NH_2\cdot + H\cdot \longrightarrow \equiv SiNH_2 + CH_4\uparrow \quad \text{(V.3)}$$

$$\equiv SiNH_2 + H_2O \longrightarrow \equiv SiOH + NH3_3\uparrow \quad \text{(V.4)}$$

The damage layer typically consists of an outer layer that is nearly carbon depleted followed by a layer of increasing carbon concentration up to the bulk, undamaged film, Figure V.1. The outer carbon depleted layer is typically denser than the pristine material due to silanol condensation reactions and ion bombardment.

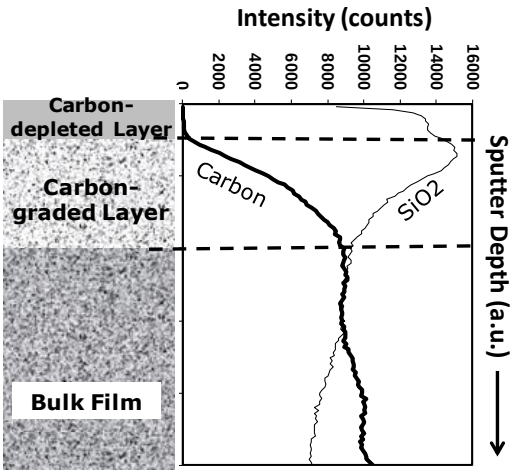

Figure V.1. An illustration of a typical plasma-induced damage layer in pSiCOH with a ToF-SIMS depth profile of the carbon and oxygen (SiO_2).

This also degrades the electrical strength of the pSiCOH as measured by voltage breakdown and leakage current. The electrical strength of the film is critical for interconnect reliability because time-dependent dielectric breakdown (TDDB) is a primary failure mode in integrated circuits.

The plasma process that most commonly damages pSiCOH is the reactive ion etch process used to etch the trench and vias into the pSiCOH to form the Cu wires. Once formed these trenches will be lined with a barrier metal and filled with Cu, Figure V.2. The plasma-based PVD deposition of barrier metal can do further damage to the pSiCOH. [376]

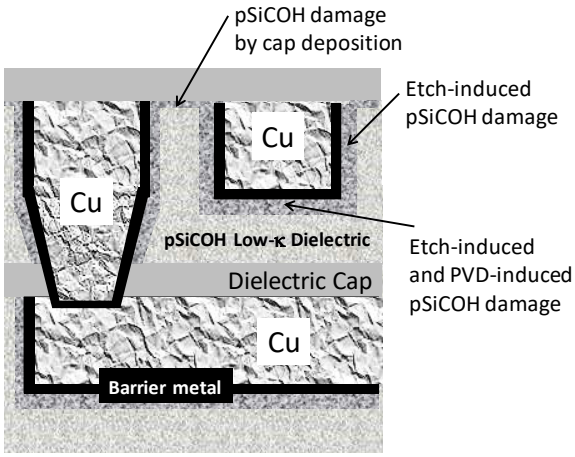

Figure V.2. An illustration of two Cu interconnect levels connected by one via showing the pSiCOH damage layers along the Cu interfaces and the pSiCOH/cap interface.

After the Cu has been deposited and excess Cu removed by chemical mechanical polishing (CMP) the top surface of the Cu wire is coated with a passivating dielectric cap, and the plasma processes used clean the Cu surface and deposit the cap can also damage the adjacent pSiCOH surface. Reducing plasmas, typically NH_3 or H_2 based, clean the Cu surface by reducing CuO_x, which forms during the air break between the CMP and cap deposition processes, and removing other contaminants.[171] However these plasmas can also damage SiCOH and pSiCOH materials. In some cases a selective metal cap, such as Co, is deposited onto the Cu to passivate it before the dielectric cap is deposited.[6] In this case the plasma cleans used to clean the Cu surface and the plasmas used for selective deposition may damage the SiCOH or pSiCOH surface adjacent to the Cu surface. These damaging plasma processes can be optimized to minimize, but not eliminate, plasma damage. This motivated development of methods to repair the pSiCOH damage.

The first attempts to repair plasma damage employed thermally activated silylation chemistry to replace SiOH with carbon containing groups such as $SiOSi(CH_3)_3$ or similar moieties, Equation V.5,

$$n(\equiv SiOH) + X_n SiR_{4-n} \longrightarrow \equiv SiOSiR_{4-n} + nHX \quad \text{(V.5)}$$

where X is a reactive group such as a halogen, alkoxy, or amine and R is a pendant such as CH_3. Shi et al., provides a brief review of low-κ repair by thermal silylation.[375] Silane coupling agents were found to preferentially react on the surface of the damaged SiCOH/pSiCOH leaving most of the damaged layer unrepaired. The silane coupling agents could not diffuse into nonporous SiCOH films, and pSiCOH films are designed to minimize the average pore size to <2.5nm and pore connectivity, which reduce the diffusivity. In addition, the surface of the plasma damaged film can be denser than a pristine film, forming a skin layer, due to silanol condensation reactions and ion bombardment during the plasma exposure. Finally, when silane coupling agents react on the surface or the walls of pores near the surface the newly bound molecule can block or narrow connections between pores and inhibit other repair molecules from diffusing deeper into the damage layer. To address the limitations of thermal silylation UV-assisted repair processes were developed. VUV was not widely considered primarily because commercial UV tools were available, the VUV photon penetration depth is limited in pSiCOH, and VUV photons can further damage (demethylate) pSiCOH by breaking the Si-CH_3 bond.[104] UV photolysis of Si-CH_3 bonds is limited.[104,109,245]

Exposing damaged SiCOH/pSiCOH to UV photons in an inert environment partially repairs plasma damage by inducing silanol condensation reactions

$$\equiv SiOH + \equiv SiOH \longrightarrow \equiv Si - O - Si \equiv + H_2O \quad \text{(V.6)}$$

Dimitrakopoulos et al.,[377] reported data in a patent application that UV exposures at 200 - 450°C (preferably 400°C) under an inert atmosphere repaired CMP-damaged SiCOH films by UV-induced silanol condensation as in reaction 6. The inert UV exposure reduced the silanol content of the films as measured by FTIR and improved the films' electrical field induced leakage current. Similarly, Varadarajan et al.,[378] reported data in a patent showing inert UV at 350-400°C recovered the κ of pSiCOH films, damaged by either CMP or an oxidizing plasma, to a greater extent than 400°C thermal annealing alone. Varadarajan further showed that UV-induced film shrinkage during UV exposure could be minimized at >300nm wavelength with no impact on κ recovery. Shi et al.,[375,379] confirmed these results with a broader set of data in a

study focused on UV-assisted repair processes. Their previous work had shown that the κ increase induced by plasma damage was dominated by the dipolar component of polarizability relative to the electronic and ionic components. Ab initio calculations revealed that physisorbed water was the primary cause of the κ increase while Si-CH=O and Si-O- showed smaller contributions.[379] Thus, reducing the silanol content of the damaged layer is critical to recover the k-value of the film. Shi used an O_2 plasma to damage a κ=2.5 pSiCOH film. The pristine film had 25% porosity and no measurable silanol by FTIR. The O_2 plasma created silanol, physisorbed water, and C=O (oxidized $SiCH_3$) absorptions in the FTIR spectrum, Figure V.3, and the κ increased to 3.26. Inert UV exposures nearly completely removed these bonds from the film and increased the Si-O-Si network and suboxide bonding. The k-value recovered to within 5% of the pristine value.

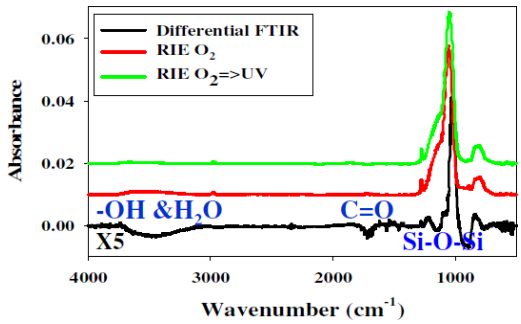

Figure V.3: FTIR spectra of a pSiCOH film exposed to an O_2-based plasma with and without an inert UV exposure. The difference spectra clearly shows the SiOH and water reduction caused by the UV exposure (from Shi, et al.[375])

The results of Dimitrakopoulos, Varadarajan, and Shi showed enough recovery of electrical properties and silanol reduction in FTIR that the effects of UV-induced silanol condensation could not be limited to the film surface but partially repaired the entire damaged layer. While substantial the repair was nonetheless partial as the κ and electrical properties did not fully recover to their pristine values. Full repair would require replenishing the $SiCH_3$ through the entire depth of the damage layer.

The next development was combining silylation and UV exposures.[378,380,381,382,383,384] Silylation alone could at least replenish $SiCH_3$ on the damaged surface while inert UV alone would partially repair deeper in the damage layer by silanol condensation. Also, the use of UV allows for photon-assisted chemical repair (including chemistries other than silylation) deeper in the damaged layer. For example Chan et al.,[383] proposed using vinyl silane containing compounds activated by UV light to effect low-κ repair, and Yim, et al.,[382] proposed using compounds containing carbon-carbon double and triple bonds, such as 1,3-butadiene and acetylene, activated by UV light to cap silanol groups in damage pSiCOH.

Huang et al.,[385] explored combinations of UV and silylation exposures to repair O_2 plasma damaged pSiCOH. Their study included inert UV exposure to remove excess silanol followed by silylation, silylation followed by inert UV exposure to repair the regions unreached by silane coupling agents, and simultaneous UV-chemical exposures. Repair effectiveness was measured using FTIR, XPS, and water contact angle measurements on blanket films damaged by an O_2 plasma. They found that inert UV exposure before silylation resulted in better repair than the opposite sequence. Previous results from the same laboratory found that silylation alone is more limited to the surface when excess silanol is present in the film because excessive reactions at the films surface resulted in the newly bonded groups blocking or inhibiting the diffusion of silane coupling agents deeper in the film. [379] Therefore UV removal of excess silanol likely facilitated repair by the subsequent silylation step. However, Huang found that simultaneous UV and silylation exposure resulted in the most repair. The patent literature also suggests that the simultaneous UV-chemical repair enables a broader choice of repair chemistries such as chemicals that produce $–CH_3$ or other radicals upon UV photolysis in the pores, which can cause repair reactions.[380,386] In this latter case the potential benefit is that non-reactive molecules have time to diffuse deeper into the damaged layer where they are chemically activated by UV light to affect repair whereas the diffusion of chemically active species such as silane coupling agents is limited primarily to surface repair because they rapidly react at the surface.

Xie et al.,[384] showed that a combination exposure of UV photons, chemistry, and heat significantly repaired k=2.2 pSiCOH films that were plasma damaged. They don't report the chemistry used or the combination of UV-chemistry exposures. Difference FTIR showed the growth of silanol and depletion of CH_3 after exposure to damaging plasmas. They used both CO_2 and NH_3 plasmas to damage the pSiCOH. FTIR after repair showed a decrease in silanol absorptions and an increase in CH_3 absorption in films damaged by either CO_2 or NH_3 plasmas. The repair process was also demonstrated using water contact angle (WCA). The films are hydrophobic before damage (WCA >100^o) and become hydrophilic (WCA <10^o) after damage. Xie's UV-chemical repair process almost fully recovered the WCA to >90^o. More importantly the electrical properties of the damage pSiCOH films improved substantially. The damage induced by either plasma increased the k-value from 2.2 to >2.5 and degraded the electrical breakdown voltage and leakage. After repair the k-value decreased to ~2.3 and the breakdown voltage and leakage partially recovered. Likewise, TDDB reliability was substantially improved for the UV-assisted repaired film relative to no repair.

Kimura et al.,[387,388] compared thermal, plasma-assisted, and UV-assisted low-κ repair processes using O_2 plasma damaged κ=2.3 and κ=2.0 pSiCOH films. The UV-assisted repair process was done at 300^{o}C. They did not reveal the restoration chemistries or additional process details about the thermal or plasma-based repair. The UV-assisted repair was most effective for recovering the κ of the κ=2.3 films. Furthermore the κ recovery, which was about 80% for the UV repair process, depended on the silanol content of the film as determined by FTIR. Elemental depth profiles showed that the damage layer was 35nm deep based on elevated O and reduced C relative to the bulk of the film as illustrated in Figure V.1. The UV-restoration process recovered a portion of the lost carbon and reduced the O content to a depth of ~20nm. The result indicates that the UV-repair process replaced silanol groups with carbon-based moieties.

Kimura found that the UV repair processed used to restore the κ=2.3 film did not repair a more porous κ=2.0 even though the κ=2.0 film suffered less damage by the same O_2 plasma treatment. The pristine κ=2.0 film had higher carbon content than the κ=2.3 film, which is why

it suffered less plasma damage despite having higher porosity. Kimura found that the UV repair process deposited an excessive amount of carbon in the κ=2.0 film due to its higher porosity. When they adjusted their process to add a more controlled carbon addition they were able to fully restore the k-value and reduce electrical leakage current.

Priyadarshini et al.,[389] applied UV-assisted repair in damascene interconnects to reduce the C component of RC. Their focus was developing a selective Co deposition to deposit a Co metal cap on top of Cu lines without depositing Co on the adjacent pSiCOH dielectric. Co on the dielectric would create electrical leakage paths between adjacent Cu lines. The selective Co process required plasma cleaning the Cu surface and multiple plasma treatments of the growing Co layer that damaged the adjacent pSiCOH surface. The damage layer on the pSiCOH surface is known to accelerate TDDB reliability failure in addition to increasing κ and capacitance. And the selective Co deposition did increase their RC delay. Priyadarshini used UV-assisted repair after the selective Co deposition to repair the pSiCOH surface, which significantly reduced, but did not fully recover, the RC delay.

V.I.2. Film Stress Engineering

As noted above, UV curing of pSiCOH films also causes incidental UV exposure for all the underlying metal interconnect and device layers.[7] One significant impact of this incidental exposure is UV-induced stress changes in the Cu cap layer, typically SiNH or SiCN, on which the pSiCOH film is deposited. [8,9] Since interconnects are composed of up to a dozen wiring layers,[6] the stress of each layer is additive and can subject the interconnect wiring levels to substantial stresses. In some cases, the tensile stress can become high enough to induce cracking in the pSiCOH film, especially when the wafer is subjected to additional stresses during the chip packaging process.[390] Thus, controlling the stress in the Cu cap layer is critical.[391]

Fortunately, the effect of p-SiOCH ILD UV curing on SiNH, SiCNH, and other SiCOH Cu cap layers is now well understood.[392] Miyagawa et al., investigated UV curing of PECVD SiNH films in detail and found that UV irradiation using a high pressure Hg lamp promoted Si-N-Si

crosslinking due to dehydrogenization and a reduction in the nanopore/vacancy diameter.[392] More specifically, they observed using FTIR that the UV cure decreased both the Si-H and N-H bonding and increased the Si-N bonding for PECVD SiNH films deposited at 300°C. Correspondingly, they also observed using PALS that the nanopore/vacancy size decreased with UV curing. The combined hydrogen loss and pore shrinkage resulted in the generation of a significant tensile strain which increased the post deposition tensile film stress from 0.3 GPa to 1.7 GPa after UV curing. Similar UV-induced structural and stress changes have also been observed in PECVD SiCNH and SiCOH Cu capping materials. Specifically, Goto et al.,[393] and Liu et al.,[394] have both observed UV cure induced hydrogen loss and more dramatic compressive-to-tensile (-250 MPa to 100 MPa) stress changes in PECVD SiCNH Cu cap materials. Even more dramatic -500 MPa to 750 MPa stress swings have been reported by Spooner et al.[9] Liu also observed using FTIR that significant UV-induced structural modifications occurred for SiCNH Cu cap materials with higher nitrogen and hydrogen content.[394] Interestingly though, small (< 1-2%) changes in dielectric constant and film thickness for SiCNH and SiOCH Cu cap materials with UV curing were observed relative to pSiOCH materials.[393] The large stress change is likely then due to the significantly higher Young's modulus (E) for Cu cap materials (60 – 200 GPa) compared to pSiOCH (5-10 GPa) where a smaller elastic strain (ε) can induce a larger stress (σ) response via Hooke's law ($\sigma = E\varepsilon$). [395] In addition, Navamathavan et al., has shown that UV curing of dense SiCOH etch stop layers using a 400W (0.6 MW/cm^2) 265 nm Hg lamp can result in up to a 15% increase in elastic modulus.[396]

Several methods have been identified to negate or minimize the UV-cure induced stress change observed in SiNH and SiCNH Cu capping layers. One method demonstrated by Spooner involves simply tuning the PECVD process to produce films with increasingly higher levels of compressive stress such that the films remain compressive after the UV cure.[9] As shown by Nguyen et al., this can be achieved by increasing the H_2 dilution flow during PECVD using trimethylsilane ($Si(CH_3)_3H$) and ammonia (NH_3).[7] Other methods for mitigating the ILD UV-cure impact on the Cu capping layer stress involve employing a SiCNH/SiNH bilayer or SiCNH/SiNH/SiNH tri-layer film stack to mitigate the κ impact of using a higher compressive

stress / higher κ material to compensate for the increased tensile stress component induced by the UV irradiation.[6,8]

In addition to affecting structural and mechanical properties, UV-curing of Cu cap materials has also been shown to impact electrical properties. Specifically, Kobayashi et al.,[328,329,397] and Bittel et al., [316] have both shown that thick ($\geq$ 200 nm) blanket films of PECVD SiNH and SiCNH Cu capping materials deposited on Si and exposed to 254 nm or 365 nm UV radiation exhibit substantially increased leakage currents under both positive and negative bias currents. Both authors were able to directly correlate the UV-induced leakage currents to an increase in unpaired spin (dangling bond) defects detected by complementary electron paramagnetic-resonance (EPR) measurements. Detailed examination of the EPR *g*-value and line width for these unpaired spins led to an initial assignment of the defects to Si dangling bonds. For SiNH, this assignment has been recently confirmed by Mutch et al., using electrically detected magnetic resonance measurements which further demonstrated that electrical transport through SiNH does directly involve Si dangling bond defects.[320,321]

In contrast, Nguyen et al., have shown that for a 20 – 35 nm UV cured SiCNH Cu cap material, UV curing at 400 °C can improve leakage current and breakdown voltage in Al contact MIS structures.[7] However, for MIM structures the UV cure was found to cause enhanced Cu diffusion/penetration into the cap material and corresponding increased leakage currents and lower breakdown voltages.[7] Similar results have been reported by Navamathavan.[396] However, Goto et al.[393] and Wang et al.[390] have observed little to slightly improved VBD and TDDB improvement in MIM structures employing a SiCNH cap exposed to UV curing. The neutral – positive impact of UV curing in this case could be due to the substantially thicker (75 – 200 nm) SiCNH films employed in the latter studies that precluded Cu diffusion across the full SiCNH film stack. Additionally, the contrasting negative impact of UV-curing observed by Kobayashi and Bittel could be a result of examining purely the SiNH/SiCNH UV-cure response using MIS structures whereas the studies by Nguyen, Goto, Wang, and Namathavan employed MIM structures utilizing Cu electrodes with and without a pSiOCH ILD. The presence of the Cu

electrode and pSiOCH ILD likely introduced other effects that may have muted or mitigated the SiNH/SiCNH UV response.

While tensile stresses are generally viewed as undesirable in metal interconnect structures,[395] they can have potential benefits at the device level where judicious strain engineering has enabled impressive gains in CMOS device performance.[398] Specifically, strain in crystalline lattices is well known to influence the effective mass, scattering probability, and consequently the mobility of charge carriers.[399] This effect has been extensively utilized to enhance the performance of CMOS devices by introducing strain into the channel region.[399] Various methods have been employed to achieve this ranging from utilizing the strain created from epitaxially grown Si_xGe_{1-x} alloy source/drain regions to the deposition of a highly stressed film over the entire transistor structure.[398] For the latter, a common example is the use of a tensile PECVD SiNH contact etch stop layer (CESL) to enhance n-channel carrier mobility and CMOS device performance.[400] In this regard, the high tensile stresses induced in PECVD SiNH by UV-curing is extremely attractive for further boosting NMOS device performance.

One of the first reports of intentionally using a UV-cure to enhance the tensile stress of a CESL was Arghavani et al., where UV curing of a PECVD SiNH film was reported to result in a tensile stress as high a 2 GPa.[401] Subsequently, Miyagawa[392] and Noori et al.[402] reported 10 – 20% improvements in drain current for < 45 nm n-MOSFET devices utilizing a UV-cured PECVD SiNH CESL film with 1.7 GPa tensile stress. Miyagawa additionally reported that UV-curing did not impact NBT (negative bias temperature instability) performance,[392] and Ortolland et al., demonstrated that UV-curing the PECVD SiNH CESL benefitted PMOS performance as well by reducing Si/gate oxide interface state density. [403] Based on a full factorial design of experiments around the PECVD SiN deposition process and detailed FTIR analysis, Morin et al., concluded that the key to obtaining such high tensile stresses in PECVD SiNH using a 400 °C UV cure was obtaining SiNH films with a N rich stoichiometry and low mass density / high hydrogen content.[404]

In summary, the stress in films used for both FEOL and BEOL needs to be controlled. In the FEOL, highly tensile films benefit device performance. In BEOL films need to have neutral to

modestly compressive stress. Inert UV exposure provides a means to tune both film stress and electrical properties to optimize film properties to specific applications.

V.2. Potential Near Term Applications

V.2.1. UV/VUV-assisted Pore Sealing

Pore sealing is necessary to enable chemical vapor deposition (CVD) or atomic layer deposition (ALD) of metals onto the surfaces of trenches etched into pSiCOH dielectric, especially more porous, lower κ pSiCOH films.[405] PVD metal deposition onto pSiCOH surfaces tends to seal the pores with little or no metal deposition inside the porous film. In contrast the conformal nature of CVD and ALD allows metal deposition deep into the pore network of pSiCOH.[1] The highly conformal, self-limiting nature of ALD deposition is especially problematic because the ALD precursor molecules can diffuse deep into the pore network and react on nucleation sites, such as residual silanol on the pore walls, Figure V.4. Metal deposition or even metal precursor binding inside the pores creates an electrical leakage path and route for TDDB reliability failure and must be avoided. The extent of the problem is related to the pSiCOH film porosity, pore size, and pore interconnectedness as well as to the ALD precursor choice and process.

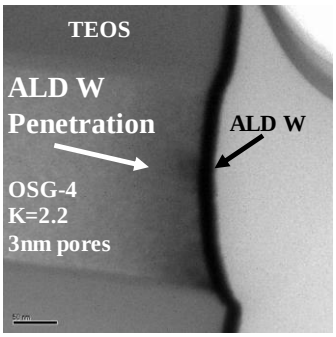

Figure V.4. TEM image of W deposited by ALD onto the sidewall of trench etched into κ=2.2 pSiCOH (labeled OSG-4). W is not confined to the sidewall but deposits >50nm from the interface. This illustrates a key problem with ALD onto pSiCOH and the need for pore sealing prior to ALD.

To enable ALD metal deposition directly onto the pSiCOH surfaces a number of pore sealing strategies have been explored.[1,405] ALD precursor ingress can be inhibited by reducing permeability at the pSiCOH surface (closing pores or reducing pore interconnections). The surfaces of etched pSiCOH may be partially densified by the plasma etch process conditions or by post etch plasma treatments to inhibit ALD precursor ingress.[1,406, 407] VUV photons emitted by plasmas likely play a role in the densification.[408] Surface pores can also be sealed by making the surface very reactive to the ALD precursor such that rapidly bound ALD precursors at the pSiCOH surface, especially in surface pores, can sterically hinder subsequent precursor diffusion deeper into the pSiCOH pore network. Another approach uses silane coupling agents, which can preferentially bind to the pSiCOH surface, to inhibit ALD precursor diffusion into the pSiCOH pores.[409] This could be especially effective if the silane coupling agent has large pendant groups.[410]

Some of the same studies of UV-assisted low-κ repair reviewed above also explored using those methods to pore seal. Replacing silanol with $Si(CH_3)_x$ or similar moieties in the pSiCOH surface pores can both sterically inhibit ALD precursor diffusion in the pSiCOH and remove silanol nucleation sites for ALD precursor binding.

Xie et al.[384] reported that UV-assisted repair reduced ALD MnN deposition in the pSiCOH pores. EELS elemental profiles show that without UV-assisted repair, ALD MnN was deposited in the pSiCOH pore network through the entire width of the pSiCOH insulating the metal lines. In contrast, the UV-assisted repair process limited MnN deposition to the Cu/pSiCOH interface.

Kimura et al.[387] and Ishikawa et al.[411] (both working in the same laboratory) explored a pore sealing process consisting of UV-assisted repair followed by deposition of a thin (~1nm) PE-ALD SiN layer. Kimura used wet chemical diffusion measurements to monitor pore sealing effectiveness on highly porous κ=2.0 pSiCOH films. Pristine samples were compared to a) samples damaged using an O_2 plasma followed by UV-assisted repair and b) O_2 plasma damaged samples + UV-assisted repair + PEALD SiN deposition. Samples with damage + UV-assisted repair showed less chemical ingress than pristine samples. The plasma damage step

may have partially densified the pSiCOH film surface and the repair process may have further blocked pores, but the pores were not completely sealed.

They then measured the minimum ALD SiN thickness necessary to completely seal the pores. 3nm thick SiN was needed to seal pristine samples whereas only 1nm was needed to seal the damaged + UV-assisted repaired samples. TEM indicated that on the pristine sample ALD SiN deposition was not confined to the surface but also deposited deep inside the pSiCOH film. In contrast, on the damage + UV-assisted repaired samples the ALD SiN deposition was much more confined to the surface as ALD precursor diffusion was blocked and/or ALD nucleation sites in the pSiCOH pores were reduced by the UV treatments. Ishikawa expanded on Kimura's study by quantifying the SiN precursor diffusion using a method to measure mass changes in the film versus the number of ALD deposition cycles. The UV-assisted repair followed by 1nm PEALD SiN enabled significant pore sealing with minimal detriment to pSiCOH electrical properties.

V.2.2. UV-based Cu/dielectric Interface Engineering

UV-assisted metal oxide reduction has also been proposed as a Cu clean prior to dielectric cap deposition. A Cu/dielectric cap interface free of metal oxide or carbonaceous residues is critical for good electromigration performance because this interface is a known fast diffusion path for Cu lines carrying electrical current. The conventional method to clean the Cu surface uses NH_3-based or H_2-based plasma processes. These effectively reduce Cu oxides and remove residual organics from the CMP process, but they also damage the adjacent pSiCOH surface leading to κ increase and TDDB degradation.

Varadarajan et al.,[412] demonstrated that simultaneously exposing an oxidized Cu surface to NH_3 and UV at 400^{o}C reduced the CuO_x much more rapidly than annealing the CuO_x under NH_3 without UV. When they exposed a κ=2.55 pSiCOH film to the UV/NH_3 they observed only a small (<1%) reduction in $SiCH_3$ by FTIR, but the k-value significantly increased although the increase was much less than that caused by a NH_3-based plasma exposure. Thus Varadarajan

showed UV/NH_3 reduced CuO_x as well as an NH_3-based plasma process but with less damage to the pSiCOH. Likewise, Chan et al.,[413] reported that simultaneous exposure to UV and NH_3 effectively reduced metal oxides at temperature above and below 300°C using reflectivity differences. Chan's UV-assisted process could be optimized to match the effectiveness of a NH_3-based plasma cleaning to reduce CuO_x. They also measured the k-value changes in a κ=2.2 pSiCOH film after exposure to the UV-assisted NH_3 clean and found it comparable to or less than that induced by the plasma-based clean although above 300°C there was an increase in κ.

Ryan and coworkers[414] also found that a 30s UV-assisted NH_3 clean, similar to that used by Chan, effectively reduced Cu oxide to the same extent as a conventional 5s NH_3 plasma exposure qualitatively confirming the results of Chan. Ryan used ToF-SIMS depth profiles to measure the Cu oxide thickness before and after exposure to the UV/NH_3 clean or a NH_3-based plasma clean. However, in contrast to Varadarajan's FTIR results above, ToF-SIMS depth profiles of pSiCOH films exposed to the UV/NH_3 clean for 30s had nearly identical damage layer thickness as the same film exposed to a 5s NH_3-based plasma clean, which indicates UV/NH_3 damages pSiCOH to the same extent as the plasma at exposure times that fully reduce CuO_x.

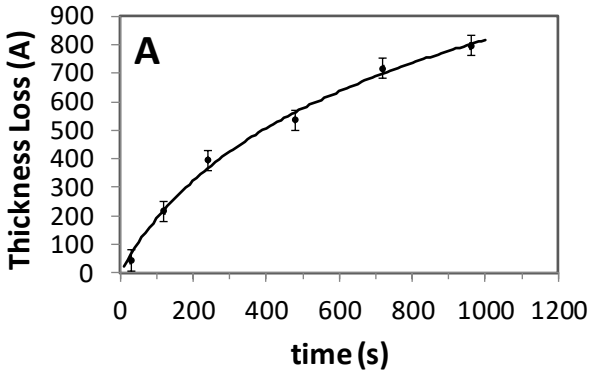

Figure V.5: Plot of HF etch-induce thickness loss as a measure of pSiCOH damage layer thickness versus UV/NH_3 exposure time at 250°C (taken from Ryan, et al.).[245] The HF wet etch selectively removes the damaged layer. A 30s UV/NH_3 caused a 4nm thick damage layer.

Ryan and Molis [245] also observed a small, but measurable 4nm thick damage layer using a wet etch method, Figure V.5, which would be difficult to detect by FTIR. The results are

qualitatively consistent with the results of Varadarajan and Chan, who both measured a small k-value increase upon UV/NH_3 exposure under different conditions.

All together these results suggest that UV/NH_3 cleans can be equally effective as plasma-based cleans in terms of CuO_x reduction and pSiCOH damage, however UV/NH_3 cleaning has not been reported in HVM to our knowledge.

V.2.3. UV-assisted Resist Strip and Cleaning

The ability of UV radiation to produce ozone and decompose organic matter has been known for several decades with reports dating back as far as the early 1970's.[415,416] This attribute quickly led to the development of UV-assisted ozone cleaning processes and their application to a variety of surfaces including semiconductors (Si,[416,417] GaAs,[418,419] InP, [420] SiC,[421] GaN,[422] ...), amorphous oxides (SiO_2,[415] ZnO,[423] ITO,[424] ...), 2D materials (graphene,[425] BN,[426] MoS_2,[427] ...), reticles,[428] and various metallic and other surfaces.[Error! Bookmark not defined.] UV/ozone treatments have also been utilized to p-type dope,[429,430] tune the work function,[431,432] and improve the adhesion to metal surfaces of graphene.[433] Additionally, UV/ozone treatments have been utilized to improve the leakage currents for various oxide based high-κ dielectrics via the proposed elimination of oxygen vacancies.[434,435]

The basic mechanism behind UV/ozone cleaning has been attributed to photosensitized oxidation of surface contamination and the substrate. [Error! Bookmark not defined.] Specifically, adventitious and organic surface contaminants are excited and/or dissociated directly by the absorption of short wavelength UV radiation ($h\nu_2$, see Figure V.6). Simultaneously, ozone and atomic oxygen are produced by photo-induced dissociation of gaseous O_2 using UV wavelengths less than 254 nm ($h\nu_1$, see Figure V.6). The excited contaminant molecules react with the atomic oxygen producing volatile species such as CO_2, H_2O, and N_2.[415,416] In parallel, the substrate surface may also be oxidized forming a thin (2 – 10 nm) surface oxide layer (see Figure V.6).[421] The thickness of the resulting surface oxide scales with the oxidation resistance / inertness of the substrate material and can play an important role in the overall effectiveness of the UV/ozone oxidation clean.[421,422] Depending on the goals of the surface cleaning and

subsequent targeted processing, this surface oxide layer may need to be removed by other methods shortly after UV/ozone exposure or could be left in place to prohibit subsequent recontamination. For example, UV/ozone cleaning of Si surfaces typically results in the formation of a thin few nm SiO_2 surface layer that is commonly removed shortly thereafter by etching in dilute HF.[415,436] However, for UV/ozone cleaning of GaAs, a thicker (10 nm) surface oxide layer is formed and typically left in place and not removed until just before the underlying GaAs needs to be exposed.[419,420]

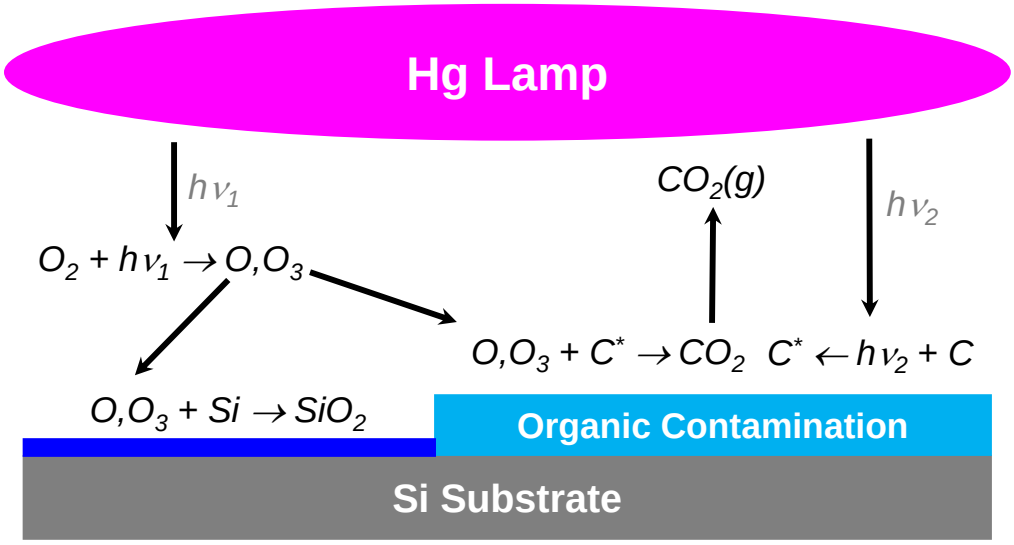

Figure V.6. Pictorial schematic of UV/Ozone cleaning illustrating the various photochemical processes involved leading to organic contamination removal and substrate oxidation. [415]

UV-assisted cleaning has recently become of renewed research interest for photoresist and post plasma etch polymer residue removal in FEOL[437] and BEOL[438] applications. For the latter, the presence of Cu and nanoporous low-κ dielectric SiOCH materials presents particular challenges due to their unique sensitivity to oxidizing chemistries.[439,440,441] For this reason several authors have investigated UV only photoresist and polymer residue removal from SiOCH surfaces. In this regard, Kesters and coworkers has shown that exposure of deep UV PMMA photoresist to 254 nm Hg lamp UV radiation in a purged Ar or N_2 environment can cause scissioning of the C-C bonds and the formation of C=C bonds, thus making the plasma etched

photoresist more amenable to dissolution in organic solvent or aqueous ozonated cleaning solutions.[438,442] Removal of the photoresist was further enhanced by performing the UV pre-exposure in the presence of O_2, but this did not completely remove the photoresist.[438] Both UV only and UV/O_2 were found to be compatible with a porous low-κ ILD material with a pristine κ value of 2.6.[443,444,445]

Similarly, Le et al.[446,447,448,449] and Mukherjee et al.,[450] have found UV radiation is also effective in reducing fluorocarbon polymeric residues produced during plasma etching of low-κ ILD and other materials in the presence of photoresist. To investigate the mechanisms involved in UV/ozone cleaning of such materials, both authors utilized as model films blanket fluoropolymer layers plasma deposited using fluorinated chemistries similar to those utilized in low-κ ILD etching. Using such films, Le found that 254 nm UV exposure in a purged Ar environment induced relatively minor changes in the chemical structure of the films as monitored by FTIR. The most significant changes were only a slight increase in C=O absorption at 1730 cm^{-1} detected by FTIR and a 10-15° decrease in water contact angle. Both observations are evidence of a slight oxidation of the fluoropolymer film. Despite these minor changes though, the UV exposure did significantly enhance the removal efficiency of the fluoropolymer (30-50 nm) using a wet chemical treatment in a solvent mixture such as dimethylsulfoxide and monomethanolamine or ozonated water – both of which were unable to completely remove the fluoropolymer without the UV pre-treatment. [445,446] As with the Kesters studies, the beneficial effect of the UV pre-treatment was attributed to UV induced C-C bond scission and oxidation of the film by atomic oxygen generated from photoexcited residual peroxy groups created in the fluoropolymer during air exposure prior to the UV treatment.[446]

Le and Mukherjee also investigated UV/ozone cleaning of fluoropolymer layers and found that the added presence of oxygen in the UV pre-exposure atmosphere led to significant material loss.[448,449,450] Most notably, Le investigated in the detail not only the influence of the background atmosphere but also the effect of pressure, temperature, UV power density, and UV dose for UV/ozone cleaning of plasma deposited fluoropolymer residues.[447,448] In this case, they found that both background atmosphere and UV dose were most critical to both material

removal during UV/ozone cleaning and by subsequent wet chemical treatments. In particular, they postulated that a minimum concentration of reactive species, such as atomic oxygen created by background O_2, was necessary to allow efficient UV assisted modification / removal of plasma deposited fluoropolymers.[448]

V.3. Potential Long Term Applications

V.3.1. UV-assisted Etching

Research on photo-assisted etching spans several decades dating back to at least the early 1960's where Hoisty demonstrated that visible white light could induce etching of GaAs wafers submerged in various acidic and basic solutions.[451] Since then, both wet[450,452] and dry[453,454] photo-assisted etching of a variety of semiconductors (Si,[455,456] Ge,[457,458] GaAs,[450,451,452,453] InP,[459,460] SiC,[461,462]), metals (Al,[463] Cu,[464,465,466] Ni,[467] Fe,[466] Co[466], W,[468] Ta[467]), insulators (SiO_2,[469,470,471] TiO_2,[472] Al_2O_3[473]) and polymers [467,471] have been demonstrated using IR,[470,474] visible, [450,456,457,458] and UV radiation. [451,452,453,454,455,460,461,462,463,464,465,466] These techniques have been utilized for forming mesas,[457] through-wafer vias,[475] optical gratings,[476] and free standing pillars,[477] highlighting crystallographic defects,[478] minimizing plasma-etch radiation damage,[454] and patterning Cu interconnect structures[464]. UV photo-assisted etching has recently proven to be a particularly popular method for etching III-V nitride semiconductors which exhibit high chemical stability and have proven difficult to etch using wet chemical or dry plasma based techniques.[479] Both UV photo-assisted wet[478,480,481] and dry[482,483] techniques have been demonstrated for GaN as well as InGaN[484] and AlGaN[485,486] alloys. For the latter, UV photo-assisted wet etching has been successfully utilized to fabricate AlGaN/GaN heterostructure field effect transistors.[484]

With regard to pSiCOH etching, Ryan and Molis[245] leveraged the mechanistic understanding of plasma-induced damage to pSiCOH to develop a plasmaless, UV-based two-step etch process. A UV/NH_3 exposure was used to demethylate the pSiCOH film to a depth determined by the exposure time, Figure V.4. UV/NH_3 exposures at 250°C damaged

(demethylated) pSiCOH in a diffusion-limited manner, and they provided possible mechanisms for the UV/NH_3 interactions in pSiCOH. Then the demethylated layer was selectively removed by an HF wet chemical etch. Since they used a commercial UV tool that produced ≥200nm for their research they also noted the significance of >200nm UV photons in plasma-induced pSiCOH damage.

UV/NH_3 etching was demonstrated by using it to replace a plasma process for removing pSiCOH from between Cu interconnect lines, which is a step in air gap nanofabrication. After the pSiCOH between Cu lines is removed a non-conformal dielectric deposition is used to create an air gap between the Cu lines. Ryan and Molis showed that the UV process accomplished the same result as the plasma process, but without ion bombardment.

Photo-assisted etching processes can also be categorized as relying either on purely pyrolytic thermal heating [463,465,473] or ablation,[487,488,489] or the direct creation of radical reactants via gas[456,452,454] or liquid phase photolysis.[490] For the former, IR radiation is typically utilized to heat the substrate and assist the desorption of etch by products (see Figure V.7).[477] For the latter, UV radiation is utilized instead to create activated species via photolysis that react with the target material to create etch byproducts (see Figure V.8). As one example, Ehrlich has demonstrated gas phase etching of GaAs and InP via gas phase photolysis of CH_3Br using a frequency doubled Ar ion laser with an output of 257.2 nm UV light.[452] In this case, they postulated that the etch process was photochemically initiated via the following reaction:

$$CH_3Br + h\nu\ (257.2\ nm) \rightarrow CH_3 + Br \qquad (V.7)$$

The Br atoms were then chemisorbed onto the III-V surface leading to adsorbed surface species such as $GaBr_x$ and $AsBr_x$ which eventually desorbed into the gas phase as reaction byproducts for GaAs etching.[101]

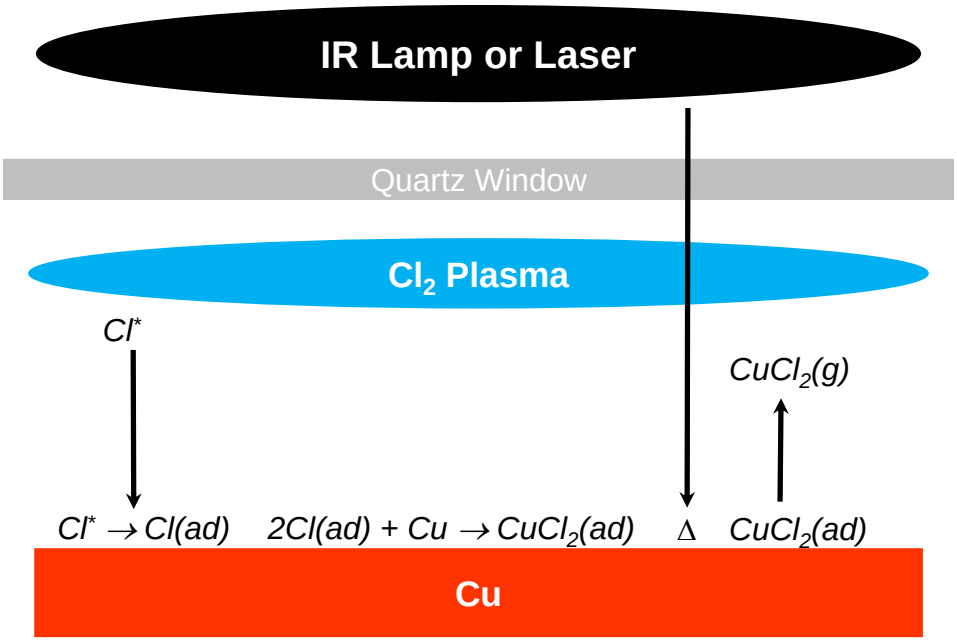

Figure V.7. Pictorial schematic for photo-assisted and pyrolytically enhanced plasma etching of Cu as demonstrated by Oshita.[473]

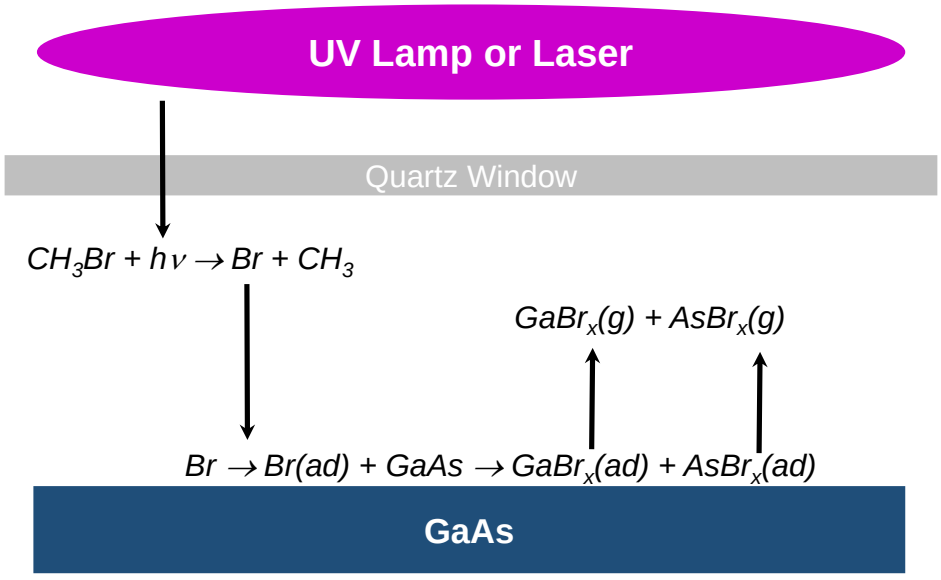

Figure V.8. Pictorial schematic for photolytically assisted Br etching of GaAs as demonstrated by Ehrlich.[452]

However, additional photo-assisted etching mechanisms have been identified and attributed to the creation and reaction of photo-generated free carriers (electrons and holes) that promote etch related surface reactions in either wet [450,451] or dry mediums (see Figure V.9).[454] Such photo-chemical processes may be further aided by the addition of an applied electrical bias resulting in so called photoelectrochemical etching[460,461,478,491] or photo-assisted anodic etching,[479,480] both of which have been demonstrated to enable highly anisotropic etching.[476,484] Further, the unintentional presence[492,493] or intentional addition[494] of UV radiation has been found in some cases to aid dry-plasma based etching techniques. Lastly, photo-assisted atomic layer etching (ALE) of Si and GaAs has also recently been reported where periodic laser pulses are utilized to create surface free carriers that aid in desorption of etch byproducts.[495]

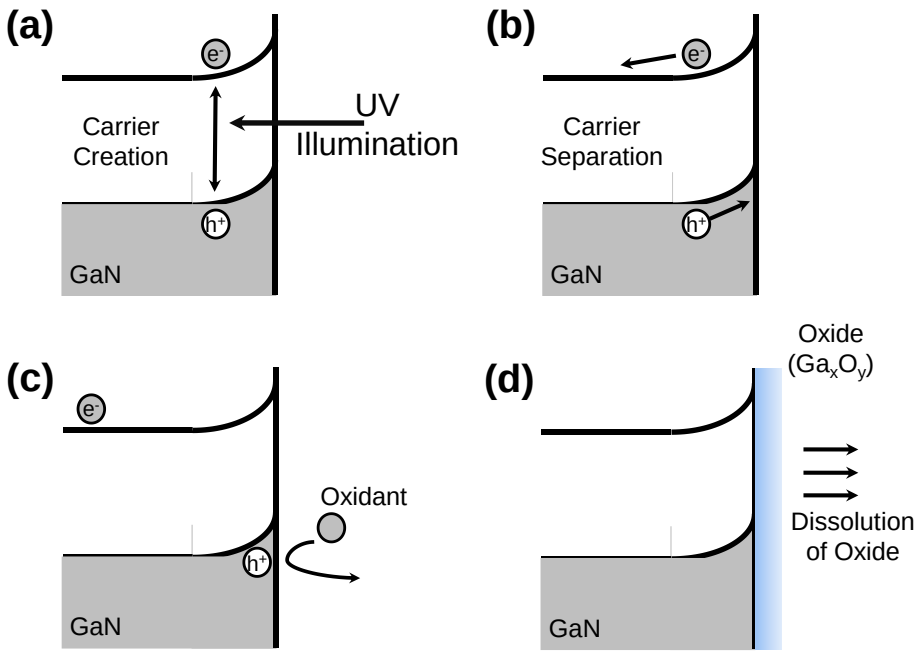

Figure V.9. Schematic illustration of GaN photoelectrochemical etching process proposed by Murata.[479] (a) UV illumination creates electron-hole pairs. (b) Carrier separation occurs due to the presence of a potential gradient. (c) Holes react with oxidants present at the semiconductor-electrolyte interface. (d) A surface oxide is formed and dissolved in the electrolyte solution.

For more complete reviews of the photo-assisted materials and processes that have been reported in the literature, the reader is referred to the article by Chuang[467] and the book by Bauerle[472]. For more details concerning the gas-surface interactions and basic mechanisms reported during photo-assisted etching, the reader is again referred to the work of Chuang[467] as well as Houle.[496,497]

V.3.2. UV-assisted Film Deposition

Like photo-assisted etching, research on photo-assisted thin film deposition goes back nearly five decades,[498] and a wide range of photo-assisted deposition methods have been reported for dielectrics (SiO_2,[499] SiN,[498,500,501] SiC,[502] Al_2O_3,[503,504] HfO_2,[505] ZrO_2,[506] TiO_2,[507] Ta_2O_5,[508] C,[509,510] B[511]), metals (Al,[502,512,] W,[513] Cu,[514] Ti,[497] Ni[497]) semiconductors (Si,[515] Ge,[516] GaAs,[517] BP,[510] GaP,[518] InP,[519] GaN,[520] InGaN,[519] ZnTe,[521] CdTe[522]), 2D materials (graphene[523,524] and MoS_2 [525]), and polymers.[526] The initial driving force for exploring photo-assisted[527] deposition was to find lower temperature deposition methods for achieving epitaxial growth,[497] reducing dopant diffusion,[498] avoiding Al metallization melting and hillock formation,[499] minimizing impurity incorporation,[503] and eliminating substrate exposure to high energy ions from plasma.[526] Since then, photo-assisted deposition methods have been explored for low temperature deposition of a-Si:H for high efficiency solar cells,[528] transparent a-SiC:H window layers[529,530,531] and conductive oxide electrodes for solar cells,[532,533] hermetic oxide moisture barriers on plastic substrates for flexible electronics,[534] polymeric bio coatings,[509] and nanoparticle surface functionalization.[535]

Like photo-assisted etching, the mechanisms for photo-assisted deposition can be broadly broken into two categories typically referred to as photolytic and pyrolitic deposition.[497] In the former, IR or UV lamps and lasers are utilized to directly excite and cause photodissociation of the gaseous growth precursors. As one example, Bergonzo has demonstrated photo-assisted CVD of SiO_2 using SiH_4 and N_2O with a Xenon excimer lamp.[536] In this case, Bergonzo postulated that O radicals were created via direct photolysis of N_2O according to the following reaction:

$$N_2O + h\nu\ (172\ nm) \rightarrow N_2 + O \qquad (V.8)$$

The atomic oxygen produced by photolysis then reacted with SiH_4 in the gas phase to produce various radicals such as SiH_3 and SiH_2 via the following proposed reactions:

$$SiH_4 + O \rightarrow SiH_3 + OH \quad \text{(V.9)}$$

$$SiH_4 + O \rightarrow SiH_2 + H_2O \quad \text{(V.10)}$$

The atomic and oxygen and $SiH_{2/3}$ radicals then adsorbed onto the growth surface to eventually combine to produce SiO_2 according to the following reactions (see Figure V.10):

$$SiH_2\ (ad) + 2O\ (ad) \rightarrow SiO_2 + H_2\ (gas) \quad \text{(V.11)}$$

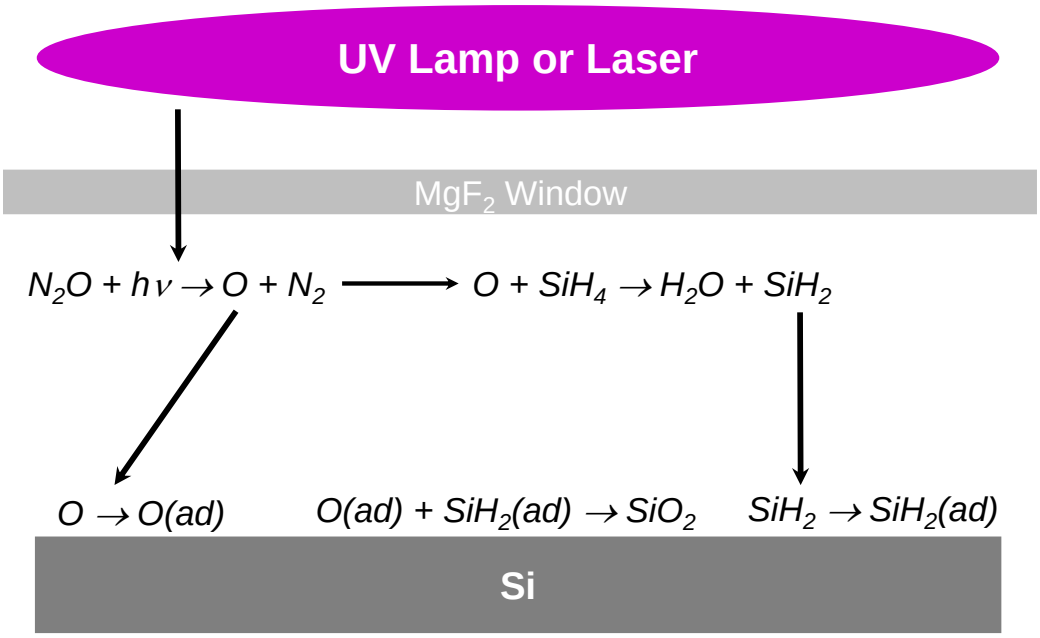

Figure V.10. Schematic illustration and reaction mechanisms proposed by Bergonzo for photo-assisted CVD of SiO_2 using SiH_4, N_2O, and a Xeon excimer lamp operating at 172 nm.[535]

In related cases, dissociation of the precursor species may be driven indirectly by photoexcitation of an intermediary species such as Hg[498] or NH_3.[515] As one example, Chen has shown that Hg

photoactivated with 254 nm radiation can be utilized to dissociate N_2O into N_2 and O according to the following reaction.[494]

$$N_2O + Hg^* \rightarrow N_2 + O + Hg \qquad (V.12).$$

The atomic O produced in this manner can be similarly utilized in combination with SiH_4 for SiO_2 CVD.[498]

For pyrolytic deposition, IR or UV radiation is instead utilized to directly heat the substrate surface and enhance film growth.[497] Pyrolytic deposition methods can also be taken to the extreme where a laser is used to heat the substrate/target to sufficient temperatures where evaporation or sublimation may occur thus producing an atomic beam of species that can in turn be used for thin film deposition. This form of pyrolytic deposition is frequently referred to as pulsed laser deposition (PLD) and has been utilized to deposit a wide variety of materials.[497,537,538,539,540]

Early work on photo-assisted thin film deposition focused primarily on Hg sensitized photolytic chemical vapor deposition (CVD) methods.[498] However, Hg sensitized methods quickly fell out of favor due to both environmental, health, and metal contamination issues,[526] and the emergence of CO_2 IR lasers[541] and a variety of halogen excimer UV lasers[542] that enabled both direct pyrolytic and photolytic CVD, respectively.[497] Beyond these initial beginnings, the evolution of photo-assisted deposition has largely followed and built upon the development and technical advancement associated with high-intensity lamps and lasers spanning the IR-visible-UV wavelength range.[543,544,545]

Due to the diversity of photo-assisted applications, we focus the remainder of this section on applications specifically pertaining to nanoelectronic device fabrication. For a more in depth general examination of photo-assisted thin film deposition, readers are referred to the review of Hanabusa[146] and the system design overview by Lian et al.[546] Concerning microelectronic device fabrication, perhaps the first application explored for photo-assisted deposition were the early reports by Frieser[547] and Kumagawa et al.,[548] to reduce the growth temperature during Si vapor phase epitaxy by incorporating UV light irradiation of the growth surface. Shortly after this

ground breaking work, Hg sensitized photo-assisted CVD was subsequently examined as a means to lower the deposition temperature of SiO_2 [498] and SiN[549,550,551] thin films for applications as lateral transistor and vertical metal interconnect electrical isolation, barrier layers, and final passivation. Due to the Hg toxicity and metal contamination concerns mentioned previously, this work was quickly followed by demonstrations of direct photolytic CVD of SiO_2 [526,552] and SiN[500,553,554] using ArF[499] excimer lasers or Hg,[500,551,553] D_2,[526] or excimer[552] lamps. While the SiO_2 and SiN films produced by both methods exhibited comparable electrical and optical properties to those for films produced by plasma-enhanced CVD methods,[497,555,556,557,558] the later became the dominant method within the industry for deposition of intra- and inter-metal electrical isolation layers.[559]

Photo-assisted deposition methods have also been explored for more front-end-of-line (FEOL) related applications such as low temperature growth of SiO_2[535,560,561] and high-κ oxide[562] gate dielectric materials on semiconductors such as Si,[535,559,560,561] SiC,[563] GaAs,[564] InP,[565] and GaN[566]. Here again, photo-assisted deposition has shown promise for gate dielectric applications, but has to date yet to displace pure thermally driven processes. More recently though, UV assisted oxidation of Si, Ge, and SiGe alloys[567,568,569] has been investigated as a means of overcoming some of the limitations of initial gate oxide formation on Ge containing materials encountered with pure thermally or plasma driven processes.[570]

For strictly BEOL applications, photo-assisted depositions of both metals and low-κ dielectrics have been explored over the past two decades. Specifically, photo-assisted CVD[497,571] and ALD[572,573] of important interconnect metals such as Al,[574,575] W,[576] and Cu[513] and photo-assisted electroplating (EP) of Cu[577] have been reported. In some cases, selective are photo-CVD processes have also been reported for Al, Cu, and W.[578] However, neither photo-assised CVD or EP have yet to supplant the current PVD, CVD, and EP methods utilized to deposit these metals in BEOL interconnect fabrication.[579] For low-κ dielectrics, there have been some reports of photo-assisted CVD of polymeric low-κ materials.[580] However, polymers have struggled to meet all the necessary integration requirements for BEOL fabrication and, while of initial interest, have been supplanted by the organosilicate materials previously reviewed in this

article.[581] One recent emerging BEOL application for photo-CVD in BEOL applications is flowable gap-filling of trenches with low-κ SiOC:H material.[582]

VI. Conclusions

In conclusion, the photo-assisted processes described in this review offer a wide range of potential technological applications for nanofabrication that are generally gentler than plasma-based techniques or allow low temperature processing. Some UV-based technological solutions, such as low-□ curing and UV-induced stress engineering have already been widely adopted for high volume manufacturing while others see more limited use or have remained in various research and development stages. Nevertheless, the challenges in nanoscaling technology may promote more widespread adoption of photon-assisted processing. We hope that fundamental insights and prospected applications described in this article will help the reader to find optimal way in this wide and rapidly developing technology area.

Acknowledgements

L. Shohet would like to thank the support from grant by the Semiconductor Research Corporation under Contact Number 2008-KJ-1871 and by the National Science Foundation under Grant CBET-1066231. The UW-Madison Synchrotron is funded by NSF under Grant DMR-0537588. M. Baklanov thanks RFBR research project 18-52-52010.

[1] K. Maex, M. R. Baklanov, D. Shamiryan, F. Iacopi, S. Brongersma, Z. S. Yanovitskaya. Appl. Phys. Rev. 93, 8793 (2003).
[2] E. T. Ryan, A. J. McKerrow, J. Leu, and P. S. Ho, Mrs Bull. 22, 49 (1997).
[3] S. Mehta, C. Dimitrakopoulos, R. Augur, J. Gambino, A. Chou, T. Hook, B. Linder, W. Tseng, T. Bolam, D. Harmon, D. Massey, S. Gates, and H. Nye, Proc. Adv. Met. Conf. (Materials Research Socity, 2005), pp. 361–367.
[4] E.T. Ogawa and O. Aubel, in Adv. Interconnects ULSI Technol. Eds. M. Baklanov, P.S.Ho, E. Zschech. (Wiley, 2012).
[5] A. Grill, Annual Rev. Mater. Res., 39, 49 (2009).
[6] A. Grill, S. M. Gates, T. E. Ryan, S. V. Nguyen, and D. Priyadarshini, Appl. Phys. Rev. 1, 011306 (2014).
[7] S.V. Nguyen, T. Haigh, T. Shaw, S. Molis, C. Dziobkowski, C. Zahakos, S. Cohen, H. Shobha, E. Liniger, C.K. Hu, G. Bonilla, N. Klymko, and A. Grill, ECS Trans. 33, 137 (2010).
[8] S.V. Nguyen, T. Haigh, M. Tagami, A. Grill, S. Cohen, H. Shobha, C.-K. Hu, E. Adams, E. Liniger, T. Shaw, T. Cheng, H. Yusuff, Y. Xu, T.-M. Ko, S. Molis, T. Spooner, S. Skordas, X.H. Liu, G. Bonilla, and D. Edelstein, ECS Trans. 41, 3 (2012).

[9] T.A. Spooner, J.C. Arnold, D. Canaperi, J. Chen, S.-T. Chen, S.M. Gates, A. Isobayashi, P. Leung, S.S. Papa Rao, M. Sankarapandian, H. Shobha, and O. Van der Straten, ECS Trans. 25, 279 (2009).
[10] S. Hasegawa, T. Tsukaoka, T. Inokuma, Y. Kurata, Journal of Non-Crystalline Solids, 240, 154 (1998).
[11] P. H. Townsend, S. J. Martin, J. Godschalx, D. R. Romer, D. W. Smith, Jr., D. Castillo, R. DeVries, G. Buske, N. Reondan, S. Froelicher, J. Marshall, E. O. Shaffer and J. H. Im: Mater. Res. Soc. Symp. Proc. 479, 9 (1997).
[12] J. O. Simpson and A. K. St. Clair: Thin Solid Films 308, 480 (1997).
[13] T. Furusawa and Y. Homma: Dig. Tech. Pap. Symp. VLSI Technol., 1997, p. 59.
[14] Y. Nomura, F. Ota, H. Kurino and M. Koyanagi. Jap. J. Appl. Phys., 44, 7876 (2005).
[15] M. Hirai, Y. Akiyama, K. Koga, H. Kawakami, K. Nakatani, and M. Tada. Interconnect Technology Conference (IITC), San Jose, 2012.
[16] M. Pantouvaki, C. Huffman, L. Zhao, N. Heylen, Y. Ono, M. Nakajima, K. Nakatani, G. P. Beyer, M. R. Baklanov. Jap. J. Appl. Phys. 50, 04DB01 (2011).
[17] Maier, G. Prog. Polym. Sci. 26, 3 (2001).
[18] Wang, Z. B.; Wang, H. T.; Mitra, A. P.; Huang, L. M.; Yan, Y. S. Adv. Mater. 13, 746 (2001).
[19] Wang, Z. B.; Mitra, A. P.; Wang, H. T.; Huang, L. M.; Yan, Y. S. Adv. Mater. 13, 1463 (2001).
[20] Li, Z. J.; Johnson, M. C.; Sun, M. W.; Ryan, E. T.; Earl, D. J.; Maichen, W.; Martin, J. I.; Li, S.; Lew, C. M.; Wang, J.; Deem, M. W.; Davis, M. E.; Yan, Y. S. Angew. Chem., Int. Ed. 45, 6329 (2006).
[21] Eslava, S.; Seo, J. W.; Kirschhock, C. E. A.; Baklanov, M. R.; Maex, K.; Martens, J. A. Adv. Funct. Mater. 20, 2377 (2010).
[22] Eslava, S.; Baklanov, M. R.; Urrutia, J.; Kirschhock, C. E. A.; Maex, K.; Martens, J. A. Adv. Funct. Mater. 18, 3332 (2008).
[23] Z. Li, M. C. Johnson, M. Sun, E. T. Ryan, D. J. Earl, W. Maichen, J. I. Martin, S. Li, C. M. Lew, J. Wang, M. W. Deem, M. E. Davis, Y. Yan, Angew. Chemie, 118, 6477 (2006).
[24] S. Umeda, T. Yuki, T. Sugiyama and T. Sugino, Diamond and Related Materials 13, 1135 (2002).
[25] H. Aoki, D. Watanabe, R. Moriyama, M. K. Mazumder, N. Komatsu, C. Kimura T. Sugino. Diamond and Related Materials. 17, 4–5, 628 (2008).
[26] Bradley J. Nordell, Thuong D. Nguyen, Anthony N. Caruso, Sudhaunshu S. Purohit, N. A. Oyler, W. A. Lanford, D. W. Gidley, J. T. Gaskins, P. E. Hopkins, P. Henry, S. W. King, and M. M. Paquette. Adv. Electron. Mater. 1700116 (2017).
[27] Zagorodniy, K.; Seifert, G.; Hermann, H. Appl. Phys. Lett. 97, 251905 (2010).
[28] S. Eslava, L. Zhang, S. Esconjauregui, J. Yang, K. Vanstreels, M. R. Baklanov, E. Saiz. Chemistry of Materials, 25, 27 (2012).
[29] M. Usman, C.-H. Lee, D.-S. Hung, S.-F. Lee, C.-C. Wang, T.-T. Luo, L. Zhao, M.-K. Wu, K.-L. Lu, J. Mater. Chem. C. 2, 3762 (2014).
[30] Eslava, S.; Baklanov, M. R.; Neimark, A. V.; Iacopi, F.; Kirschhock, C. E. A.; Maex, K.; Martens, J. A. Adv. Mater. 20, 3110 (2008).
[31] M. R. Baklanov, C. Adelmann, L. Zhao, S. De Gendt, ECS J. Sol. St. Sci. and Technol., 4 (1) Y1 (2015).
[32] M. R. Baklanov and K. Maex. Phil. Trans. R. Soc. A, 364, 201 (2006).
[33] V. Jousseaume, A. Zenasni, O. Gourhant, L. Favennec, M. R. Baklanov. Ultra-Low-k by CVD: Deposition and Curing. In: Advanced Interconnects for ULSI Technology, M. R. Baklanov, P. S. Ho, and E. Zschech, Eds, Wiley, New York, (2012).
[34] W. Volksen, R. D. Miller, and G. Dubois, G. Chem. Rev., 110, 56–110 (2010).
[35] C. J. Brinker and G. W. Scherer, The Physics and Chemistry of Sol-Gel Processing, Academic Press, Inc., San Diego, 1990.
[36] F. Goethals. PhD thesis. Gent University, Belgium, 2012.
[37] T. Asefa, M. MacLachlan, N. Coombs, G. Ozin, Nature 402, 867 (1999).
[38] S. Inagaki, S. Guan, Y. Fukushima, T. Ohsuna, O. Terasaki, J. Am. Chem. Soc. 121, 9611 (1999).
[39] B. J. Melde, B. T. Holland, C. F. Blanford, A. Stein, Chem. Mater. 11, 3302 (1999).
[40] S. K. Kwak, K. H. Jeong and S. W. Rhee, J Electrochem Soc, 151, F11 (2004).
[41] T. Asefa, M. J. MacLachlan, H. Grondey, N. Coombs, G. A. Ozin, Angew. Chemie Int. Ed. 39, 1808 (2000).
[42] H. Li, J. M. Knaup, E. Kaxiras, and J. J. Vlassak, Acta Mater., 59(1), 44 (2011).
[43] K. Vanstreels, H. Li, and J. Vlassak, Mechanical reliability of low-k dielectrics. In: M. Baklanov, P. S. Ho, and E. Zschech, (Eds.) Advanced Interconnects for ULSI Technology, Wiley & Sons, 2012, pp. 339.

[44] H. Kazi, R. James, S. Gaddam, U. Chiluwal, J. Rimsza, J. Du and J. Kelber. 2014 IEEE International Interconnect Technology Conference / Advanced Metallization Conference (IITC/AMC). San Jose, CA, USA
[45] A. Grill, Materials for Advanced Inerconnects and Packaging, Bejing, China, 2017.
[46] A. Grill, and V. Patel, Appl. Phys. Lett., 79, 803 (2001).
[47] R. N.Vrtis, M.L. O'Neill, J. L. Vincent, A. S. Lukas, B. K. Peterson, M. D. Bitner, and E. J. Karwacki, Materials Research Society Symposium Proceedings, vol. 766, p. 259 (2003).
[48] S. M. Bilodeau, A. S. Borovik, A. A. Ebbing, D. J. Vestyck, C. Xu, J. F. Roeder, and T. H. Baum. Materials Research Society Symposium Proceedings, vol. 812, pp. F6.18.1–F6.18.6 (2004).
[49] D. D. Burkey, and K. K. Gleason, J. Vac. Sci. Technol. A, 22, 61 (2004).
[50] L. Favennec, V. Jousseaume, V. Rouessac, J. Durand, and G. Passemard. Materials Research Society Symposium Proceedings, vol. 863, pp. 49 (2005).
[51] V. Jousseaume, A. Zenasni, L. Favennec, G. Gerbaud, M. Bardet, J. P. Simon, A. and Humbert. J. Electrochem. Soc., 154, 1 (2007).
[52] O. Gourhant, G. Gerbaud, A. Zenasni, L. Favennec, P. Gonon, and V. Jousseaume. J. Appl. Phys., 108, 124105 (2010).
[53] S. M. Bilodeau, P. Chen, W. Giannetto, C. Xu, W. Hunks, T. H. Baum, J. F. Roeder, J.F. Proceedings of the Advanced Metallization Conference, vol. 367 (2006).
[54] S. M. Gates, G. Dubois, E. T. Ryan, A. Grill, M. Liu, and D. Gidley. J. Electrochem. Soc., 156, G156 (2009).
[55] A. Grill, and V. Patel. J. Appl. Phys., 104, 024113 (2008).
[56] R. Nenashev, Y. Wang, C. Liu, N. Kotova, K. Vorotilov, J. Zhang, S. Wei, D. Seregin, A. Vishnevskiy, J. Leu, and M. R. Baklanov. ECS Journal of Solid State Science and Technology, 6 (10) N182 (2017).
[57] P. Lazzeri, L. Vanzetti, M. Anderle, and M. Bersani, J. J. Park, Z. Lin, R. M. Briber, and G. W. Rubloff, H. C. Kim and R. D. Miller. J. Vac. Sci. Technol. B 23, 908 (2005).
[58] C. J. Brinker, Mrs Bull, 29, 631 (2004).
[59] A. Urbanowicz, PhD thesis, KULeuven, Leuven, Belgium, 2010
[60] M. R. Baklanov, K. P. Mogilnikov, V. G. Polovinkin, and F. N. Dultsev, J. Vac. Sci. Technol. B 18, 1385 (2000).
[61] V. Jousseaume, A. Zenasni, L. Favennec, G. Gerbaud, M. Bardet, J. P. Simon, and A. Humbert. J. Electrochem. Soc., 154, 1 (2007).
[62] L. Favennec, V. Jousseaume, G. Gerbaud, A. Zenasni, and G. Passemard. J. Appl. Phys., 102, 064107 (2007).
[63] A. Zenasni, V. Jousseaume, P. Holliger, L. Favennec, O. Gourhant, P. Maury, and G. Gerbaud, G. J. Appl. Phys., 102, 094107 (2007).
[64] S. I. Nakao, J. Ushio, T. Ohno, T. Hamada, Y. Kamigaki, M. Kato, K. Yoneda, S. Kondo, and N. Kobayashi. Proceedings of the IEEE Interconnect Technology Conference, p. 66 (2006).
[65] V. Jousseaume, M. Payet, P. Maury, and G. Passemard. Abstracts of Electrochemical Society, 601, 370 (2006).
[66] A. Zenasni, V. Jousseaume, O. Gourhant, L. Favennec, and P. Maury. Microelectron. Eng., 85, 2102 (2008).
[67] J. A. Lubguban, J. Sun, T. Rajagopalan, B. Lahlouh, S. L. Simon, and S. Gangopadhyay, S. Appl. Phys. Lett., 81, 4407 (2002).
[68] V. Jousseaume, J. Beynet, B. Rémiat, F. Gaillard, G. Lumia, G Didier, B. Fournel, D. Rebiscoul, D. Louis, and G. Passemard, G. Proceedings of the Advanced Metallization Conference, pp. 317–323 (2005).
[69] E. Kondoh, K. Segawa, M. Watanabe, L. Jin, L. Zhang, and M. R. Baklanov. Jap. J. Appl. Phys. 56, 07KF02 (2017).
[70] A. M. Urbanowicz, K. Vanstreels, P. Verdonck, D. Shamiryan, S. De Gendt, and M. R. Baklanov. J. Appl. Phys. 107, 104122 (2010).
[71] C. Waldfried, A. Margolis, O. Escorcia, Q. Han, R. Albano, I. Berry. Proc. of the 1st Internat. Conf. on Semicond. Techn. (ISTC 2001), vol. 2, p.234.
[72] W. Volksen, G. Dubois, A. Kellock, T. P. Magbitang, R. D. Miller, D. Miller, S. Cohen, E. E. Simonyi, L. Ramirez, D. Markle, S. Chen, S. Zhou, X. Wang and Y. Wang. J. Electrochem. Soc., 155, G224 (2008).
[73] M. Redzheb, S. Armini, K. Vanstreels, J. Meersschaut, M. R. Baklanov, Y. Wang, S. Chen, V. Le, M. Awdshiew, P. Van Der Voort, 2016 IEEE International Interconnect Technology Conference / Advanced Metallization Conference (IITC/AMC), 156-158 (2016).
[74] T. Rajagopalan, B. Lahlouh, J. A. Lubguban, N. Biswas, and S. Gangopadhyay, J. Sun, D. H. Huang, and S. L. Simon, A. Mallikarjunan, H.-C. Kim, W. Volksen, M. F. Toney, E. Huang, P. M. Rice, E. Delenia, and R. D. Miller. Appl. Phys. Lett. 82, 4328 (2003).

[75] J.A. Lubguban, S. Gangopadhyay, B. Lahlouh, T. Rajagopalan, N. Biswas, J. Sun, D.H. Huang, S.L. Simon, A. Mallikarjunan, H-C. Kim, J. Hedstrom, W. Volksen, R.D. Miller and M.F. Toney. J. Materials Research, 19, 11, 3224 (2004).
[76] J. Liu, E. M. Lee, D. I. Toma. Patent No.: US 7.622,378 B2 (Nov. 24, 2009).
[77] J. Liu, D. I. Toma. E. M. Lee. Patent No.: US 7,858,533 B2 (Dec. 28, 2010).
[78] H. Zheng, X. Guo, D. Pei, W. Li, J. Blatz, K. Hsu, D. Benjamin, Y.-H. Lin, H.-S. Fung, C.-C. Chen, Y. Nishi, and J. L. Shohet. Appl. Phys. Lett. 108, 242906 (2016).
[79] Dielectric Films for advanced microelectronics, Eds. M. Baklanov, K. Maec. M. Green, Wiley, 2008.
[80] A. Grill. J. Appl. Phys., 93, 1785 (2003).
[81] O. Gourhant, G. Gerbaud, A. Zenasni, L. Favennec, P. Gonon, and V. Jousseaume. J. Appl. Phys., 108, 124105 (2010).
[82] M. Krishtab, V. Afanas' ev, A. Stesmans, S. De Gendt. Appl. Phys. Lett. 111, 032908 (2017).
[83] S. I. Nakao, J. Ushio, T. Ohno, T. Hamada, Y. Kamigaki, M. Kato, K. Yoneda, S. Kondo, and N. Kobayashi. Proceedings of the IEEE Interconnect Technology Conference, p. 66 (2006),
[84] J. USHIO, T. OHNO, T. HAMADA, S-I. NAKAO, K.YONEDA, M. KATO, and N. KOBAYASHI. Jap. J. Appl. Phys., 46, L405 (2007).
[85] F. Iacopi, Y. Travaly, B. Eyckens, C. Waldfried, T. Abell, E. P. Guyer, D. M. Gage, R. H. Dauskardt, T. Sajavaara, K. Houthoofd, P. Grobet, P. Jacobs, K. Maex. J. Appl. Phys. 99, 053511 (2006).
[86] F. Lorut, A. Roggero, and G. Imbert, J. Appl. Phys. 114, 084508 (2013).
[87] E. Mickler, C.-T. Lin, A. T. Krishnan, C. Jin, and M. Jain. Proceedings of the 7th International Interconnect Technology Conference, pp. 190–192 (2004).
[88] C. Guedj, G. Imbert, E. Martinez, C. Licitra, N. Rochat, V. Arnal. Microelectronics Reliability 47, 764 (2007).
[89] E. Martinez, N. Rochat, C. Guedj, C. Licitra, G. Imbert, and Y. Le Friec. J. Appl. Phys. 100, 124106 (2006).
[90] D. M. Gage, L. Peng, J. Stebbins, K. S. Yim, A. Al-Bayati, A. Demos, R. H. Dauskardt. Int. J. Mat. Res. (formerly Z. Metallkd.) 101, 2 (2010).
[91] T.C. Chang, T.M. Tsai, P.T. Liu, C.W. Chen, T.Y. Tseng. Thin Solid Films 469–470, 383 (2004).
[92] K. Saito and A. J. Ikushima. Phys. Rev. B, 62, 13, 8584 (2000).
[93] H. Hosono, Y. Ikuta, T. Kinoshita, K. Kajihara, and M. Hirano. Phys. Rev. Lett. 87, 17, 175501 (2001).
[94] T. Tatsumi, S. Fukuda, S. Kadomura. Jap. J. Appl. Phys., 33, 2175 (1994).
[95] J. R. Woodworth, M. E. Riley, V. A. Amatucci, T. W. Hamilton, and B. P. Aragon. J. Vac. Sci. Technol. A 19, 45 (2001);
[96] H. S. Witham an P. M. Lenahan. Appl. Phys. Lett., 51.1007 (1987).
[97] K. Yokogawa, Y. Yajima, T. Mizutani, S. Nishimatsu, K. Suzuki. Jpn. J. Appl. Phys., 29, 2265 (1990).
[98] K. Yunogami, T. Mizutani, K. Tsujimoto, K. Suzuki. Jpn. J. Appl. Phys. 29, 2269 (1990).
[99] H. Sinha, H. Ren, M. T. Nichols, J. L. Lauer, et al., J. Appl. Phys. (Appl. Phys. Rev.) 112, 111101 (2012);
[100] P. Marsik, P. Verdonck, D. De Roest, M. R. Baklanov. Thin Solid Films 518 (2010) 4266 (2010).
[101] F. A. Choudhury et al. Appl. Phys. Lett., 112, 082902 (2018)
[102] T. V. Rakhimova et al., J. Phys. D: Appl. Phys. 47, 025102 (2014).
[103] P. Marsik, A. M. Urbanowicz, P. Verdonck, D. De Roest, H. Sprey, M. R. Baklanov. Thin Solid Films, 519, 3619 (2011).
[104] L. Prager, P. Marsik, L. Wennrich, M. R. Baklanov, S. Naumov, L. Pistol, D. Schneider, J. Gerlach, P. Verdonck, and M. Buchmeiser, M. Microelectron. Eng., 85, 2094 (2008).
[105] C. Chatchilialoglu. Organosilanes in Radical Chemistry, John Wiley & Sons, Ltd, Chichester., 2004.
[106] S. Nakao, Y. Kamigaki, J. Ushio, T. Hamada, T. Ohno, M. Kato, K. Yoneda, S. Kondoh, and N. Kobayashi. Jpn. J. Appl. Phys., 46, 3351 (2007).
[107] N. Tajima, Y. Ohashi, S. Nagano, Y. Xu, S. Matsumoto, T. Kada, and T. Ohno. Proceedings of the International Interconnect Technology Conference, p. 116 (2009).
[108] K. Seo, Y. Oka, K. Nomura, M. Tsutsue, E. Kobori, K. Goto, Y. Mizukami, T. Ohtsuka, K. Tsukamoto, S. Matsumoto, and T. Ueda. Proceedings of the International Interconnect Technology Conference, pp. 101 (2009).
[109] T. V. Rakhimova, A. T. Rakhimov, Y. A. Mankelevich, D. V. Lopaev, A. S. Kovalev, A. N. Vasilieva, O. V. Proshina, O. V. Braginsky, S. M. Zyryanov, K. Kurchikov, N. N. Novikova, and M. R. Baklanov, Appl. Phys. Lett. 102, 111902 (2013).
[110] K.-C. Kao, W.-Y. Chang, Y.-M. Chang, J. Leu, and Y.-L. Cheng, J. Vac. Sci. Technol., A 32, 061514 (2014).

[111] Z. Ming, H. Deng, Shu, Y. Xie, B. Zhang, Materials Science in Semiconductor Processing. 39, 235 (2015).
[112] M. R. Baklanov, J.-F. De Marneffe, D. Shamiryan, A. Urbanowicz, H. Shi, T. Rakhimova, H. Huang, and P. S. Ho. J. Appl. Phys., 113(4), 041101 (2013).
[113] G. Gerbaud, S. Hediger, M. Bardet, L. Favennec, A. Zenasni, J. Beynet, O. Gourhant, and V. Jousseaume, Phys. Chem. Chem. Phys., 11, 9729 (2009).
[114] M. Matsuura, K. Goto, N. Miura, S. Hashii, and K. Asai. Materials Research Society Symposium Proceedings, vol. 914, pp. F01 (2006).
[115] P.-Y. Mabboux, and K. K. Gleason, J. Electrochem. Soc., 152, F7 (2005).
[116] S. M. Gates, G. Dubois, E. T. Ryan, A. Grill, M. Liu, D. Gidley. J. Electrochem. Soc. 156, G156 (2009).
[117] M. R. Baklanov, L. Zhao, E. Van Besien, and M. Pantouvaki. Microelectron. Eng., 88, 990 (2011).
[118] O. Gourhant. (2008) Élaboration et caractérisation de matériaux à très faible constante diélectrique de type a-SiCOH élaborés par PECVD: application aux interconnexions des circuits intégrés. PhD thesis, INP Grenoble, France.
[119] G. Imbert, D. Vo-Than, C. Trouiller, and F. Lorut, J. Appl. Phys., 114, 224110 (2013).
[120] F. Ciaramella, V. Jousseaume, S. Maitrejean, M. Verdier, B. Remiat, A. Zenasni, and G. Passemard. Thin Solid Films, 495, 124 (2006).
[121] L. J. Gibson, and M. F. Ashby, M.F. Cellular Solids: Structure and Properties, 2nd edn, Cambridge University Press, 1997.
[122] F. Ito, T. Takeuchi, and Y. Hayashi, Y. Proceedings of the Advanced Metallization Conference, 32–33 (2004).
[123] V. Jousseaume, L. Favennec, A. Zenasni, and O. Gourhant. Surf. Coat. Technol., 201, 9248 (2007).
[124] Y. Lin, Y. Xiang, T. Tsui, and J. Vlassak. Acta Materialia, 56, 4932–4943.
[125] C. H. Huang, H. L. Huang, C. I. Hung, N. F. Wang, Y. H. Wang, and M. P. Houng. J. Appl. Phys., 47, 1532 (2008).
[126] V. Jousseaume, Ch. Le Cornec, F. Ciaramella, L. Favennec, A. Zenasni, G. Simon, J. P. Simon, G. Gerbaud and G. Passemard. Materials Research Society Symposium Proceedings, vol. 914, pp. F04 (2006).
[127] A. Grill, and D. A. Neumayer. J. Appl.Phys., 94, 6697 (2003).
[128] A. Grill, D. Edelstein, D. Restaino, M. Lane, S. Gates, E. Liniger, T. Shaw, X. H. Liu, D. Klaus, V. Patel, S. Cohen, E. Simonyi, N. Klymko, S. Lane, K. Ida, S. Vogt, T. Van Kleeck, C. Davis, M. Ono, T. Nogami, and T. Ivers. Proceedings of the 7th IEEE International Interconnect Technology Conference, pp. 54–56 (2004).
[129] S. Eslava, G. Eymery, P. Marsik, F. Iacopi, C. E. A. Kirschhock, K. Maex, J. A. Martens, M. R. Baklanov. J. Electrochem. Soc., 155, G115 (2008).
[130] T.-S. Kim, N. Tsuji, N. Kemeling, K. Matsushita, D. Chumakov, K. Geisler, E. Zschech, and R. H. Dauskardt. J. Appl. Phys., 103, 064108 (2008).
[131] T.-S. Kim, N. Tsuji, K. Matsushita, N. Kobayashi, D. Chumakov, H. Geisler, E. Zschech, and R. H. Dauskardt. J. Appl. Phys., 104, 074113 (2008).
[132] A. Grill, S. M. Gates, T. E. Ryan, S. V. Nguyen, and D. Priyadarshini. Appl. Phys. Rev. 1, 011306 (2014).
[133] S. M. Gates, G. Dubois, E. T. Ryan, A. Grill, M. Liu, D. Gidley. J. Electrochem. Soc. 156, G156 (2009).
[134] G. Dubois, T. Magbitang, W. Volksen, E. Simonyi, and R.D. Miller. Proceedings of the IEEE International Interconnect Technology Conference, 2005, pp. 226 (2005).
[135] D. J. Michalak, J. M. Blackwell, J. M. Torres, A. Sengupta, L. E. Kreno, J. S. Clarke, D. Pantuso. J. Mater. Res. 30 3363 (2015).
[136] K.-I. Usami, S. Sugahara, M. Kobayashi, K. Sumimura, T. Hattori, and M. Matsumura. J. Non-Cryst. Solids 260, 199 (1999).
[137] W. Volksen, S. Purushothaman, M. Darnon, M. F. Lofaro, S. A. Cohen, J. P. Doyle, N. Fuller, T. P. Magbitang, P. M. Rice, L. E. Krupp, H. Nakagawa, Y. Nobe, T. Kokubo, and G. Dubois. ECS J. Solid State Sci. Technol. 1, N85 (2012).
[138] M. Redzheb, L. Prager, M. Krishtab, S. Armini, K. Vanstreels, A. Franquet, P. Van Der Voort, M.R Baklanov. Microelecron. Eng. 156, 103 (2016).
[139] H. You, P. Mennell, M. Shoudy, D. Sil, D. Dorman, S. Cohen, E. Liniger, T. Shaw, T.-L. Leo, D. Canaperi, M. Raymond, A. Madan, and A. Grill. J. Vac. Sci. Technol. B 36, 012202 (2018).
[140] D. Priyadarshini, S. V. Nguyen, H. Shobha, E. Liniger, J. H.-C. Chen, H. Huang, S. A. Cohen, and A. Grill. J. Vac. Sci. Technol. B 35, 021201 (2017).
[141] J. El Sabahy, G. Castellan, F. Ricoul and V. Jousseaume. J. Phys. Chem. C, 120, 9184 (2016).
[142] Z.A. Weinberg, G.W. Rubloff, E. Bassous. PHYSICAL REVIEW B 19, 3107 (1979).
[143] S.W. King, B. French, and E. Mays. J. Appl. Phys. 113, 044109 (2013).
[144] F. N. Dultsev. Phys. Status Solidi C 8, No. 6, 1946–1949 (2011).

[145] H. Zheng, E. T. Ryan, Y. Nishi, and J. L. Shohet. Appl. Phys. Lett., 105, 202902 (2014).
[146] J. Lee and D.B. Graves, J. Phys. D: Appl. Phys. 44 325203 (2011).
[147] J. Lee and D. B. Graves, J. Vac. Sci. Technol. A 31 041302 (2013).
[148] D.V. Lopaev, V.V. Rakhlinsky, S.M. Zyryanov,Yu.A. Mankelevich, T.V. Rakhimova, K.A. Kurchikov, M.R. Baklanov. Plasma Processes and Polymers 15, 1700166 (2018).
[149] J.-F. de Marneffe, L. Zhang, M. Heyne, M. Lukaszewicz, S. B. Porter, F. Vajda, V. Rutigliani, Z. el Otell, M. Krishtab, A. Goodyear, M. Cooke, P. Verdonck, and M. R. Baklanov, J. Appl. Phys. 118 133302 (2015).
[150] S. Yasuhara, J. Chung, K. Tajima, H. Yano,S. Kadomura, M. Yoshimaru, N. Matsunagaand, S. Samukawa. J. Phys. D: Appl. Phys. 42 235201(2009).
[151] E. T. Ryan, S. M. Gates, A. Grill, S. Molis, P. Flaitz, J. Arnold, M. Sankarapandian, S. A. Cohen, Y. Ostrovski, and C. Dimitrakopoulos, J. Appl. Phys. 104, 094109 (2008).
[152] A. Grill and V. Patel, J. Electrochem. Soc. 153, F169 (2006)
[153] J. Bao, H. Shi, J. Liu, H. Huang, P. S. Ho, M. D. Goodner, M. Moinpour, and G. M. Kloster, J. Vac. Sci. Technol., B: Microelectron. Nanometer Struct. 26, 219 (2008).
[154] H. J. Lee, C. L. Soles, E. K. Lin, W. L. Wu, and Y. Liu, Appl. Phys. Lett. 91, 172908 (2007).
[155] D Eon, V Raballand, G Cartry and C Cardinaud, J. Phys. D: Appl. Phys. 40,3951(2007).
[156] Y. Iba, T. Kirimura, M. Sasaki, Y. Kobayashi, Y.Nakata, and M. Nakaishi, Jap. J. Appl. Phys. 47, 6923 (2008).
[157] M. Darnon, N. Casiez, T. Chevolleau, G. Dubois, W.Volksen, T. J. Frot, R. Hurand, T.L. David, N. Posseme, N. Rochat, and C. Licitra, J. Vac. Sci. Technol. B 31, 011207 (2013).
[158] Uchida S, Takashima S, Hori M, Fukasawa M, Ohshima K, Nagahata K and Tatsumi T. J. Appl. Phys. 103,073303 (2008).
[159] M.A. Goldman, D.B. Graves, G.A. Antonelli, S.P. Behera, and J.A. Kelber, J. Appl. Phys. 106, 013311 (2009).
[160] J. L. Lauer, H. Sinha, M. T. Nichols, G. A. Antonelli, Y. Nishi, and J. L. Shohet, J. Electrochem. Soc. 157(8), G177 (2010).
[161] H. Ren, G. A. Antonelli, Y. Nishi, and J. L. Shohet, J. Appl. Phys. 108, 094110 (2010).
[162] P. Tian and M. J. Kushner. Plasma Sources Sci. Technol. 24, 034017 (2015).
[163] Titus M. J., Nest D. and Graves D. B. Appl. Phys. Lett. 94, 171501 (2009).
[164] C. Petit-Etienne, M. Darnon, L. Vallier, E. Pargon, G. Cunge, F. Boulard, and O. Joubert, J. Vac. Sci. Technol. B 28(5), 926 (2010).
[165] D.J. Economou, J. Phys. D: Appl. Phys. 47, 303001 (2014).
[166] Song Sang-Heon and Kushner M.J. Plasma Sources Science and Technology, 21, 055028 (2012).
[167] Wen De-Qi, Zhang Quan-Zhi, Jiang W, Song Yuan-Hong, Bogaerts A and Wang You-Nian, J. Appl. Phys. 115, 233303 (2014).
[168] Y. Ichihashi, Y. Ishikawa, R. Shimizu, S. Samukawa, J. Vac. Sci. Technol. B 28, 577 (2010)
[169] P. Tian and M. J. Kushner, Plasma Sources Sci. Technol. 26, 024005 (2017).
[170] Y. Sun, M. Krishtab, H. Struyf, P. Verdonck, S. De Feyter, M. R. Baklanov, S. Armini, Langmuir, 30, 3832 (2014).
[171] F. Ito, H. Shobha, M. Tagami, T. Nogami, S. Cohen, Y. Ostrovski, S. Molis, K. Maloney, J. Femiak, J. Protzman, T. Pinto, E. T. Ryan, a. Madan, C.-K. Hu, and T. Spooner, Microelectronic Engineering, 92, 62 (2012).
[172] Xin Liu, Sandeep Gill, and Fu Tang, Sean W. King, Robert J. Nemanich, J. Vac. Sci. Technol. B 30, 031212 (2012).
[173] N. Posseme, T. Chevolleau, T. David, M. Darnon, O. Louveau and O. Joubert, J. of Vacuum Science & Technology B, 25, 1928 (2007).
[174] H. G. Peng, D. Z. Chi, W. D. Wang, J. H. Li, K. Y. Zeng, R. S. Vallery, W. E. Frieze, M. A. Skalsey, D. W. Gidley and A. F. Yee, J. Electrochem. Soc., 154, G85 (2007).
[175] F. N. Dultsev, A. M. Urbanowicz and M. R. Baklanov, Mat. Res. Soc. Proc. (2008).
[176]L. Zhang, R. Ljazouli, P. Lefaucheux, T. Tillocher, R. Dussart, Y. A. Mankelevich, J.-F.de Marneffe, S. de Gendt, and M. R. Baklanov. ECS Solid State Letters, 2(2):N5-N7 (2012).
[177] L. Zhang, R. Ljazouli, P. Lefaucheux, T. Tillocher, R. Dussart, Y. A. Mankelevich, J.-F. deMarneffe, S. de Gendt, and M. R. Baklanov. // ECS Journal of Solid State Science and Technology, 2(6):N131 (2013).
[178] L. Zhang, J.F. de Marneffe, F. Leroy, P. Lefaucheux, T. Tillocher, R. Dussart, K. Maekawa, K. Yatsuda, C. Dussarrat, A. Goodyear, M. Cooke, S. De Gendt, and M. R Baklanov. // Journal of Physics D: Applied Physics, 49, 175203 (2016).

[179] R. Dussart, T. Tillocher, P. Lefaucheux, and M. Boufnichel. Journal of Physics D: Applied Physics, 47, 123001 2014.
[180] A. Rezvanov, A. V. Miakonkikh, A. S. Vishnevskiy, K. V. Rudenko, and M. R. Baklanov. J. Vac. Sci. Technol. B, 35, 021204, (2017).
[181] D. V. Lopaev, Yu. A. Mankelevich, T. V. Rakhimova, A. I. Zotovich, S. M. Zyryanov, and M. R. Baklanov. Journal of Physics D: Applied Physics, 50, 485202, (2017).
[182] Z. Liu, Yi. Wu, B. Harteneck and D. Olynick, Nanotechnology, 24, 015305 (2013).
[183] Armon McPherson, Ned Rouze, W. B. Westerveld, and John S. Risley. APPLIED OPTICS, Vol. 25, No. 2 (1986).
[184] A. Zotovich, O. Proshina, Z. el Otell, D. Lopaev, T. Rakhimova, A. Rakhimov, J.-F. de Marneffe and M. R. Baklanov, Plasma Sources Sci. Technol. 25, 055001 (2016).
[185] E. J. Iglesias, F. Mitschker, M. Fiebrandt, N. Bibinov and P. Awakowicz, Meas. Sci. Technol. 28, 085501 (2017).
[186] D.V. Lopaev, S.M. Zyryanov, A.I. Zotovich, T.V. Rakhimova. Yu.A. Mankelevich, A.T. Rakhimov, and M.R. Baklanov, Plasma Process Polym. 1700213 (2018).
[187] U. Fantz, S. Briefi, D. Rauner, and D. Wünderlich,, Plasma Sources Sci. Technol. 25, 045006(2016).
[188] B. Jinnai, S. Fukuda, H. Ohtake and S. J. Samukawa. Appl. Phys.107,043302 (2010).
[189] O. V. Proshina, T. V. Rakhimova, D. V. Lopaev, V. Šamara, M. R. Baklanov and J.-F. de Marneffe, Plasma Sources Sci. Technol. 24, 055006 (2015)
[190] O. V. Proshina, T. V. Rakhimova, A. I. Zotovich, D. V. Lopaev, S. M. Zyryanov and A. T. Rakhimov. Plasma Sources Sci. Technol. 26, 075005 (2017).
[191] K. Takeda, Y. Miyawaki, S. Takashima, M. Fukasawa, K. Oshima, K. Nagahata, T. Tatsumi, and M. Hori, J. Appl. Phys. 109, 033303 (2011).
[192] H. Yamamoto, K. Takeda, K. Ishikawa, M.Ito, M. Sekine, M. Hori, T. Kaminatsui, H. Hayashi, I. Sakai, and T. Ohiwa, JOURNAL OF APPLIED PHYSICS 109, 084112 (2011),
[193] H. Yamamoto, K. Asano, K. Ishikawa, M. Sekine, H. Hayashi, I. Sakai, T. Ohiwa, K. Takeda, H. Kondo, and M.Hori, J. Appl. Phys. 110, (2011).
[194] H. Shi, H. Huang, J. Bao, J. Im, P. S. Ho, Y. Zhou, J. T. Pender, M. Armacost, and D. Kyser, in Proceedings of the IEEE International Interconnect Technology Conference, p. 78 (2009).
[195] H. Shi, H. Huang, J. Bao, J. Liu, P. S. Ho, Y. Zhou, J. T. Pender, M. D. Armacost, and D. Kyser, J. Vac. Sci. Technol. B 30, 011206 (2012).
[196] A. C. Fozza, J. E. Klemberg-Sapieha, and Michael R. Wertheimer. Plasmas and Polymers, 4, 183 (1999).
[197] J. Lee and D.B. Graves, J. Phys. D: Appl. Phys. 43 (2010) 425201
[198] N. Matsunaga, H. Okumura, B. Jinnai, and S. Samukawa, Jpn. J. Appl. Phys. 49, 04DB06 (2010).
[199] H. Kazi and J. A. Kelber, J. Vac. Sci. Technol. A 32, 021302 (2014).
[200] S. Behera, J. Lee, S. Gaddam, S. Pokharel, J. Wilks, F. Pasquale, D. Graves, and J. A. Kelber, Appl. Phys. Lett. 97, 034104 (2010).
[201] F. A. Choudhury, E. T. Ryan, H. M. Nguyen, Y. Nishi, and J. L. Shohet, AIP Adv. 6, 075012 (2016).
[202]O.V. Braginsky, A.S. Kovalev, D.V. Lopaev, E.M. Malykhin, Yu.A. Mankelevich, T.V. Rakhimova, A.T. Rakhimov, A.N. Vasil'eva, S.M. Zyryanov, and M.R. Baklanov, J. Appl. Phys. 108, 073303 (2010).
[203] A. M. Urbanowicz, D. Shamiryan, A. Zaka, P. Verdonck, S. De Gendt, and M. R. Baklanov, J. Electrochem. Soc. 157, H565 (2010).
[204] J. Lee, H. Kazi, S. Gaddam, J. A. Kelber, and D. B. Graves. J. Vac. Sci. Technol. A 31, 041303 (2013).
[205] M. A. Worsley, S. F. Bent, S. M. Gates, N. C. M. Fuller, W. Volksen, M. Steen, and T. Dalton, J. Vac. Sci. Technol. B 23, 395 (2005).
[206] A. Grill, V. Sternhagen, D. Neumayer, V. Patel, and T.J. Watson, J. Appl. Phys. 98, 074502 (2005)
[207] M. Fukasawa et al. Japan. J. Appl. Phys.51, 026201 (2012).
[208] Shoeb, J.; Kushner, M. J. Vac. Sci. Technol. A: Vac., Surf., Films 29, 051305 (2011)
[209] J. Shoeb, M.M. Wang and M. Kushner M, J. Vac. Sci. Technol. A 30, 041303 (2012).
[210] H. Kazi, R. James, S. Gaddam, U. Chiluwal, J. Rimsza, J. Du and J. Kelber, 2014 IEEE international Interconnect Technology Conference/Advanced Metallization Conference (IITC/AMC) doi 10.1109/IITC.2014. 6831884
[211] M. Redzheb, L. Prager, S. Naumov, M. Krishtab, S. Armini, P. Van Der Voort, and M.R. Baklanov, Appl.Phys.Lett., 108, 012902-1, 2016
[212] M. Okigawa, Y. Ishikawa, S, Kumagari, and S. Samukawa, 2002 7th International Symposium on plasma- and Plasma-Induced Damage, June 6-7, Maui, HI, USA.

[213] H.F. Winters and J.W. Coburn. Surface Science Reports 14, 161 (1992).
[214] D.L. Flamm, C.J. Mogab, and E.R. Sklaver, J. Appl. Phys. 50, 6211 (1979).
[215] T.V. Rakhimova, D.V. Lopaev, Yu.A. Mankelevich, A.T. Rakhimov, S.M. Zyryanov, K.A. Kurchikov, N.N. Novikova, and M.R. Baklanov, J. Phys. D: Appl. Phys. 48, 175203 (2015)
[216] T.V. Rakhimova, D.V. Lopaev, Yu.A. Mankelevich, K.A. Kurchikov, S.M. Zyryanov, A.P. Palov, O.V. Proshina, K.I. Maslakov, and M.R. Baklanov, J. Phys. D: Appl. Phys. 48, 175204 (2015).
[217] Yu.A. Mankelevich, E.N. Voronina, T.V. Rakhimova, A.P. Palov, D.V. Lopaev, S.M. Zyryanov, and M.R. Baklanov, J. Phys. D: Appl. Phys. 49, 345203 (2016).
[218] E Soda, S Kondo, S Saito, Y Ichihashi, A Sato, H Ohtake and S Samukawa. J. Vac. Sci. Technol. A 26, 875 (2008).
[219] S Samukawa, Y Ichihashi, H Ohtake, E Soda and S Saito. J. Appl. Phys. 103, 053310 (2008).
[220] Z el Otell, V Šamara, A Zotovich, T Hansen, J-F de Marneffeand M R Baklanov. J. Phys. D: Appl. Phys. 48, 395202 (2015).
[221] D V Lopaev, Yu A Mankelevich, T V Rakhimova, A I Zotovich, S M Zyryanov, and M R Baklanov. Journal of Physics D: Applied Physics, 50(48):485202, (2017).
[222] Yu.A. Mankelevich, E.N. Voronina, T.V. Rakhimova, A.P. Palov, D.V. Lopaev, S.M. Zyryanov, A.I. Zotovich, and M.R. Baklanov, Eur. Phys. J. D 71, 126 (2017).
[223] E.N. Voronina, Yu.A. Mankelevich, and T.V. Rakhimova, Eur. Phys. J. D 71, 184 (2017).
[224] E. N. Voronina, Yu. A. Mankelevich, and T. V. Rakhimova. Journal of Surface Investigation: X-ray, Synchrotron and Neutron Techniques, 12, 535 (2018).
[225] M. Redzheb. PhD thesis. Gent University, Belgium, 2018.
[226] A. M. Urbanowicz, M. R. Baklanov, J. Heijlen, Y. Travaly, and A. Cockburn. Electrochem. Sol.-St. Letters, 10 (10) G76-G79 (2007).
[227] S. P. Behera, Q. Wangand J. A . Kelber. J. Phys. D: Appl. Phys. 44, 155204 (2011).
[228] J. M. Calvert, M. K.Gallagher, Semicond. Int., 26, 56 (2003)
[229] V. Jousseaume, M. Assous, A. Zenasni, S. Maitrejean, B. Remiat, P. Leduc, H. Trouve, Le C. Cornec, M. Fayolle, A. Roule, F. Ciaramella, D. Bouchu, T. David, A. Roman, D. Scevola, T. Morel, D. Rebiscoul, G. Prokopowicz, M. Jackman, C. Guedj, D. Louis, M. Gallagher, G. Passemard, Proc. of the IEEE International Interconnect Technology Conference, 60 (2005)
[230] V. Jousseaume, L. Favennec, A. Zenasni, G. Passemard, Appl. Phys. Lett., 88, 182908 (2006).
[231]T. Frot, W. Volksen, S. Purushothaman, R. Bruce, G. Dubois, Adv. Mater. 23, 2828 (2011)
[232] T. Frot, W. Volksen, S. Purushothaman, R.S. Bruce, T. Magbitang, D.C. Miller, V.R. Deline, G. Dubois, Adv. Funct. Mater. 22 3043 (2012).
[233] M.H. Heyne, L. Zhang, J. Liu, I. Ahmad, D. Toma, J.-F. de Marneffe, S. De Gendt, M.R. Baklanov, Journal of Vacuum Science & Technology B 32, 062202 (2014)
[234] L. Zhang, J.-F. de Marneffe, M. H. Heyne, S. Naumov, Y. Sun, A. Zotovich, Z. el Otell, F. Vajda, S. De Gendt, and M. R. Baklanov. ECS J. Solid State Sci. Technol. 4, N3098 (2014).
[235] F. Iacopi, J. H. Choi, K. Terashima, P. M. Rice, G. Dubois. Physical Chemistry Chemical Physics, 13, 3634 (2011).
[236] M. Baklanov, F. Iacopi, S. Vanhaelemeersch. US patent 8540890, 2013.
[237] F. Leroy, L. Zhang, T. Tillocher, K. Yatsuda, K. Maekawa, E. Nishimura, P. Lefaucheux, J.-F. de Marneffe, M.R. Baklanov, R. Dussart, J. Phys. D: Appl. Phys. 48, 435202 (2015)
[238] M.R. Baklanov, J.-F. de Marneffe, L. Zhang, I. Ciofi, Z. Tokei, Solid State Technol. 57, 25 (2014).
[239] M. R. Baklanov. US patent US 8961803 B1, 2015.
[240] R. Chanson, L. Zhang, S. Naumov, Yu. A. Mankelevich, T. Tillocher, P. Lefaucheux, R. Dussart, S. De Gendt, and J.-F. de Marneffe, Scientific REPORTS 8, 1886 (2018).
[241] M. Krishtab, K Vanstreels, S. De Gendt, and M. Baklanov. IEEE International Interconnect Technology Conference and 2015 IEEE Materials for Advanced Metallization Conference (IITC/MAM), pages 103-106, (2015).
[242] M. Krishtab, J. F. de Marneffe, S. De Gendt, and M. R. Baklanov. Appl. Phys. Lett. 110, 2, (2017).
[243] A. Wills, M. Movassat, H. Pakbaz and N. Hacker. 2016 IEEE International Interconnect Technology Conference / Advanced Metallization Conference (IITC/AMC).
[244] J.-F.de Marneffe, A. Rezvanov, L. Zhang, M. Watanabe, M. B. Krishtab, L. Zhang, N. Hacker, P. Verdonck, S. Armini. J. Vac. Sci. Technol. B 35, 021211 (2017).
[245] E.T. Ryan and S. E. Molis, J. Appl. Phys. 122, 244104 (2017).

[246] C. K. Choi, C. Y. Kim, R. Navamathavan , H. S. Lee, J.-K. Woo, M. T. Hyun, H. J. Lee, and W. Y. Jeung, Current Appl. Phys. 11, S109 (2011).
[247] T. H. DiStefano and D. E. Eastman, Solid State Commun. 9, 2259 (1971).
[248] V. K. Adamchuk and V. V. Afanas'ev, Phys. Stat. Solidi (a) 132, 371(1992).
[249] R. J. Powell and G. F. Derbenwick, IEEE Trans. Nucl. Sci. NS-18, 99 (1971).
[250] D. J. DiMaria, Z. A. Weinberg, and J. M. Aitken, J. Appl. Phys. 48, 898 (1977).
[251] A. R. Stivers and C. T. Sah, J. Appl. Phys. 51, 6292 (1980).
[252] V. K. Adamchuk, V. V. Afanas'ev and A. Ph. Akulov, Phys. Stat. Solidi (a), 122, 347 (1990).
[253] For a review see, e.g., V. V. Afanas'ev and V. K. Adamchuk, Progr. Surface Sci. 47, 301 (1994).
[254] H. Li, C. Xu, N. Srivastava, and K. Banerjee, IEEE Trans. Electron Dev. 56, 1799 (2009).
[255] J. M. Aitken and D. R. Young, J. Appl. Phys. 47, 1196 (1976).
[256] J. M. Aitken, C. M. Serrano, and J. A. VanVechten, J. Electrochem. Soc. 125, C127 (1978).
[257] J. M. Aitken, D. R. Young, and K. Pan, J. Appl. Phys. 49, 3386 (1978).
[258] J. M. Aitken, J. Non-Cryst. Solids 40, 31 (1980).
[259] V. V. Afanas'ev, J. M. M. de Nijs, P. Balk, and A. Stesmans, J. Appl. Phys. 78, 6481 (1995).
[260] V. V. Afanas'ev, A. Stesmans, A. G. Revesz, and H. L. Hughes, J. Electrochem. Soc., 144, 749 (1997).
[261] V. V. Afanas'ev and A. Stesmans, Appl. Phys. Lett. 71, 3844 (1997).
[262] V. V. Afanas'ev and A. Stesmans, Mat. Res. Soc. Symp. Proc. 592, 195 (2000).
[263] V. V. Afanas'ev and A. Stesmans, J. Electrochem. Soc. 146, 3409 (1999).
[264] V. V. Afanas'ev and A. Stesmans, Mater. Sci. Eng. B 71, 56 (2000).
[265] D. J. DiMaria and J.W. Stasiak, J. Appl. Phys. 65, 2342 (1989).
[266] D. J. DiMaria, E. Cartier, and D. Arnold, J. Appl. Phys. 73, 3367 (1993).
[267] D. J. DiMaria and E. Cartier, J. Appl. Phys. 78, 3883 (1995).
[268] D. J. DiMaria, Appl. Phys.Lett 75, 2427 (1999).
[269] D. J. DiMaria, J. Appl. Phys. 87, 8707 (2000).
[270] D. J. DiMaria and J. H. Stathis, J. Appl. Phys. 89, 5015 (2001).
[271] V. V. Afanas'ev. Internal Photoemission Spectroscopy, 2nd ed. (Elsevier, Oxford, 2014).
[272] V. V. Afanas'ev, J. M. M. de Nijs, and P. Balk, Appl. Phys. Lett. 66, 1738 (1995).
[273] E. H. Nicollian, C. N. Berglund, P. F. Schmidt, and J. M. Andrews, J. Appl. Phys. 42, 5654 (1971).
[274] A. Hartstein and D. R. Young, Appl. Phys. Lett. 38, 631 (1981).
[275] V. V. Afanas'ev, F. Ciobanu, G. Pensl, and A. Stesmans, Solid State Electron. 46, 1815 (2002).
[276] H. Hosono, H. Kawazoe, and N. Matsunami, Phys. Rev. Lett. 80, 317 (1998).
[277] J. Krauser, F. Wulf, M. A. Briere, J. Steiger, and D. Braunig, Microelectron. Eng. 22, 65 (1993).
[278] M. Wilde and K. Fukutani, Surf. Sci. Reports 69, 196 (2014).
[279] A. Pusel, U. Wetterauer, and P. Hess, Phys. Rev. Lett. 81, 645 (1998).
[280] T. Vondrak and X.-Y. Zhu, Phys. Rev. Lett. 82, 1967 (1999).
[281] K. Kajihara, L. Skuja, M. Hirano, and H. Hosono, Phys. Rev. Lett. 89, 135507 (2002).
[282] D. L. Griscom, Nucl. Instr. Meth. Phys. Res. B 46, 12 (1990).
[283] V. V. Afanas'ev and A. Stesmans, J. Phys.: Condens. Matter 12, 2285 (2000).
[284] V. V. Afanas'ev and A. Stesmans, Europhys. Lett. 53, 233 (2001).
[285] V. V. Afanas'ev and A. Stesmans, Mater. Sci. Semicond. Proc. 4, 149 (2001).
[286] R. E. Stahlbush, A. H. Edwards, D. L. Griscom, and B. J. Mrstik, J. Appl. Phys. 73, 658 (1993).
[287] A. G. Revesz, IEEE Trans. Nucl. Sci. 24, 2102 (1977).
[288] F. B. McLean, IEEE Trans. Nucl. Sci. 27, 1651 (1980).
[289] J. M. M. de Nijs, K. G. Druijf, V. V. Afanas'ev, E. van der Drift, and P. Balk, Appl. Phys. Lett. 65, 2428 (1994).
[290] E. Cartier, J. H. Stathis, and D. A. Buchanan, Appl. Phys. Lett. 63, 1510 (1993).
[291] R. E. Stahlbush, E. Cartier, and D. A. Buchanan, Microelectron. Eng. 28, 15 (1995).
[292] V. V. Afanas'ev, J. M. M. de Nijs, and P. Balk, J. Appl. Phys. 76, 7990 (1994).
[293] V. V. Afanas'ev and A. Stesmans, Phys. Rev. Lett. 78, 2437 (1997).
[294] V. V. Afanas'ev and A. Stesmans, Microelectron. Eng. 36, 149 (1997).
[295] A. M. El-Sayed, M. B. Watkins, T. Grasser, V. V. Afanas'ev, and A. L. Shluger, Phys. Rev. Lett. 114, 115503 (2015).
[296] A. M. El-Sayed, Y. Wimmer, W. Goes, T. Grasser, V. V. Afanas'ev, and A. L. Shluger, Phys. Rev. B 92, 014107 (2015).

[297] D. Z. Gao, A. M. El-Sayed, and A. L. Shluger, Nanotechnology 27, 505207 (2016).
[298] J. Strand, M. Kaviani, D. Gao, A. M. El-Sayed, V. V. Afanas'ev and A. L. Shluger, J. Phys.: Condens. Matter 30, 233001 (2018).
[299] A. Padovani, D. Z. Gao, A. L. Shluger, and L. Larcher, J. Appl. Phys. 121, 155101 (2017).
[300] A. Stesmans, R. A. B. Devine, A. G. Revesz, and H. L. Hughes, IEEE Trans. Nucl. Sci. 37, 2008 (1990).
[301] D. Herve, J. L. Leray, and R. A. B. Devine, J. Appl. Phys. 72, 3634 (1992).
[302] W. L. Warren, M. R. Shaneyfelt, J. R. Schwank, D. M. Fleetwood, P. S. Winokur, R. A. B. Devine, W. P. Mazara, and J. B. McKitterick, IEEE Trans. Nucl. Sci. 40, 1755 (1993).
[303] R. A. B. Devine, W. L. Warren, J. B. Xu, I. H. Wilson, P. Pailet, and J. L. Leray, J. Appl. Phys. 77, 175 (1995).
[304] V. V. Afanas'ev, A. Stesmans, A. G. Revesz, and H. L. Hughes, J. Appl. Phys. 82, 2184 (1997).
[305] S. Shamuilia, V. V. Afanas'ev, P. Somers, A. Stesmans, Y. L. Li, Zs. Tokei, G. Groeseneken, and K. Maex, Appl. Phys. Lett. 89, 202909 (2006).
[306] P. Turek, M. Bernard, N. Lardon, J. C. Maisonobe and G. Passemad, In: Proc. 2000 Intl. Interconnect Technol. Conf., p. 173. DOI:10.1109/IITC.2000.854316
[307] V.V. Afanas'ev, K. Keunen, A. Stesmans, M. Jivanescu, Zs. Tokei, M.R. Baklanov, and G.P. Beyer, Microelectron. Eng.88, 1503 (2011).
[308] A.Stesmans and F. Scheerlinck, Phys. Rev. B 50, 5204 (1994).
[309] A.Stesmans and F. Scheerlinck, Phys. Rev. B 51, 4987 (1995).
[310] V. V. Afanas'ev, K. Keunen, A. P. D. Nguyen, M. Jivanescu, A. Stesmans, Zs. Tokei, M. R. Baklanov and G. P. Beyer MRS Proc. 1335, mrss11-1335-o04-04 (2011). doi:10.1557/opl.2011.1288.
[311] V. V. Afanas'ev, A. P. D. Nguyen, M. Houssa, A. Stesmans, Zs. Tokei, and M. R. Baklanov, Appl. Phys. Lett. 102, 172908 (2013).
[312] V. Nikas, S. Gallis, M. Huang, A. E. Kaloyeros, A. P. D. Nguyen, A. Stesmans, and V. V. Afanas'ev, Appl. Phys. Lett. 104, 061906 (2014).
[313] M. Krishtab, V. V. Afanas'ev, A. Stesmans, and S. De Gendt, Appl. Phys. Lett. 111, 032908 (2017).
[314] C. Wu, Y. Li, A. Lesniewska, O. Varela Pedreira, J.-F. de Marneffe, I. Ciofi, P. Verdonck, M. R. Baklanov, J. Bommels, I. De Wolf, Zs. Tokei, and K. Croes, J. Appl. Phys. 118, 164101 (2015).
[315] A. Konashuk, E. Filatova, S. Sakhonenkov, and V. Afanas'ev, Microelectron. Eng. 178, 209 (2017).
[316] B. C. Bittel, P. M. Lenahan, and S. W. King, Appl. Phys. Lett. 97, 063506 (2010).
[317] H. Sinha, H. Ren, M. T. Nichols, J. L. Lauer, M. Tomoyasu, N. M. Russell, G. Jiang, G. A. Antonelli, N. C. Fuller,S. U. Engelmann, Q. Lin, V. Ryan, Y. Nishi, and J. L. Shohet, J. Appl. Phys. 112, 111101 (2012).
[318] T. A. Pomorski, B. C. Bittel, C. J. Cochrane, P. M. Lenahan, J. Bielefeld, and S. W. King, J. Appl. Phys. 114, 074501 (2013).
[319] T. A. Pomorski, B. C. Bittel, P. M. Lenahan, E. Mays, C. Ege, J. Bielefeld, D. Michalak, and S. W. King, J. Appl. Phys. 115, 234508 (2014).
[320] M. J. Mutch, P. M. Lenahan, and S. W. King, J. Appl. Phys. 119, 094102 (2016).
[321] M. J. Mutch, T. Pomorski, B. C. Bittel , C. J. Cochrane, P. M. Lenahan, X. Liu, R. J. Nemanich, J. Brockman, M. French, M. Kuhn, B. French, and S. W. King, Microelectron. Reliab. 63, 201 (2016).
[322] J. M. Atkin, D. Song,T. M. Shaw, E. Cartier, R. B. Laibowitz, and T. F. Heinz, J. Appl. Phys. 103, 094104 (2008).
[323] J. L. Lauer, H. Sinha, M. T. Nichols, G. A. Antonelli, Y. Nishi, and J. L. Shohet, J. Electrochem. Soc. 157, G177 (2010).
[324] A. S. Zakirov, T. W. Kang, R. Navamathavan , C. Y. Kim, and C. K. Choi, J. Korean Phys. Soc. 58, 1393 (2011).
[325] C. Wu, Y. Li, I. Ciofi, Th. Kauerauf, J. Bommels, I. De Wolf, Zs. Tokei, and K. Croes, J. Appl. Phys. 117, 064101 (2015).
[326] A. S. Zakirov, R. Navamathavan , T. W. Kang, C. Y. Kim, and C. K. Choi, AIP Conf. Proc. 1399, 71 (2011). (DOI: 10.1063/1.3666262)
[327] H. Zheng, E. T. Ryan, Y. Nishi, and J. L. Shohet, Appl. Phys. Lett. 105, 202902 (2014).
[328] K. Kobayashi, H. Yokoyama, and M. Endoh, Appl. Surf. Sci. 254, 6222 (2008).
[329] K. Kobayashi and T. Ide, Jpn. J. Appl. Phys. 49, 05FE02 (2010).
[330] S. Nakao, Y. Kamigaki, J. Ushio, T. Hamada, T. Ohno, M. Kato, K. Yoneda, S. Kondo, and N. Kobayashi, Jpn. J. Appl. Phys. 46, 3351 (2007).
[331] E. T. Ogawa, J. Kim, G. S. Haase, H. C. Mogul, and J. W. McPherson, *Proc. IEEE Int. Rel. Physics Symp*, p.166.

[332] Kok-Yong Yiang, H. W. Yao, A. Marathe, and O. Aubel, *Reliability Physics Symposium Proceedings, 44th Annual IEEE International* (2009).
[333] F. Chen, O. Bravo, K. Chanda, P. McLaughlin, T. Sullivan, J. Gill, J. Lloyd, R. Kontra, J. Aitken, *Reliability Physics Symposium Proceedings, 44th Annual IEEE International* (2006)
[334] C. Cismaru and J.L. Shohet, *Appl. Phys. Lett*. **74**, 2599-2601 (1999).
[335] J.R. Woodworth, M. G. Blain, R. L. Jarecki, T.W. Hamilton, and B.P. Aragon, *J. Vac. Sci. Technol. A* **17**, 3209-3217 (1999).
[336] M. Joshi, J. P. McVittie, and K. Saraswat *7th Intern. Sym. Plasma- and Process-Induced Damage* 23 (2002).
[337] J. L. Lauer, J. L. Shohet, C. Cismaru, R. W. Hansen, M. Y. Foo, and T. J. Henn *J. Appl. Phys.* **91**, 1242 (2002).
[338] J.L. Lauer, J.L. Shohet and Y.Nishi, *Appl. Phys. Lett.* **94**, 162907 (2009)
[339] G.S. Upadhyaya, J.L. Shohet and J.B. Kruger, *Appl. Phys. Lett.* **91** 182108 (2007).
[340] C. Cismaru, J. L. Shohet, J. L. Lauer, R. W. Hansen and S. Ostapenko *Appl. Phys. Lett.* **77**, 3914 (2000).
[341] J. M. Atkin, E. Cartier, T. M. Shaw, R. B. Laibowitz, and T. F. Heinz, *Appl. Phys. Lett.* **93**, 122902 (2008).
[342] J. R. Lloyd, E. Liniger, and T. M. Shaw, *J. Appl. Phys.* **98**, 084109 (2005).
[343] J. M. Atkin, D. Song, T. M. Shaw, E. Cartier, R. B. Laibowitz, and T. F. Heinz, *J. Appl. Phys.* **103**, 094104 (2008).
[344] G. B. Alers, K. Jow, R. Shaviv, G. Kooi, and G. W. Ray, *IEEE Trans. Device and Materials Reliability* **4**, 148 (2004).
[345] H. Ren, H. Sinha, A. Sehgal, M. T. Nichols, G. A. Antonelli, Y. Nishi, and J. L. Shohet, *Appl. Phys. Lett.***97** 072901 (2010)
[346] H. Sinha, J. L. Lauer, M. T. Nichols, G. A. Antonelli, Y. Nishi, and J. L. Shohet, *Appl. Phys. Lett.* **96**, 052901 (2010)
[347] H. Sinha, M. T. Nichols, A. Sehgal, M. Tomoyasu, N. M. Russell, G. A. Antonelli, Y. Nishi and J. L. Shohet, *J. Vac. Sci. Technol. A* **29** 010601 (2011)
[348] R. S. Muller and T. I Kamins, *Device Electronics for Integrated Circuits*, New York: John Wiley & Sons (2003).
[349] H. Sinha, G. A. Antonelli, Y. Nishi and J. L. Shohet, J. Vac. Sci. Technol A 29 030602 (2011).
[350] J. L. Lauer, *The effect of vacuum ultraviolet irradiation on dielectric materials*, (Doctoral dissertation). University of Wisconsin-Madison, Madison, WI (2010)
[351] G.S. Upadhyaya, J.L. Shohet and J.L. Lauer, *Applied Physics Letters* **86** 102101 (2005)
[352] H. Sinha, H. Ren, A. Sehgal, G. A. Antonelli, Y. Nishi, and J. L. Shohet, *Appl. Phys. Lett.* **96**, 142903 (2010).
[353] M. Hosoya, K. Ichimura, Z. H. Wang, G. Dresselhaus, and P. C. Eklund, Phys. Rev. B 49, 4981 (1994).
[354] H. J. Queisser, Phys. Rev. Lett. 54, 234–236 (1985).
[355] A. Grill, D. Edelstein, M. Lane, V. Patel, S. Gates, D. Restaino, and S. Molis, J. Appl. Phys. 103, 054104 (2008).
[356] A. Stesmans and V. V. Afanas'ev, Appl. Phys. Lett. 82, 4074 (2003).
[357] L.L. Chapelon, E. Petitprez, P. Brun, A. Farcy, J. Torres, Microelectronic Engineering 84, 11 (2007).
[358] I. L. Berry, C. Waldfried, K. Durr, *Mater. Res.Soc.Symp.Proc.* **990** (2007).
[359] S. Eslava, F. Iacopi, A. M. Urbanowicz, C. E. A. Kirschhock, K. Maex, J. A. Martens, and M. R. Baklanov, *J. Electrochem. Soc.* **155**, G231 (2008).
[360] R.F. Pierret, *Semiconductor Device Fundamentals*, Addison-Wesley, Reading, MA, 1996.
[361] H. Sinha, G. A. Antonelli, Y. Nishi and J. L. Shohet, *J. Vac. Sci. Technol* A **29** 030602 (2011).
[362] M. Hosoya, K. Ichimura, Z. H. Wang, G. Dresselhaus, and P. C. Eklund, Phys. Rev. B 49, 4981 (1994).
[363] H. J. Queisser and D. E. Theodorou, *Phys. Rev. B* **33,** 4027–4033 (1986).
[364] M. Fayolle, G. Passemard, O. Louveau, F. Fusalba and J. Cluzel, Microelectronic Engineering 70, 2-4 (2003).
[365] H. J. Queisser, *Phys. Rev. Lett***. 54,** 234–236 (1985).
[366] A. Grill, D. Edelstein, M. Lane, V. Patel, S. Gates, D. Restaino, and S. Molis, *J. Appl. Phys.* **103**, 054104 (2008).
[367] J. H. Stathis, D. A. Buchanan, D. L. Quinlan, A. H. Parsons, and D. E. Kotecki, *Appl. Phys. Lett.* **62**, 2682 (1993).
[368] H. Sinha, A. Sehgal, H. Ren, M.T. Nichols, M. Tomoyasu, N. M. Russell, Y. Nishi and J.L. Shohet, *Thin Solid Films* **519** (16) 5464-5466 (2011).
[369] L.L. Chapelon, E. Petitprez, P. Brun, A. Farcy, J. Torres, *Microelectronic Engineering* **84**, 11 (2007).
[370] C. S. Chang, S. Chattopadhyay, L. C. Chen, K. H. Chen, C. W. Chen, Y. F. Chen, R. Collazo, and Z. Sitar, *Phys. Rev. B* **68**, 125322 (2003).
[371] Y. Lan, M. Yan, W. Liu, Y. Hu, and T. Lin, *J. Vac. Sci. Technol. B* **24**, 918 (2006).
[372] Jong-Min Park and Shi-Woo Rhee, *J. Electrochem. Soc.* **149**, F92 (2002).
[373] J. Planelles and J. L. Movilla, *Physical Review B* **73**, 235350 (2006).

[374] C. Guedj, E. Martinez and G. Imbert, *Mater. Res. Soc. Symp.* **990** (2007).
[375] H. Shi, D. Shamiryan, J.-F. de Marneffe, H. Huang, P.S. Ho, and M.R. Baklanov, Plasma Processing of Low-K Dielectrics (Wiley, 2012).
[376] M. Delavant, J. Guillan, D. Galpin, S. Chhun, M. Juhel, D. Guiheux, P. Jian, T.H. Ha, J. Forster, S. Guggilla, S. Hong, and B. Bozon, Microelectron. Eng. 92, 38 (2012).
[377] C.D. Dimitrakopoulos, S.M. Gates, V.J. McGahay, and S.C. Mehta, US7253105B2 (2007).
[378] B.N. Varadarajan, K.M. McLaughlin, and B. van Schravendijk, US8465991B2 (2013).
[379] H. Shi, J. Bao, J. Liu, R.S. Smith, Y. Sun, P.S. Ho, M.L. McSwiney, M. Moinpour, and G.M. Kloster, in Mater. Process. Adv. Interconnects Microelectron. (Materials Research Society, Pittsburgh, 2008), pp. N02–10.
[380] B. Van Schravendijk and W. Crew, US7851232B2 (2010).
[381] H. Huang, J.J. Bao, H. Huang, J.J. Liu, R.S. Smith, Y. Sun, P.S. Ho, M.L. McSwiney, M. Moinpour, and G.M. Kloster, in Mater. Res. Soc. Symp. Proc. D. (2008), pp. N02–10.
[382] K.S. Yim, T. Nowak, B. Xie, and A.T. Demos, US8216861B1 (2012).
[383] K. Chan and A.T. Demos, US20140004717A1 (2014).
[384] B. Xie, K. Chan, D. Cui, H. Ren, D. Raj, E. Hollar, S. Baluja, J. Rocha, M. Naik, and A. Demos, in IEEE Int. Interconnect Technol. Conf. (2014), pp. 335–338.
[385] H. Huang, H. Shi, J. Bao, P.S. Ho, Y. Zhou, J.T. Pender, M. Armacost, and D. Kyser, in Mater. Res. Soc. Proc. (2010), p. F5.3.
[386]B. Van Schravendijk and V.S. Benzing, US20100267231 (2010).
[387] Y. Kimura, A. Kobayashi, D. Ishikawa, A. Nakano, K. Matsushita, and N. Kobayashi, in 2012 IEEE Int. Interconnect Technol. Conf. (2012), pp. 1–3.
[388] Y. Kimura, D. Ishikawa, A. Nakano, A. Kobayashi, K. Matsushita, D. de Roest, and N. Kobayashi, Jpn. J. Appl. Phys. 51, 05 (2012).
[389] D. Priyadarshini, S. Nguyen, H. Shobha, S. Cohen, T. Shaw, E. Liniger, C.K. Hu, C. Parks, E. Adams, J. Burnham, A.H. Simon, G. Bonilla, A. Grill, D. Canaperi, D. Edelstein, D. Collins, M. Balseanu, M. Stolfi, J. Ren, and K. Shah, in IEEE Int. Interconnect Technol. Conf. (2014), pp. 185–188.
[390] G. Wang, P.S. Ho, and S. Groothuis, Microelectron. Reliab. 45, 1079 (2005).
[391] S. Van Nguyen, S. Hosadugra, T. Haigh, Y. Yao, L. Tai, S. Cohen, T. Shaw, C.K. Hu, E. Liniger, K. Virwani, A.J. Kellock, and D. Canaperi, ECS J. Solid State Sci. Technol. 6, 429 (2017).
[392] Y. Miyagawa, T. Murata, Y. Nishida, T. Nakai, A. Uedono, N. Hattori, M. Matsuura, K. Asai, and M. Yoneda, Jpn. J. Appl. Phys. 46, 1984 (2007).
[393] K. Goto, D. Kodama, N. Suzumura, S. Hashii, M. Matsumoto, N. Miura, T. Furusawa, M. Matsuura, and K. Asai, in 2006 Int. Interconnect Technol. Conf. (2006), pp. 95–97.
[394] H. Liu, J. Widodo, S.L. Liew, Z.H. Wang, Y.H. Wang, B.F. Lin, L.Z. Wu, C.S. Seet, W. Lu, C.H. Low, W.P. Liu, M.S. Zhou, and L.C. Hsia, in 2009 IEEE Int. Interconnect Technol. Conf. (2009), pp. 258–260.
[395] S.W. King, ECS J. Solid State Sci. Technol. 4, 3029 (2015).
[396] R. Navamathavan, C.Y. Kim, H.J. Lee, Y. Yu, and C.K. Choi, Thin Solid Films 547, 151 (2013).
[397] K. Kobayashi and K. Ishikawa, Jpn. J. Appl. Phys. 50, 031501 (2011).
[398] 46 P.R. Chidambaram, C. Bowen, S. Chakravarthi, C. Machala, and R. Wise, IEEE Trans. Electron Devices 53, 944 (2006).
[399] S. Reboh, P. Morin, M.J. Hÿtch, F. Houdellier, and A. Claverie, APL Mater. 1, 042117 (2013).
[400] W.-S. Liao, M.-C. Wang, Y. Hu, S.-H. Chen, K.-M. Chen, Y.-G. Liaw, C. Ye, W. Wang, D. Zhou, H. Wang, and H. Gu, Appl. Phys. Lett. 99, 173505 (2011).
[401] R. Arghavani, L. Xia, H. M'Saad, M. Balseanu, G. Karunasiri, A. Mascarenhas, and S.E. Thompson, IEEE Electron Device Lett. 27, 114 (2006).
[402] A.M. Noori, M. Balseanu, P. Boelen, A. Cockburn, S. Demuynck, S. Felch, S. Gandikota, A.J. Gelatos, A. Khandelwal, J.A. Kittl, A. Lauwers, W.C. Lee, J. Lei, T. Mandrekar, R. Schreutelkamp, K. Shah, S.E. Thompson, P. Verheyen, C.Y. Wang, L.Q. Xia, and R. Arghavani, IEEE Trans. Electron Devices 55, 1259 (2008).
[403] C. Ortolland, Y. Okuno, P. Verheyen, C. Kerner, C. Stapelmann, M. Aoulaiche, N. Horiguchi, and T. Hoffmann, IEEE Trans. Electron Devices 56, 1690 (2009).
[404] P. Morin, D. Benoit, and J. Metz, Eur. Phys. J. Appl. Phys. 43, 315 (2008).
[405] E. Todd Ryan, C. Labelle, S. Nitta, N.C.M. Fuller, G. Bonilla, K. McCullough, C. Taft, H. Lin, A. Simon, and E. Simonyi, Simonyi, MRS Proc. 863, 2 (2005).

[406] T. Abell and K. Maex, Microelectron. Eng. 76, 16 (2004).
[407] A.M. Urbanowicz, M.R. Baklanov, J. Heijlen, Y. Travaly, and A. Cockburn, Electrochem. Solid-State Lett. 10, 76 (2007).
[408] J. Lee, "Interactions of Plasma-Generated Species on Porous Dielectric Thin Films," (Doctoral Thesis: UC Berkeley, 2013).
[409] J. Liu, W. Kim, J. Bao, H. Shi, W. Baek, and P.S. Ho, J. Vac. Sci. & Technol. B: Microelectron. Nanom. Struct. Process. Meas. Phenom. 25, 906 (2007).
[410] E.T. Ryan, US 6,919,636 (2005).
[411] D. Ishikawa, A. Kobayashi, A. Nakano, Y. Kimura, K. Matsushita, N. Kobayashi, G. Ditmer, and A. Kiermasz, Jpn. J. Appl. Phys. 52, 05 (2013).
[412] B. Varadarajan, G.A. Antonelli, and B. van Schravendijk, US20110111533A1 (2011).
[413] K. Chan and A.T. Demos, US20150375275A1 (2015).
[414] E.T. Ryan, unpublished results.
[415] J.R. Vig, J. Vac. Sci. & Technol. 3, 1027 (1985).
[416] D.B. Fenner, D.K. Biegelsen, and R.D. Bringans, J. Appl. Phys. 66, 419 (1989). Now 416
[417] V.Y. Fominski, O.I. Naoumenko, V.N. Nevolin, A.P. Alekhin, A.M. Markeev, and L.A. Vyukov, Appl. Phys. Lett. 68, 2243 (1996).
[418] S. Ingrey, W.M. Lau, N.S. McIntyre, J. Vac. Sci. & Tech. 4, 984 (1986).
[419] J.A. McClintock, R.A. Wilson, and N.E. Byer, J. Vac. Sci. Technol. 20, 241 (1982).
[420] S. Ingrey, W.M. Lau, N.S. McIntyre, and R. Sodhi, J. Vac. Sci. & Technol. 5, 1621 (1987).
[421] S.W. King, R.J. Nemanich, and R.F. Davis, J. Electrochem. Soc. 146, 2648 (1999).
[422] S.W. King, J.P. Barnak, M.D. Bremser, K.M. Tracy, C. Ronning, R.F. Davis, and R.J. Nemanich, J. Appl. Phys. 84, 5248 (1998).
[423] J.S. Park, T.S. Kim, K.S. Son, W.-J. Maeng, H.-S. Kim, M. Ryu, and S.Y. Lee, Appl. Phys. Lett. 98, 012107 (2011).
[424] W. Song, S.K. So, D. Wang, Y. Qiu, and L. Cao, Appl. Surf. Sci. 177, 158 (2001).
[425] W. Li, Y. Liang, D. Yu, L. Peng, K.P. Pernstich, T. Shen, A.R.H. Walker, G. Cheng, C.A. Hacker, C.A. Richter, Q. Li, D.J. Gundlach, and X. Liang, Appl. Phys. Lett. 102, 183110 (2013).
[426] S.W. King, R.J. Nemanich, and R.F. Davis, Surf. Interface Anal. 47, 798 (2015).
[427] A. Azcatl, S. McDonnell, S.K. C., X. Peng, H. Dong, X. Qin, R. Addou, G.I. Mordi, N. Lu, J. Kim, M.J. Kim, K. Cho, and R.M. Wallace, Appl. Phys. Lett. 104, 111601 (2014).
[428] A.E. Duisterwinkel, A.T.G.M. Bastein, and W. van Schaik, Microelectron. Eng. 67-68, 3 (2003).
[429] W.J. Liu, X.A. Tran, X.B. Liu, J. Wei, H.Y. Yu, and X.W. Sun, ECS Solid State Lett. 2, 1 (2013).
[430] J. Yuan, L.-P. Ma, S. Pei, J. Du, Y. Su, W. Ren, and H.-M. Cheng, ACS Nano 7, 4233 (2013).
[431] Y.-J. Lin and J.-J. Zeng, Appl. Phys. Lett. 102, 183120 (2013).
[432] G. Imamura and K. Saiki, ACS Appl. Mater. & Interfaces 7, 2439 (2015).
[433] J. Seo, W.S. Chang, and T.-S. Kim, Thin Solid Films 584, 170 (2015).
[434] Y. Zhao, K. Kita, K. Kyuno, and A. Toriumi, Jpn. J. Appl. Phys. 46, 4189 (2007).
[435] L. Wu, H. Yu, K.S. Yew, J. Pan, W.J. Liu, and T.L. Duan, IEEE Trans. Electron Devices 58, 2177 (2011).
[436] T. Takahagi, I. Nagai, A. Ishitani, H. Kuroda, and Y. Nagasawa, J. Appl. Phys. 64, 3516 (1988).
[437] D. Tsvetanova, R. Vos, K. Vanstreels, D. Radisic, R. Sonnemans, I. Berry, C. Waldfried, D. Mattson, J. DeLuca, G. Vereecke, P.W. Mertens, T.N. Parac-Vogt, and M.M. Heyns, J. Electrochem. Soc. 158, 150 (2011).
[438] E. Kesters, Q.T. Le, M. Lux, L. Prager, and G. Vereecke, Microelectron. Eng. 87, 1674 (2010).
[439] X. Liu, C. Zhu, B.S. Eller, T. Sun, C.J. Jezewski, S.W. King, and R.J. Nemanich, J. Vac. Sci. & Technol. B 30, 052203 (2012).
[440] X. Liu, S. Gill, F. Tang, S.W. King, and R.J. Nemanich, J. Vac. Sci. & Technol. B 30, 031212 (2012).
[441] X. Liu, S.W. King, and R.J. Nemanich, J. Vac. Sci. & Technol. B 31, 022205 (2013).
[442] E. Kesters, Q.T. Le, M. Lux, L. Onandia, C. Baerts, and G. Vereecke, ECS Trans. 25, 63 (2009).
[443] E. Kesters, Q.T. Le, M. Lux, G. Vereecke, H. Struyf, and S. De Gendt, ECS Trans. 41, 269 (2011).
[444] E. Kesters, Q.T. Le, M. Lux, J. Pittevils, G. Vereecke, H. Struyf, and S.D. Gendt, J. Electrochem. Soc. 159, 287 (2012).
[445] G. Vereecke, E. Kesters, Q.T. Le, M. Claes, M. Lux, H. Struyf, R. Carleer, and P. Adriaensens, Microelectron. Eng. 105, 119 (2013).

[446] Q.T. Le, F. Drieskens, T. Conard, M. Lux, J.F. de Marneffe, H. Struyf, and G. Vereecke, in Ultra Clean Process. Semicond. Surfaces X (Trans Tech Publications, 2012), pp. 207–210.
[447] Q.T. Le, J.-F. de Marneffe, T. Conard, I. Vaesen, H. Struyf, and G. Vereecke, J. Electrochem. Soc. 159, 208 (2012).
[448] Q. Toan Le, S. Naumov, T. Conard, A. Franquet, M. Müller, B. Beckhoff, C. Adelmann, H. Struyf, S. De Gendt, and M.R. Baklanov, ECS J. Solid State Sci. Technol. 2, 93 (2013).
[449] Q.T. Le, I. Simms, H. Yue, I. Brown, E. Kesters, G. Vereecke, H. Struyf, and S.D. Gendt, Microelectron. Eng. 114, 136 (2014).
[450] T. Mukherjee, S.A. Berhe, A. Goswami, O. Chyan, K.J. Singh, and I. Brown, ACS Appl. Mater. & Interfaces 7, 5051 (2015).
[451] R.W. Hoisty, J. Electrochem. Soc. 108, 790 (1961).
[452] D.V. Podlesnik, H.H. Gilgen, and R.M. Osgood, Appl. Phys. Lett. 45, 563 (1984).
[453] D.J. Ehrlich, R.M. Osgood, and T.F. Deutsch, Appl. Phys. Lett. 36, 698 (1980).
[454] P. Brewer, S. Halle, and R.M. Osgood, Appl. Phys. Lett. 45, 475 (1984).
[455] H. Okano, Y. Horiike, and M. Sekine, Jpn. J. Appl. Phys. 24, 68 (1985).
[456] U. Streller, A. Krabbe, and N. Schwentner, Appl. Phys. Lett. 69, 3004 (1996).
[457] M.R. Baklanov, I.M. Beterov, S.M. Repinskii, A.V. Rzhanov, V.P. Chebotaev, and N.I. Yurshina, Sov. Phys. Dok. 19, 31 (1974).
[458] G.P. Davis, C.A. Moore, and R.A. Gottscho, J. Appl. Phys. 56, 1808 (1984).
[459] D. Lubzens, Electron. Lett. 13, 171 (1977).
[460] A.E. Willner, D.V. Podlesnik, H.H. Gilgen, and R.M. Osgood, Appl. Phys. Lett. 53, 1198 (1988).
[461] J.S. Shor, X.G. Zhang, and R.M. Osgood, J. Electrochem. Soc. 139, 1213 (1992).
[462] J.S. Shor and R.M. Osgood, J. Electrochem. Soc. 140, 123 (1993).
[463] D.J. Ehrlich, R.M. Osgood, and T.F. Deutsch, Appl. Phys. Lett. 38, 399 (1981).
[464] J.H. Brannon and K.W. Brannon, J. Vac. Sci. & Technol. B: Microelectron. Process. Phenom. 7, 1275 (1989).
[465] K. Choi and C. Han, J. Electrochem. Soc. 145, 37 (1998).
[466] W. Sesselmann, E.E. Marinero, and T.J. Chuang, Appl. Phys. 41, 209 (1986).
[467] Y.B. Hahn, S.J. Pearton, H. Cho, and K.P. Lee, Mater. Sci. Eng. 79, 20 (2001).
[468] T.J. Chuang, J. Vac. Sci. Technol. 21, 798 (1982).
[469] S. Yokoyama, Y. Yamakage, and M. Hirose, Appl. Phys. Lett. 47, 389 (1985).
[470] M. Hirose, S. Yokoyama, and Y. Yamakage, J. Vac. Sci. & Technol. B: Microelectron. Process. Phenom. 3, 1445 (1985).
[471] J.I. Steinfeld, T.G. Anderson, C. Reiser, D.R. Denison, L.D. Hartsough, and J.R. Hollahan, J. Electrochem. Soc. 127, 514 (1980).
[472] T. Sugiura, T. Yoshida, and H. Minoura, Electrochem. Solid-State Lett. 1, 175 (1998).
[473] D.W. Bäuerle, Chemical Processing with Lasers (Springer-Verlag Berlin Heidelberg, 1986).
[474] Y. Ohshita and N. Hosoi, Thin Solid Films 262, 67 (1995).
[475] R.M. Osgood, A. Sanchez-Rubio, D.J. Ehrlich, and V. Daneu, Appl. Phys. Lett. 40, 391 (1982).
[476] D.V. Podlesnik, H.H. Gilgen, R.M. Osgood, and A. Sanchez, Appl. Phys. Lett. 43, 1083 (1983).
[477] H.W. Lau, G.J. Parker, R. Greef, and M. Hölling, Appl. Phys. Lett. 67, 1877 (1995).
[478] F. Kuhn-Kuhnenfeld, J. Electrochem. Soc. 119, 1063 (1972).
[479] J. Murata and S. Sadakuni, Electrochimica Acta 171, 89 (2015).
[480] H. Lu, Z. Wu, and I. Bhat, J. Electrochem. Soc. 144, 8 (1997).
[481] M. Ohkubo, Mater. Sci. Eng. 59, 355 (1999).
[482] R.T. Leonard and S.M. Bedair, Appl. Phys. Lett. 68, 794 (1996).
[483] A. Tempez, N. Medelci, N. Badi, I. Berishev, D. Starikov, and A. Bensaoula, J. Vac. Sci. & Technol. 17, 2209 (1999).
[484] X. Xiao, A.J. Fischer, M.E. Coltrin, P. Lu, D.D. Koleske, G.T. Wang, R. Polsky, and J.Y. Tsao, Electrochimica Acta 162, 163 (2015).
[485] H. Maher, D.W. DiSanto, G. Soerensen, C.R. Bolognesi, H. Tang, and J.B. Webb, Appl. Phys. Lett. 77, 3833 (2000).
[486] H.J. Quah, W.F. Lim, Z. Hassan, F.K. Yam, and N. Zainal, J. Alloy. Compd. 662, 32 (2016).
[487] J.J. Ritsko, F. Ho, and J. Hurst, Appl. Phys. Lett. 53, 78 (1988).
[488] B.S. Agrawalla, B.T. Dai, and S.D. Allen, J. Vac. Sci. & Technol. B: Microelectron. Process. Phenom. 5, 601 (1987).
[489] J.E. Andrew, P.E. Dyer, R.D. Greenough, and P.H. Key, Appl. Phys. Lett. 43, 1076 (1983).
[490] R.W. Haynes, G.M. Metze, V.G. Kreismanis, and L.F. Eastman, Appl. Phys. Lett. 37, 344 (1980).

[491] F.W. Ostermayer and P.A. Kohl, Appl. Phys. Lett. 39, 76 (1981).
[492] H. Shin, W. Zhu, V.M. Donnelly, and D.J. Economou, J. Vac. Sci. & Technol. A: Vacuum, Surfaces, Films 30, 021306 (2012).
[493] W. Zhu, S. Sridhar, L. Liu, E. Hernandez, V.M. Donnelly, and D.J. Economou, J. Appl. Phys. 115, 203303 (2014).
[494] N. Hayasaka, H. Okano, M. Sekine, and Y. Horiike, Appl. Phys. Lett. 48, 1165 (1986).
[495] P.R. Chalker, Surf. Coatings Technol. 291, 258 (2016).
[496] F.A. Houle, Phys. Rev. B 39, 10120 (1989).
[497] F.A. Houle, Appl. Phys. 41, 315 (1986).
[498] M. Hanabusa, Mater. Sci. Reports 2, 51 (1987).
[499] J.Y. Chen, R.C. Henderson, J.T. Hall, and J.W. Peters, J. Electrochem. Soc. 131, 2146 (1984).
[500] P.K. Boyer, G.A. Roche, W.H. Ritchie, and G.J. Collins, Appl. Phys. Lett. 40, 716 (1982).
[501] Y. Numasawa, K. Yamazaki, and K. Hamano, Jpn. J. Appl. Phys. 22, 792 (1983).
[502] S.Y. Myong, T.H. Kim, K.S. Lim, K.H. Kim, B.T. Ahn, S. Miyajima, and M. Konagai, Sol. Energy Mater. Sol. Cells 81, 485 (2004).
[503] R. Solanki, W.H. Ritchie, and G.J. Collins, Appl. Phys. Lett. 43, 454 (1983).
[504] M. Ishida, A. Eto, T. Nakamura, and T. Suzaki, J. Vac. Sci. & Technol. 7, 2931 (1989).
[505] Q. Fang, J.-Y. Zhang, Z.M. Wang, J.X. Wu, B.J. O'Sullivan, P.K. Hurley, T.L. Leedham, H. Davies, M.A. Audier, C. Jimenez, J.-P. Senateur, and I.W. Boyd, Thin Solid Films 427, 391 (2003).
[506] J.J. Yu and I.W. Boyd, Appl. Surf. Sci. 208-209, 374 (2003).
[507] N. Kaliwoh, J.-Y. Zhang, and I.W. Boyd, Appl. Surf. Sci. 186, 241 (2002).
[508] J.-Y. Zhang, B. Lim, and I.W. Boyd, Thin Solid Films 336, 340 (1998).
[509] M. Danno and M. Hanabusa, Mater. Lett. 4, 261 (1986).
[510] O. Kubová, V. Švorčík, J. Heitz, S. Moritz, C. Romanin, P. Matějka, and A. Macková, Thin Solid Films 515, 6765 (2007).
[511] Y. Kumashiro, T. Enomoto, K. Sato, Y. Abe, K. Hirata, and T. Yokoyama, J. Solid State Chem. 177, 529 (2004).
[512] T. Motooka, S. Gorbatkin, D. Lubben, and J.E. Greene, J. Appl. Phys. 58, 4397 (1985).
[513] Y.K. Fang, S.B. Hwang, and C.Y. Sun, J. Electrochem. Soc. 138, 1720 (1991).
[514] Y.-L. Wu, M.-H. Hsieh, and H.-L. Hwang, Thin Solid Films 483, 10 (2005).
[515] M.K. Mazumder, Y. Takakuwa, and N. Miyamoto, Appl. Phys. Lett. 61, 2881 (1992).
[516] C.J. Kiely, V. Tavitian, C. Jones, and J.G. Eden, Appl. Phys. Lett. 55, 65 (1989).
[517] P.K. York, J.G. Eden, J.J. Coleman, G.E. Fernández, and K.J. Beernink, J. Appl. Phys. 66, 5001 (1989).
[518] R. Solanki, U. Sudarsan, and J.C. Johnson, Appl. Phys. Lett. 52, 919 (1988).
[519] V.M. Donnelly, M. Geva, J. Long, and R.F. Karlicek, Appl. Phys. Lett. 44, 951 (1984).
[520] M.S. Tomar, R. Rutherford, C. New, and K.A. Kuenhold, Sol. Energy Mater. Sol. Cells 63, 437 (2000).
[521] S. Fujita, T. Asano, K. Maehara, and S. Fujita, Appl. Surf. Sci. 79-80, 270 (1994).
[522] B. Liu, R.F. Hicks, and J.J. Zinck, J. Cryst. Growth 129, 111 (1993).
[523] J. Riikonen, W. Kim, C. Li, O. Svensk, S. Arpiainen, M. Kainlauri, and H. Lipsanen, Carbon 62, 43 (2013).
[524] Y.Y. Tan, K.D.G.I. Jayawardena, A.A.D.T. Adikaari, L.W. Tan, J.V. Anguita, S.J. Henley, V. Stolojan, J.D. Carey, and S.R.P. Silva, Carbon 50, 668 (2012).
[525] Y. Li, H. Wang, and S. Peng, J. Phys. Chem. C 118, 19842 (2014).
[526] C.A.D. Dion, W. Raphael, E. Tong, and J.R. Tavares, Surf. Coatings Technol. 244, 98 (2014).
[527] M. Okuyama, Y. Toyoda, and Y. Hamakawa, Jpn. J. Appl. Phys. 23, 97 (1984).
[528] T. Shirafuji, M. Yoshimoto, T. Fuyuki, and H. Matsunami, Sol. Energy Mater. 23, 256 (1991).
[529] T. Fujii, M. Yoshimoto, T. Fuyuki, and H. Matsunami, Appl. Surf. Sci. 79-80, 316 (1994).
[530] O. Chevaleevski, S.Y. Myong, and K.S. Lim, Solid State Commun. 128, 355 (2003).
[531] J. Kwak, S.W. Kwon, S.I. Park, J.H. Yang, and K.S. Lim, Sol. Energy Mater. Sol. Cells 92, 1081 (2008).
[532] K. Saito, Y. Watanabe, K. Takahashi, T. Matsuzawa, B. Sang, and M. Konagai, Sol. Energy Mater. Sol. Cells 49, 187 (1997).
[533] Y. Yamamoto, K. Saito, K. Takahashi, and M. Konagai, Sol. Energy Mater. Sol. Cells 65, 125 (2001).
[534] B.H. Lee, S. Cho, J.K. Hwang, S.H. Kim, and M.M. Sung, Thin Solid Films 518, 6432 (2010).
[535] C.A.D. Dion and J.R. Tavares, Powder Technol. 239, 484 (2013).
[536] P. Bergonzo, U. Kogelschatz, and I.W. Boyd, Appl. Surf. Sci. 69, 393 (1993).
[537] A.A. Voevodin and M.S. Donley, Surf. Coatings Technol. 82, 199 (1996).

[538] V. Craciun and R.K. Singh, Appl. Surf. Sci. 168, 239 (2000).
[539] M.N.R. Ashfold, F. Claeyssens, G.M. Fuge, and S.J. Henley, Chem. Soc. Rev. 33, 23 (2004).
[540] T.J. Jackson and S.B. Palmer, J. Phys. D: Appl. Phys. 27, 1581 (1994).
[541] M. Hanabusa, A. Namiki, and K. Yoshihara, Appl. Phys. Lett. 35, 626 (1979).
[542] R.W. Andreatta, C.C. Abele, J.F. Osmundsen, J.G. Eden, D. Lubben, and J.E. Greene, Appl. Phys. Lett. 40, 183 (1982).
[543] I.W. Boyd and J.-Y. Zhang, Solid-State Electron. 45, 1413 (2001)..
[544] P. Bergonzo, P. Patel, I.W. Boyd, and U. Kogelschatz, Appl. Surf. Sci. 54, 424 (1992).
[545] U. Kogelschatz, H. Esrom, J.-Y. Zhang, and I.W. Boyd, Appl. Surf. Sci. 168, 29 (2000).
[546] S. Lian, B. Fowler, S. Krishnan, L. Jung, C. Li, I. Manna, D. Samara, and S. Banerjee, J. Vac. Sci. & Technol. 11, 2914 (1993).
[547] R.G. Frieser, J. Electrochem. Soc. 115, 401 (1968).
[548] M. Kumagawa, H. Sunami, T. Terasaki, and J. Nishizawa, Jpn. J. Appl. Phys. 7, 1332 (1968).
[549] M.G. Collet, J. Electrochem. Soc. 116, 110 (1969).
[550] C.H.J. v. d. Brekel and P.J. Severin, J. Electrochem. Soc. 119, 372 (1972).
[551] K. Hamano, Y. Numazawa, and K. Yamazaki, Jpn. J. Appl. Phys. 23, 1209 (1984).
[552] Y. Tarui, J. Hidaka, and K. Aota, Jpn. J. Appl. Phys. 23, 827 (1984).
[553] P. Bergonzo and I.W. Boyd, Appl. Phys. Lett. 63, 1757 (1993).
[554] M. Yoshimoto, K. Takubo, M. Komoda, and H. Matsunami, Appl. Surf. Sci. 79-80, 264 (1994).
[555] M. Berti, M. Meliga, G. Rovai, S. Stano, and S. Tamagno, Thin Solid Films 165, 279 (1988).
[556] M. Lemiti, S. Audisio, J.C. Dupuy, and B. Balland, J. Non-Crystalline Solids 144, 261 (1992).
[557] G.M. Nikolić, Vacuum 40, 143 (1990).
[558] V.K. Rathi, M. Gupta, R. Thangaraj, K.S. Chari, and O.P. Agnihotri, Thin Solid Films 266, 219 (1995).
[559] D.R. Cote, S.V. Nguyen, A.K. Stamper, D.S. Armbrust, D. Tobben, R.A. Conti, and G.Y. Lee, IBM J. Res. Dev. 43, 5 (1999).
[560] P. Patel and I.W. Boyd, Appl. Surf. Sci. 46, 352 (1990).
[561] V. Sánchez, J. Munguía, and M. Estrada, Microelectron. Reliab. 44, 885 (2004).
[562] Q. Fang, J.Y. Zhang, Z.M. Wang, G. He, J. Yu, and I.W. Boyd, Microelectron. Eng. 66, 621 (2003).
[563] C.H. Liu, C.S. Chang, S.J. Chang, Y.K. Su, Y.Z. Chiou, S.H. Liu, and B.R. Huang, Mater. Sci. Eng. 100, 142 (2003).
[564] C.H. Liu, T.K. Lin, and S.J. Chang, Solid-State Electron. 49, 1077 (2005).
[565] C. Licoppe, F. Wattine, C. Meriadec, J. Flicstein, and Y.I. Nissim, J. Appl. Phys. 68, 5636 (1990).
[566] K.H. Lee, P.C. Chang, S.J. Chang, and Y.K. Su, Solid-State Electron. 72, 38 (2012).
[567] I.W. Boyd, V. Craciun, and A. Kazor, Jpn. J. Appl. Phys. 32, 6141 (1993).
[568] J.-Y. Zhang and I.W. Boyd, Appl. Surf. Sci. 186, 64 (2002).
[569] J.-Y. Zhang, Q. Fang, A.J. Kenyon, and I.W. Boyd, Appl. Surf. Sci. 208-209, 364 (2003).
[570] E. Chagarov, K. Sardashti, T. Kaufman-Osborn, S. Madisetti, S. Oktyabrsky, B. Sahu, and A. Kummel, ACS Appl. Mater. & Interfaces 7, 26275 (2015).
[571] D.J. Ehrlich, R.M. Osgood Jr., and T.F. Deutsch, J. Vac. Sci. Technol. 21, 23 (1982).
[572] V. Miikkulainen, K. Väyrynen, V. Kilpi, Z. Han, M. Vehkamäki, K. Mizohata, J. Räisänen, and M. Ritala, ECS Trans. 80, 49 (2017).
[573] K.M. Vayrynen, "Photo-Assisted Atomic Layer Deposition and Chemical Vapor Deposition of Metal and Metal Oxide Thin Films," (Doctoral Thesis, University of Helsinki, 2015).
[574] A.R. Calloway, T.A. Galantowicz, and W.R. Fenner, J. Vac. Sci. & Technol. 1, 534 (1983).
[575] M. Hanabusa, A. Oikawa, and P.Y. Cai, J. Appl. Phys. 66, 3268 (1989).
[576] D.K. Flynn, J.I. Steinfeld, and D.S. Sethi, J. Appl. Phys. 59, 3914 (1986).
[577] J.-Y. Zhang, S.L. King, I.W. Boyd, and Q. Fang, Appl. Surf. Sci. 109-110, 487 (1997).
[578] W.L. Gladfelter, Chem. Mater. 5, 1372 (1993).
[579] S.M. Merchant, S.H. Kang, M. Sanganeria, B. van Schravendijk, and T. Mountsier, JOM 53, 43 (2001).
[580] J.-Y. Zhang and I.W. Boyd, Opt. Mater. 9, 251 (1998).
[581] A. Grill, J. Vac. Sci. & Technol. B 34, 020801 (2016).
[582] W.-J. Lee, H. Fukuda, T.H. Kim, and Y.-H. Choa, ECS J. Solid State Sci. Technol. 5, 32 (2016).

VII. ADDENDUM.

VII.1. Nomenclature.

1MS	Methylsilane
2MS	Dimethylsilane
3MS	Trimethylsilane
4MS	Tetramethylsilane
AFM	Atomic force microscopy
ALD	Atomic layer deposition
ARC	Anti-reflecting coating
ARXPS	Angle-resolved x-ray photoelectron spectroscopy
ATR-FTIR	Attenuated total reflectance Fourier transform infra red spectroscopy
BEOL	Back end of the line
BTS	Bias-temperature stress
CCP	Capacitively coupled plasma
CD	Critical dimensions
CMP	Chemical mechanical polishing
CTE	Coefficient of thermal expansion
CVD	Chemical vapour deposition
DEMS	Diethoxy-methyl-silane
DMCPS	Deca-methyl-cyclo-pentasiloxane
DMSO	Dimethyl sulfoxide
DSP	Downstream plasma
EFTEM	Energy-filtered transmission electron microscopy
ELD	Electroless plating
ELK	Extreme low-k
EP	Ellipsometric porosimetry
FTIR	Fourier transform infra red spectroscopy
GISAXS	Grazing incidence small angle x-ray scattering
HAFA	Hydrogen Abstraction Flourine Addition
HMDS	Hexamethyldisilazane
ICP	Inductively coupled plasma
IR	Infrared
IR-RAS	Infrared reflection absorption spectroscopy
ILD	Inter-layer dielectric
LWR	Line width roughness
NCS	Nanocrystalline silica
MSQ	Methylsilsesquioxane
NMR	Nuclear magnetic resonance
OSG	Organo-silicate glass
PALS	Positronium annihilation lifetime spectroscopy
PAPE	pallet for plasma evaluation
PECVD	Plasma-enhanced chemical vapor deposition

PID	Plasma induced damage
PR	Photoresist
PVD	Physical vapor deposition
RMS	Root mean square (roughness)
SEM	Scanning electron microscope
SIMS	Secondary ion mass spectroscopy
TDDB	Time-dependent dielectric breakdown
TDS	Thermal desorption spectroscopy
TEM	Transmission electron microscopy
TMAH	Tetramethylammonium hydroxide
TMCTS	Tetramethyl-cyclotetrasiloxane
TVS	Triangular voltage sweep
ULK	Ultra low-k
UV	Ultra violet
UVSE	UV spectroscopic ellipsometry
VUV	Vacuum ultra violet
XPS	X-ray photoelectron spectroscopy
XRD	X-ray diffraction
XRF	X-ray fluorescence
XRR	X-ray reflectivity

VII.2. The most common physical methods used for evaluation of low-k materials.

Materials Properties	Method of Evaluation
Chemical composition	FTIR, XPS, TOF SIMS, NMR
Porosity and Pore size	EP, PALS, GISAXS, SANS
Porogen residue evaluation	UV spectroscopy, ESR
Density	RBS, SXR
Mechanical Properties	Nanoidentation, SAWS, BLS
CTE, Stress	SXR, SE, Bending beam
Thermal Stability and Outgassing	TDS
Thermal conductivity	3-Omega test
Adhesion	4 point bending
Roughness	AFM
Cross-section, shape of patterned low-*k* films.	TEM
Composition gradient in patterned structures.	EFTEM, EELS